Title
Fragment-Based Identification of Phosphatase Inhibitors

Author
Rawls, Katherine Anne

Publication Date
2010

Peer reviewed|Thesis/dissertation

Fragment-Based Identification of Phosphatase Inhibitors

by

Katherine Anne Rawls

A dissertation submitted in partial satisfaction of the

requirements for the degree of

Doctor of Philosophy

in

Chemistry

in the

Graduate Division

of the

University of California, Berkeley

Committee in charge:

Professor Jonathan A. Ellman, Chair
Professor Carolyn R. Bertozzi
Professor Tom Alber

Spring 2010

Abstract

Fragment-Based Identification of Phosphatase Inhibitors

by

Katherine Anne Rawls

Doctor of Philosophy in Chemistry

University of California, Berkeley

Professor Jonathan A. Ellman, Chair

Chapter 1. A new fragment-based method for the identification of phosphatase inhibitors, Substrate Activity Screening, is described. Application of the method to *Mycobacterium tuberculosis* protein tyrosine phosphatase PtpB resulted in the identification of novel, nonpeptidic substrate scaffolds that were optimized by rapid analog synthesis and evaluation. These substrate scaffolds were then converted to low molecular weight inhibitors for PtpB by incorporation of a variety of established phosphate mimetics, resulting in nanomolar affinity inhibitors that were highly selective for PtpB over mycobacterial and human phosphatases.

Chapter 2. The design and synthesis of new inhibitor analogs based on the scaffold identified in Chapter 1 is described. The synthesis of more challenging inhibitor scaffolds was achieved, resulting in a panel of low molecular weight, nanomolar to micromolar affinity inhibitors for the *Mycobacterium tuberculosis* protein tyrosine phosphatase PtpB. These compounds represent chemical tools for further dissection of the biochemical role of PtpB in tuberculosis infection.

Chapter 3. Application of the method described in Chapter 1 to *Mycobacterium tuberculosis* protein tyrosine phosphatase PtpA is described. Inhibitors incorporating a well established phosphate mimetic were explored, resulting in compounds with low micromolar affinity for PtpA. Modeling studies provided a rationale for the observed structure-activity relationships and guided further compound optimization. The most potent compound was additionally shown to be selective for PtpA over a variety of human enzymes as well as the other *Mycobacterium tuberculosis* phosphatase PtpB. This inhibitor represents a chemical tool that can be used in conjunction with the inhibitors described in Chapters 1-2 to further probe the role of PtpA and PtpB in tuberculosis infection, and to examine potential synergistic effects.

Chapter 4. The application of inhibitors developed in Chapters 1-3 to the pathogenic target *Staphylococcus aureus*, the causative agent of Staph infection, is described. Several of the inhibitors described in Chapter 1 were found to have activity versus *Staphylococcus aureus* bacteria, prompting further probing of structure-activity relationships. The synthesis of new analogs was realized by developing a new synthetic strategy to allow for rapid analog synthesis

and evaluation. The cellular target is postulated to be *Staphylococcus aureus* protein tyrosine phosphatases SaPtpA and SaPtpB, newly discovered enzymes which may play a role in pathogenesis. Compounds were evaluated directly in cell assays, and the mechanism of action of these compounds, which show activity in *Staphylococcus aureus* strains that are resistant to traditional beta-lactam antibiotics, is under investigation.

Fragment-Based Identification of Phosphatase Inhibitors

Table of Contents

Acknowledgements

First and foremost, I would like to thank my advisor, Professor Jonathan Ellman. His in-depth knowledge of all things science and his incredible attention to detail has always inspired and amazed me, and motivated me to succeed. I also appreciate his advice and guidance in my career search, and his nonstop desire to help his students excel. I wish him the best of luck in his east coast endeavors.

I would also like to thank Prof. Carolyn Bertozzi and Prof. Chris Chang, who were gracious enough to let me rotate through their labs as part of the Chemical Biology Program during my first year at Berkeley. Carolyn was a source of inspiration over the years; I admire her ability to seamlessly manage her many scientific commitments while running a research laboratory and spearheading valuable programs like the CBP. I am incredibly grateful for all of the advice and mentorship she has provided to me over the years. Chris has an amazing scientific mind, and is full of great ideas. I appreciate his enthusiasm for science, and am grateful to have been able to work on just a few of the projects in his lab. I learned a great deal of science in both rotations and valuable skills that enhanced my overall graduate career. Thanks also to my undergraduate advisor, Prof. Michael Carrasco, who encouraged me to apply to Berkeley, and for his continued support throughout graduate school.

My research rotation mentors also deserve a great deal of thanks. Andy Patterson was a great mentor, both during my rotation and once I joined the Ellman lab, and I (and my parents!) will certainly never forget his GRS introduction. He is the only person I know who can "sleep it off" at his desk after a crazy night out in Berkeley, and the only mentor who deserted me during my rotation to get married. Jenn "under" Prescher was also an amazing mentor, and I thank her for allowing me to invade her (already crowded) hood and bench space, which I dutifully shared with her and her "superstar" undergrad, Anderson "ALo" Lo. I also have to thank Nick Agard for his nonstop taunting and joking, which I know he meant in only the nicest of ways. His advice meant a great deal to me and helped me make a major decision in my graduate career. Thanks also to Evan Miller for helping me navigate through the Chang lab, despite the fact that I tried my best to set him on fire during my first week, and thanks to Aaron Albers for including me in one of the biggest "surprises" I've ever heard during graduate school!

I also have to thank the many Ellmanians who have influenced and helped me over the years. Jared Lewis was a great example of graduate school done right, and he was always willing to lend a hand. I'll never forget the day he left a permanent mark on the lab while nearly breaking his fist, or the days when I caught him blasting industrial techno in the early morning hours. Jeff "Macho" McMahon was always willing to listen, and made softball far more enjoyable for everyone involved. Katrien "stinks" Brak was a great colleague and friend, and I wish her and Nate the best of luck in their postdoc positions. Thanks also to Mike Gribble, who is still the only person I know to give a chemistry talk about benzodiazepines while on benzodiazepines. Melissa Leyva is my only "famous friend" and my goal in life is to one day follow her on Twitter too. I'll never forget the (many) coffee breaks we took to keep our energy up in lab and dish about the latest chemistry department gossip. Thanks also to younger members of the lab for making things interesting; Pete Marsden taught me more SoCal lingo than I care to know, Andy "AA" Tsai has taken on more group jobs than the whole lab combined, and Van Yotphan was my favorite Biotage buddy.

Thanks to all of my friends, inside and outside of lab, for keeping in touch and keeping me in tune with the real world. Thanks to Sarah Bell for the many lunches out and girls' nights

in – I wish her and Scott the best of luck in Michigan! I also enjoyed shopping trips with Kasuen and Kawai Mauldin, my only twin friends. I wish Kasuen and Clayton the best of luck with their new baby. Thanks to my friends on the east coast, whom I've never forgotten and am now thrilled to rejoin. Cathy Casey (now Edmonds) and Kate Rybicki (now Diehl) were gracious enough to include me in their "big day", which was a welcome reprieve from the graduate school life. I am so happy for them both, and am honored to still be considered a good friend.

Thanks especially to my family for their continued support. My Grandpa Dan has always been my biggest chemistry fan, and my parents have supported me even though the concept of going to school for five *more* years after undergrad was somewhat bewildering to them. I have thoroughly enjoyed their visits, including the many trips to wine country and SF and the fancy dinners at Chez Panisse, all of which could not have been done on a graduate student salary. Thanks also to my brother Kris who was (thankfully) smarter than me and decided to pursue a nonscientific career. I'm sure he'll be running the show in D.C. before we know it. Thanks to my Grandma Rawls and Aunt Carol for helping me through my undergraduate years, without which I never would have made it to Berkeley.

Last but not least, I want to thank Brian Pujanauski, who has been not only a fantastic partner, but also my best friend. I am sure I wouldn't have made it through the past five years without him. He always made me laugh, even when things weren't going well, and he made the best "popsicles" and "french toast" around. He also got me used to the idea of entropy, and I'm a messier person for it. For better or worse, he also convinced me that sports are not a complete waste of time (go Yankees!), and I've watched more football and baseball games in the past five years than I care to admit. I can't wait to start our new life together on the east coast!

Chapter 1. Fragment-Based Method for the Identification of Inhibitors of the *Mycobacterium tuberculosis* Phosphatase PtpB

Abstract: *In this chapter, the development of a novel fragment-based method for the identification of phosphatase inhibitors and its application to the Mycobacterium tuberculosis (Mtb) phosphatase PtpB is described. The method consists of three basic steps: (1) a library of O-aryl phosphates with diverse, low molecular weight O-aryl groups is screened to identify phosphatase substrates using a simple spectrophotometric-based assay, (2) the identified phosphate substrates are optimized by rapid analog synthesis and evaluation, and (3) the optimized substrates are converted to inhibitors by direct replacement of the phosphate with known phosphate isosteres. This method was used to identify submicromolar, low molecular weight isoxazole carboxylic acid inhibitors of PtpB, with our most potent inhibitor at* K_i *= 220 nM. This inhibitor was found to be selective over a panel of human phosphatases, in addition to the other secreted Mtb phosphatase PtpA. The majority of this work has been published (Soellner M. B.; Rawls, K. A.; Grundner, C.; Alber, T.; Ellman, J. A., J. Am. Chem. Soc.* ***2007****, 129, 9613-9615).*

Authorship

This work was conducted in collaboration with Dr. Matthew Soellner, a postdoctoral fellow in the Ellman laboratory. The *O*-aryl phosphate substrate library was made by Matt and myself. The focused biphenyl *O*-aryl phosphate substrate library was made by Matt and myself, and a select few substrates were made by Karen Dehnert. The inhibitor library was made by Matt and myself. All compounds were assayed by Matt and myself. Dr. Christoph Grundner provided enzyme for compound assays, and Dr. Jerome Hert carried out 2D connectivity analysis on commercially available phenol fragments.

Introduction

Phosphatases

Phosphatases are enzymes that catalyze the dephosphorylation of biomolecules. They work in conjunction with kinases, which catalyze the phosphorylation of biomolecules, to control a variety of essential cellular processes, including cell growth, differentiation, and the immune response.[1] There are two major classes of phosphatases: Ser/Thr phosphatases, which target phosphoserine (pSer) and phosphothreonine (pThr) residues in proteins, and Tyr phosphatases (PTPs), which primarily accommodate phosphotyrosine (pTyr) residues. The PTP family can be further divided into three subfamilies, including classical PTPs, which dephosphorylate only pTyr residues, dual-specificity PTPs, which can accommodate all of pTyr, pSer, and pThr residues as substrates, and low molecular weight PTPs (LMW-PTPs), which share no significant sequence homology with the other two PTP family members but accommodate only pTyr residues.[2] Ser/Thr phosphatases are metalloenzymes, while PTPs catalyze dephosphorylation through the formation of a covalent phosphocysteine intermediate (Figure 1.1),[1,3] and consequently the catalytic domains of Ser/Thr phosphatases differ completely from that of PTPs.

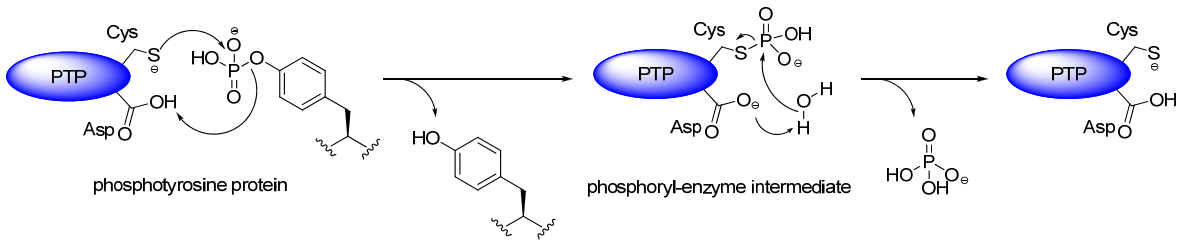

Figure 1.1. Protein Tyrosine Phosphatase (PTP) catalytic mechanism.

Abnormal phosphorylation is associated with a variety of diseases, including diabetes (PTP1B), cancer (Cdc25), autoimmune disease (CD45) and infectious diseases (Yersinia PTP, *Mycobacterium tuberculsosis* PtpA and PtpB, and *Staphylococcus aureus* SaPtpA and SaPtpB). Unfortunately, phosphatases have proven to be difficult drug targets, as demonstrated by the significant industrial efforts towards the development of inhibitors of PTP1B, an enzyme involved in insulin signaling.[4] Though many potent PTP1B inhibitors have been reported, only a few have advanced to clinical trials, and of those none has been approved for use in the clinic.[4a,5] For phosphatase inhibitors, the mono- or di-anionic nature of the pharmacophore required for phosphatase binding can hinder both cell permeability and oral bioavailability. Moreover,

because the catalytic domain in each family is highly conserved, achieving inhibitor selectivity poses an additional challenge.

Tuberculosis Phosphatases

Tuberculosis (TB) is a chronic, infectious disease caused by *Mycobacterium tuberculosis*. Each year, nearly 2 million deaths occur out of over 13 million active cases of TB,[6] and current treatment of drug-sensitive strains requires 6-9 months to fully eradicate the infection. This lengthy treatment time is due in large part to the requirement for current frontline treatments[7] to penetrate the unusually thick mycobacterial cell wall[8] in order to be effective. Compounding the problem is the development of drug-resistant strains, caused in large part by a lack of compliance with the lengthy treatment regimin.[6] New *Mtb* drugs that act on novel targets are needed to shorten treatment time and address the emergence of antibiotic resistance.

Mtb encodes two protein tyrosine phosphatases, PtpA and PtpB, that are promising new targets for TB drug development.[9] These PTPs are secreted by *Mtb*[10] into the cytosol of infected macrophages, precluding the need for inhibitors to enter bacterial cells.[11] Although genetic deletion of *ptpA* or *ptpB* does not affect *Mtb* growth in culture,[11-12] these deletions severely attenuate growth in sensitive infected macrophages.[11] These data suggest that the *Mtb* PTPs act on macrophage signaling pathways to promote *Mtb* survival in the infected host. Although not classical drug targets because they are not essential *in vitro*, targeting the secreted PTPs in the host macrophage circumvents two central resistance mechanisms of *Mtb*; *i.e.* poor drug permeability due to the *Mtb* cell wall,[8] and pump-mediated drug efflux.[13]

PtpB is a classical PTP that contains structural elements reminiscent of dual-specificity phosphatases.[14] In addition to a highly conserved PTP active site, the enzyme contains a unique two-helix lid that likely serves to protect the catalytic cysteine from oxidative inactivation. The first crystal structure of this enzyme was reported in 2005 (PDB ID 1YWF),[14] prompting our interest in the enzyme, and a co-crystal structure between PtpB and a nanomolar potency inhibitor has since been reported (PDB ID 2OZ5).[15] Although the biochemical role of PtpB still remains to be completely elucidated, recent studies have uncovered that PtpB assists TB bacterial survival and replication by preventing apoptosis of the macrophage host.[16]

Methods for Identifying Phosphatase Inhibitors

High Throughput Screening

In high throughput screening (HTS), collections of thousands of compounds are screened to identify leads with nanomolar to low micromolar affinity that can then be optimized to provide more potent inhibitors. HTS of compound libraries has been used to successfully identify drug-like molecules that interact with clinically relevant enzyme targets.[17] In the case of phosphatases, however, these screens have resulted in a high incidence of false positives. This may be due to a number of factors, including: (1) the tendency of phosphatase inhibitors to form micelles at high concentrations and thus nonspecifically inhibit enzyme function,[18] (2) the high reactivity of the active site Cys nucleophile,[19] and (3) irreversible oxidative inactivation of the catalytic Cys.[19-20] Wyeth has commented on this problem, reporting that in a HTS of PTP1B inhibitors, out of over 6,000 "hits" found in their initial screen, none were real inhibitors upon cross-validation.[20]

X-Ray and NMR Fragment Screens

Alternative fragment-based approaches have also been applied to phosphatases, wherein collections of low molecular weight compounds (typically with MW <300 Da) are screened to identify fragments with weak affinity that are subsequently optimized to potent lead compounds.[21] Fragment-based drug design relies on screening smaller compound libraries (typically, several thousand) to identify fragments with weak activity (micromolar to millimolar) that can then be combined and optimized to provide potent inhibitors.[21a] While fragment molecules can be screened against phosphatase targets in a high throughput manner, these screens typically are performed at higher concentrations than traditional inhibitor screens and result in an even greater prevalence of false positives. This has necessitated the use of more rigorous methods to directly observe fragment binding to phosphatase targets.

Two fragment approaches, NMR ("SAR by NMR") and X-ray based methods, have in particular been utilized to provide potent inhibitors of PTP1B.[22] In SAR by NMR approaches, changes in the protein NMR are detected upon fragment binding.[23] X-ray based screening methods, in which fragments are crystallized in the active site, have also been applied to phosphatase inhibitor development, often in tandem with NMR-based screens to confirm binding modes and further probe SAR.[21b,c] This method, like NMR-based methods, drastically reduces the number of false positives and provides detailed binding information, but crystal structures often take time to acquire and thus SAR determination by this method alone can be sluggish, especially for targets without previously published structural data.[24] Despite successful application to PTP1B inhibitor development, however, both X-ray and NMR-based methods are limited by the requirement for large amounts of protein and dedicated use of expensive instrumentation. Additionally, X-ray and NMR data cannot be obtained for all phosphatases, and thus alternative methods are desirable to address these issues and expand the chemical space explored by fragment discovery methods.[21a]

Substrate Activity Screening Method for Phosphatases

To identify phosphatase inhibitors, we have developed a novel substrate-based fragment identification method termed substrate activity screening (SAS).[25] This approach addresses two key challenges in fragment-based screening; *i.e.* the accurate and efficient identification of weak binding fragments, and finding an effective means for rapid optimization of the weak binding fragments into compounds with higher affinity. The SAS method and its application to the development of phosphatase inhibitors is outlined in Scheme 1.1. In the first step, a library of *O*-aryl phosphates with diverse, low molecular weight *O*-aryl groups is screened to identify phosphatase substrates using a simple spectrophotometric-based assay. In the second step, identified *O*-aryl phosphate substrates are optimized by rapid analog synthesis and evaluation. In the last step, the optimized substrates are converted to inhibitors by direct replacement of the phosphate with known phosphate isosteres.

There are several key features of the SAS method that distinguish it from established fragment-based screens. Most importantly, in the identification step, the false positives commonly seen in HTS methods are eliminated, since active site binding and catalysis are required for identification. In both the identification and optimization steps, an increase in signal is monitored, which is in contrast to HTS methods that monitor a decrease in signal, which is inherently more difficult to quantify. The assay also has the added benefit of signal

amplification due to catalytic substrate turnover. Optimization at the substrate stage affords easy access to a library of compounds for rapid SAR exploration, before development of more synthetically challenging inhibitors. Because the pharmacophore is incorporated in the last step, there is a high degree of flexibility in terms of the choice of phosphate mimetic.

Scheme 1.1. Substrate Activity Screening (SAS) method for the identification of phosphatase inhibitors

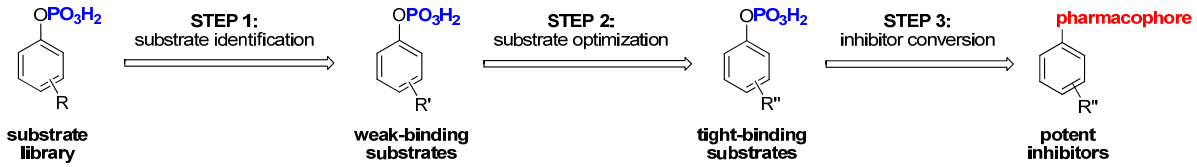

Development and Synthesis of the *O*-Aryl Phosphate Library

O-Aryl phosphate fragments were chosen as the framework for the initial substrate library, since these small compounds are the simplest mimic of natural phosphotyrosine substrates. These fragments (**1.2**) could also be synthesized in one step from commercially available phenols (**1.1**), which are abundant in number (>3000), using phosphorus oxychloride followed by aqueous workup (Scheme 1.2). Each phosphate was additionally purified via reversed-phase HPLC (RP-HPLC) to remove impurities that might otherwise inhibit enzyme function.

Scheme 1.2. Synthesis of *O*-aryl phosphates from phenol fragments

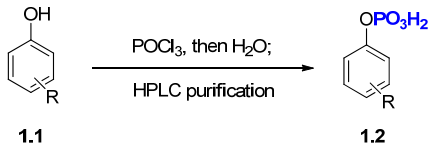

To maximize the diversity that was incorporated into the substrate library while also confining the number of total compounds to a practical limit, Dr. Jerome Hert (Prof. Brian Shoichet's group, UCSF) organized commercially available phenol fragments with a MW of <300 into structurally similar clusters based on their 2D connectivity using Pipeline Pilot (see Figure 1.2 for an example cluster).[26] One to two compounds were then selected from each cluster for incorporation into the library. Each of the selected phenols (120 compounds total) was converted to the corresponding *O*-aryl phosphate (vide infra), resulting in a fragment library with a wide range of functionality and substitution patterns (Table 1.1 and Table 1.2).

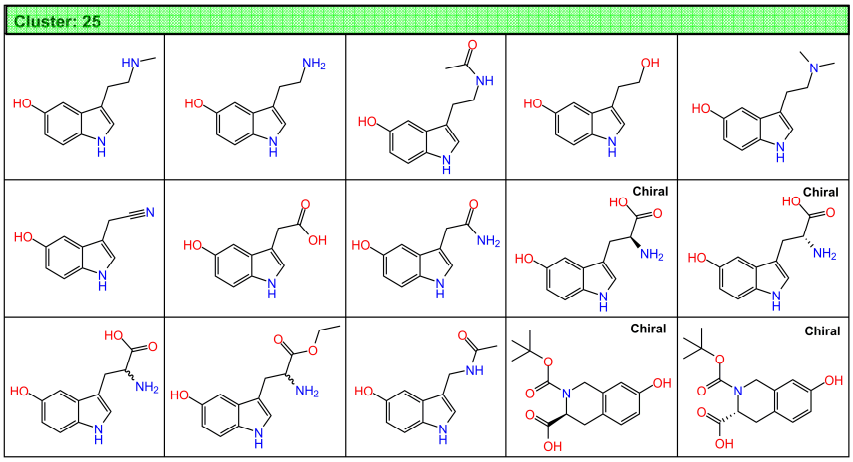

Figure 1.2. Example phenol cluster obtained from Pipeline Pilot.[26]

Table 1.1. Structure of *O*-aryl phosphate substrates that are singly substituted at the *ortho*, *meta*, or *para* position of the benzene ring

R	R	R	R	R	R
H	F	Cl			

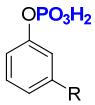

R	R	R	R	R	R
F	Cl				

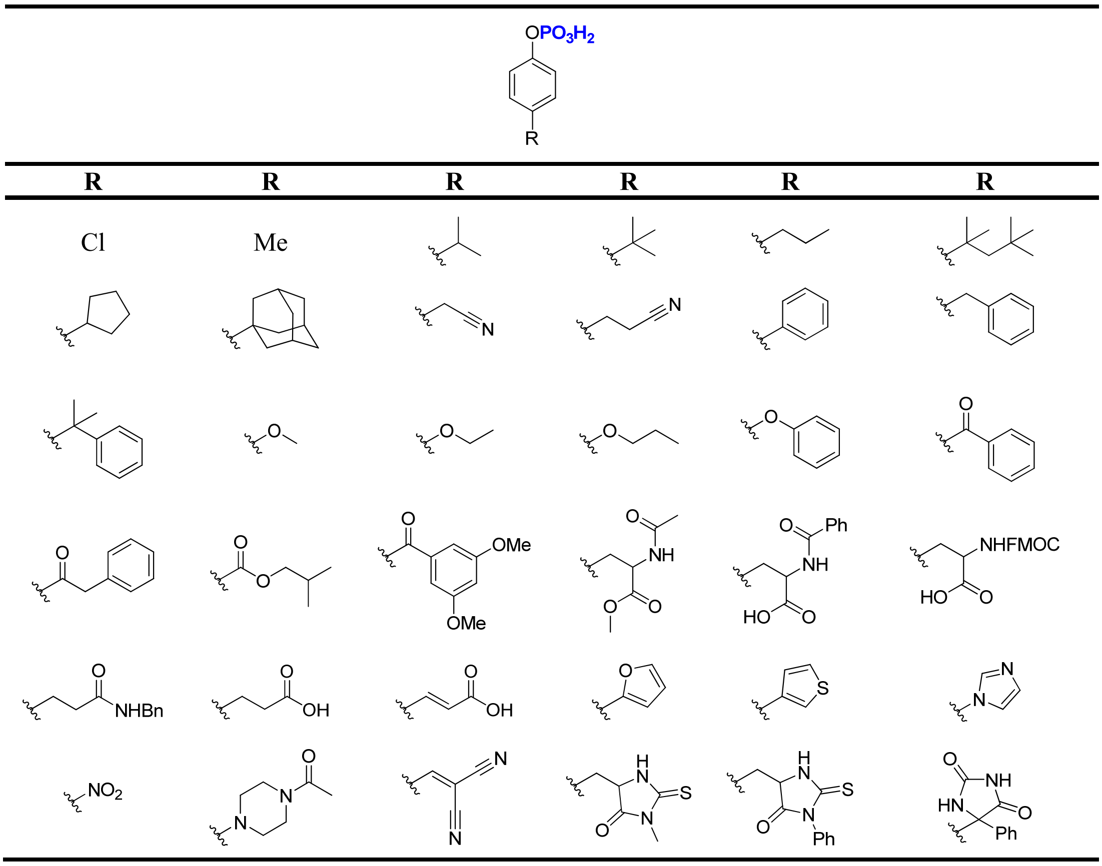

Table 1.2. Structure of *O*-aryl phosphate substrates multiply substituted on benzene

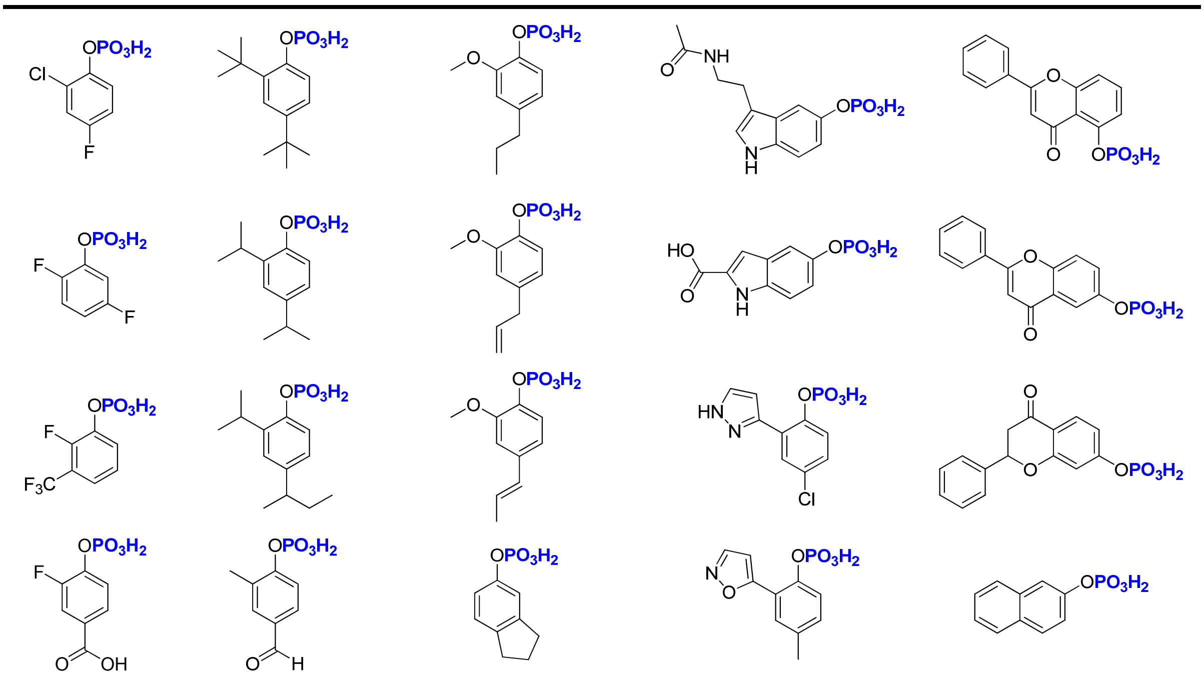

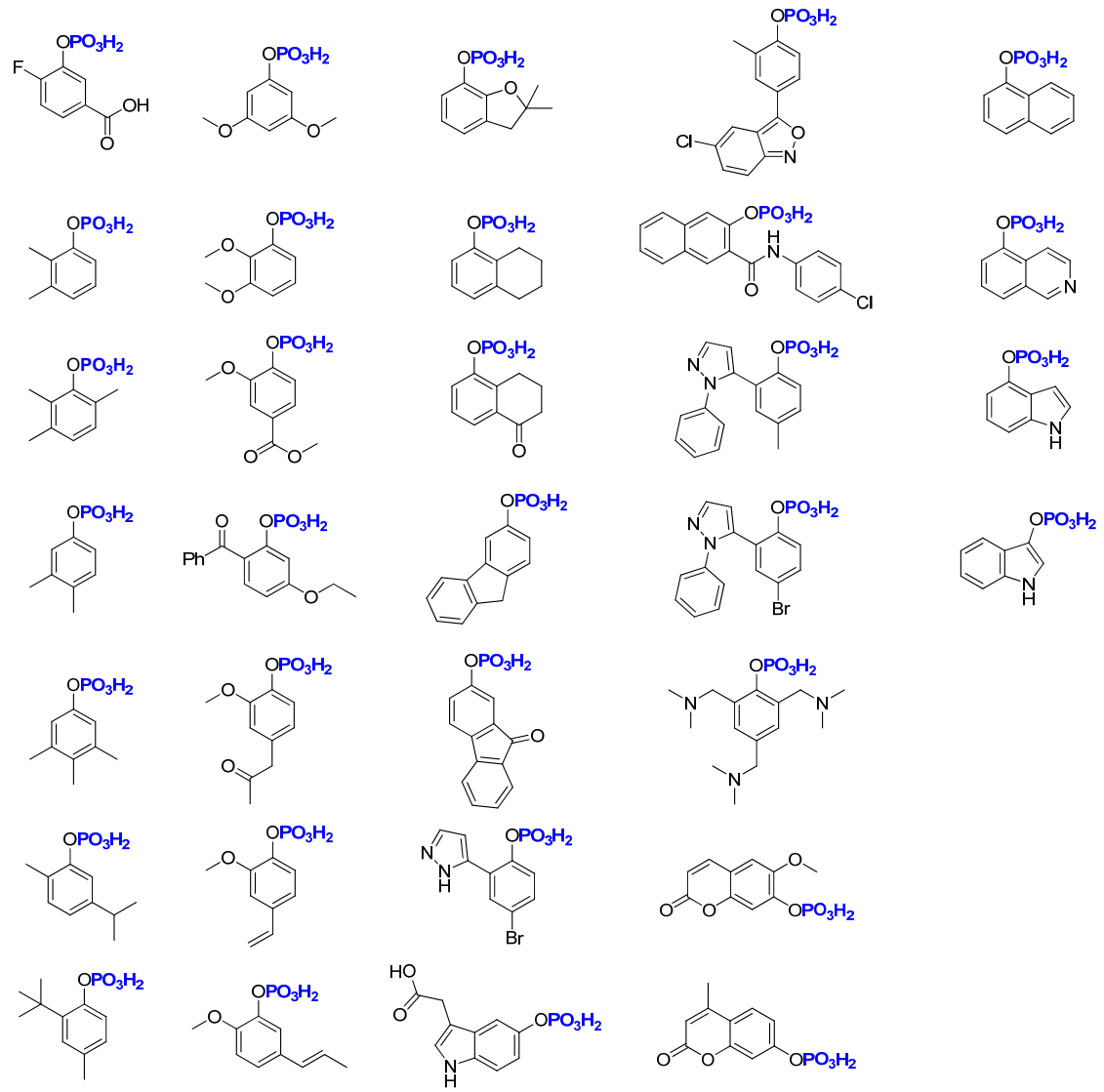

Identification of PtpB Substrates

Following synthesis, the *O*-aryl phosphate fragment library was screened against PtpB to identify compounds that were actively turned over by the enzyme. Because inorganic phosphate is not UV or fluorescence active, compounds were screened using a spectrophotometric coupled assay (Scheme 1.3).[27] This sensitive and high-throughput assay relies on the action of a secondary enzyme, purine nucleoside phosphorylase (PNP), which phosphorylates the ribose ring of nucleobase substrate **1.3**, releasing phosphorylated ribose **1.4** and UV-active purine base **1.5**. Substrate turnover results in a spectrophotometric shift in maximum absorbance from 330 nm for substrate **1.3** to 360 nm for product **1.5**, and thus this assay can be used to continuously monitor the kinetics of inorganic phosphate released by phosphatase-catalyzed hydrolysis of *O*-aryl phosphate substrates.

Scheme 1.3. Spectrophotometric method for detection of inorganic phosphate

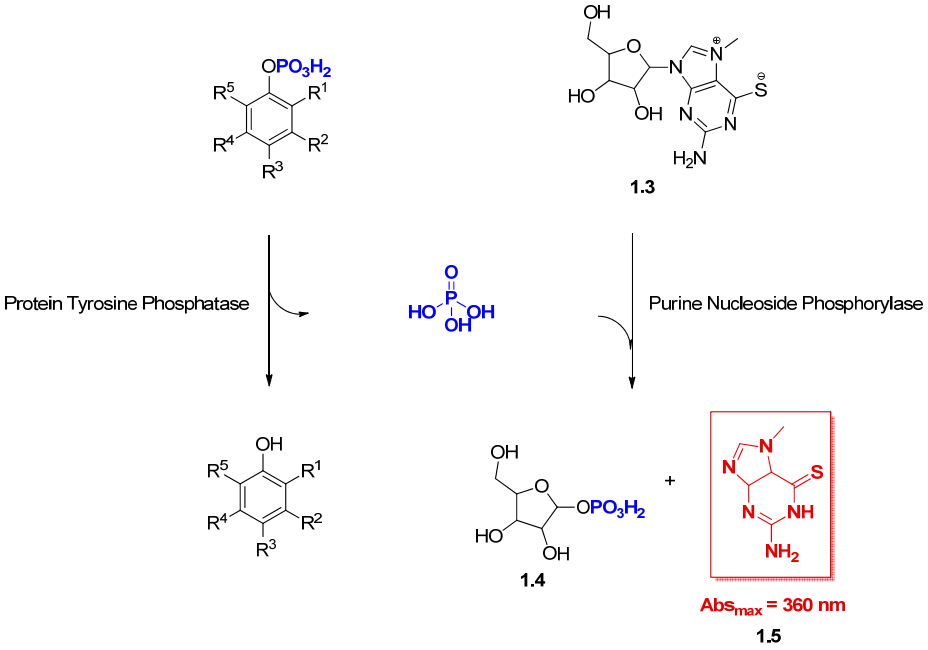

Importantly, the reaction catalyzed by PNP is essentially irreversible (K_{eq} >130), ensuring that read-out is entirely correlated with inorganic phosphate production.[27a] Additionally, this substrate-based assay eliminates the false positives commonly found in HTS, including false positives due to irreversible inactivation of the protein target, protein precipitation, and aggregation. Because inhibition of PNP by a phosphatase substrate could lead to false negatives in our assay, as a control, a subset of compounds was evaluated for inhibition of PNP. Gratifyingly, none of these compounds was found to inhibit PNP at all concentrations examined. Phosphatase inhibitors that incorporate stable phosphate mimetics are designed to be substrate and not transition state analogs,[28] and therefore substrate K_M values rather than k_{cat}/K_M values would be expected to best correlate with the K_i values of the corresponding inhibitors incorporating stable phosphate mimetics. For this reason, K_M values were determined from this assay and compared for structure-activity relationship (SAR) investigation.

Screening the initial library of *O*-aryl phosphates yielded several active substrates with various substitution patterns (see Figure 1.3 for selected hits, and Table 1.3 for complete substrate screen results). Compared to the benchmark compound phenyl phosphate (**1.6**), the acylated phosphotyrosine derivative **1.8**, which most closely mimics natural PTP substrates, surprisingly had much weaker activity than a variety of nonpeptidic scaffolds. Substitution at the *ortho*, *meta*, and *para* positions was well-tolerated, including several promising fragment substrates with greatly improved K_M values (**1.9**-**1.17**) relative to the standard assay substrate *p*-nitrophenyl phosphate (**1.7**). Initial optimization focused on the biphenyl scaffold **1.13**, because it is regarded as a "privileged structure" with drug-like properties,[29] and is additionally highly amenable to synthetic diversification.

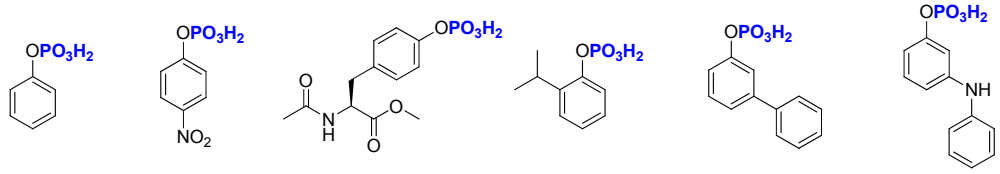

Substrate	1.6	1.7	1.8	1.9	1.10	1.11
K_M, μM (PtpB)	3439	1336	818	267	137	116
rel. k_{cat}/K_M	1.0	1.5	2.9	13.0	20.6	19.1

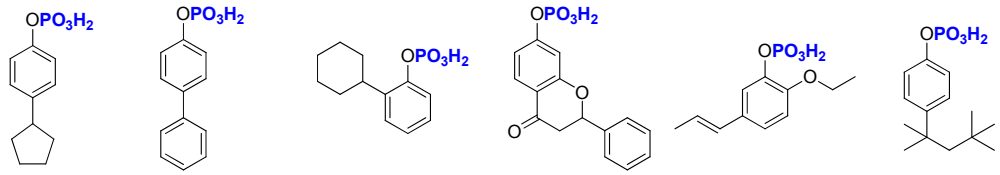

Substrate	1.12	1.13	1.14	1.15	1.16	1.17
K_M, μM (PtpB)	113	86	78	77	47	24
rel. k_{cat}/K_M	31.5	36.9	10.8	18.2	29.7	52.3

Figure 1.3. Selected initial substrate hits versus PtpB.

Table 1.3. Initial substrate screen versus PtpB (full panel)

#	Structure	K_M (μM)	#	Structure	K_M (μM)	#	Structure	K_M (μM)
1.17	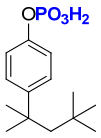	24.0	**1.50**	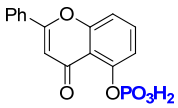	461	**1.89**	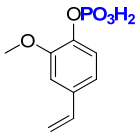	1880
1.18	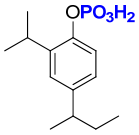	25.0	**1.51**	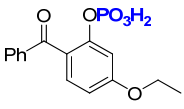	474	**1.90**	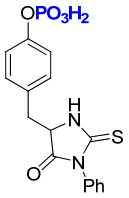	1907
1.19	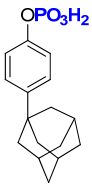	33.0	**1.52**	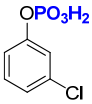	494	**1.91**	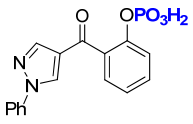	1962
1.16	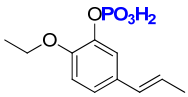	47.0	**1.53**	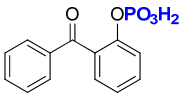	530	**1.92**	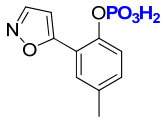	2298
1.20	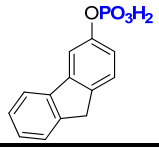	49.0	**1.54**	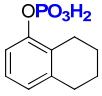	529	**1.93**	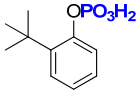	2403

1.21	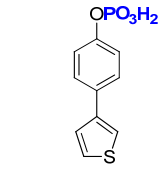	53.0	**1.55**	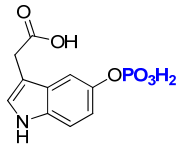	537	**1.94**	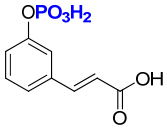	2401
1.22	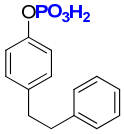	68.0	**1.56**	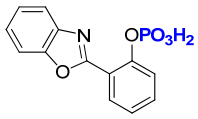	540	**1.95**	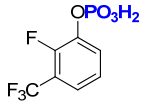	2393
1.15	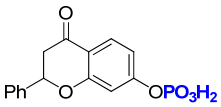	77.0	**1.57**	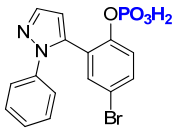	545	**1.96**	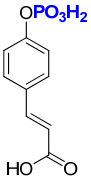	2430
1.14	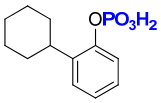	78.0	**1.58**	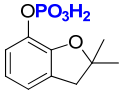	616	**1.97**	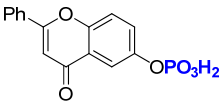	2568
1.23	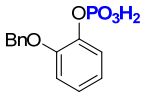	84.0	**1.59**	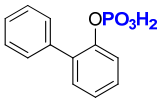	620	**1.98**	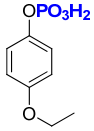	2647
1.24	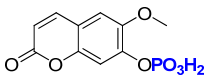	85.0	**1.60**	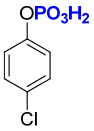	701	**1.99**	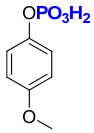	2901
1.13	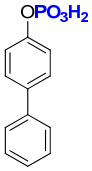	86.0	**1.61**	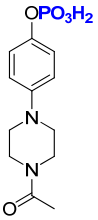	737	**1.100**	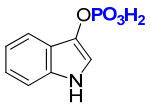	2996
1.12	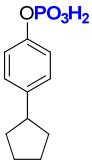	113	**1.62**	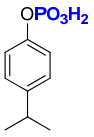	758	**1.101**	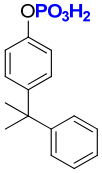	3417
1.25	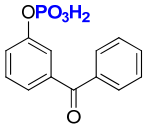	114	**1.63**	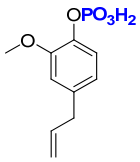	792	**1.6**		3439
1.26	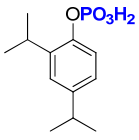	114	**1.64**	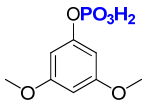	811	**1.102**	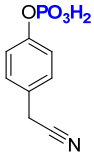	3715

1.11	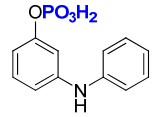	116	**1.8**	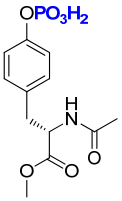	818	**1.103**	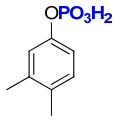	3862
1.27	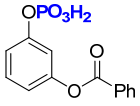	119	**1.65**	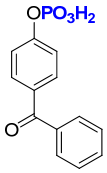	825	**1.104**	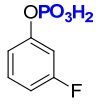	4149
1.28	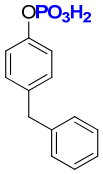	124	**1.66**	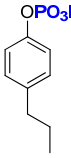	836	**1.105**	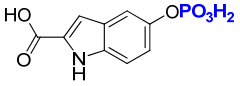	4643
1.10	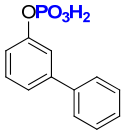	137	**1.67**	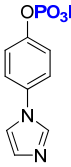	368	**1.106**	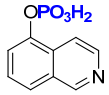	4818
1.29	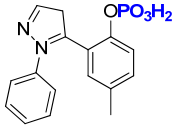	144	**1.68**	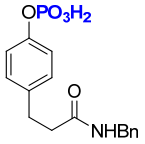	857	**1.107**	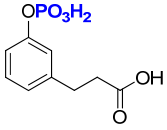	5269
1.30	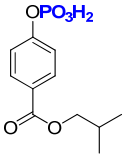	147	**1.69**	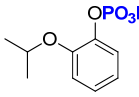	879	**1.108**	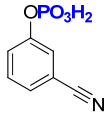	6762
1.31	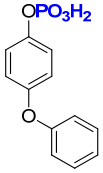	150	**1.70**	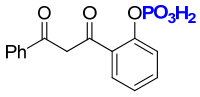	918	**1.109**	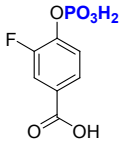	7046
1.32	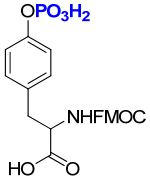	155	**1.71**	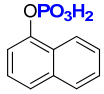	956	**1.110**	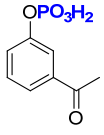	7643
1.33	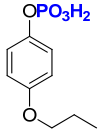	184	**1.72**	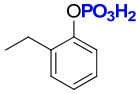	965	**1.111**	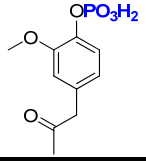	8089

1.34	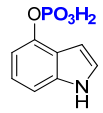	202	**1.73**	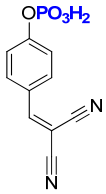	980	**1.112**	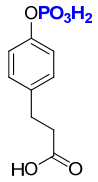	8580
1.35	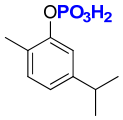	213	**1.74**	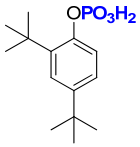	988	**1.113**	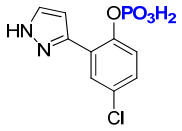	8605
1.36	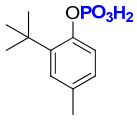	225	**1.75**	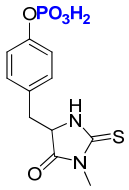	1103	**1.114**	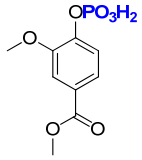	8788
1.9	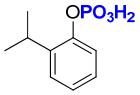	267	**1.76**	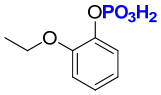	1106	**1.115**	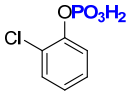	9373
1.37	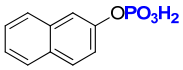	271	**1.77**	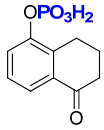	1127	**1.116**	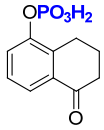	9504
1.38	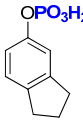	287	**1.78**	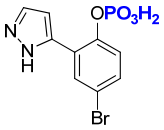	317	**1.117**	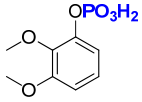	>9500
1.39	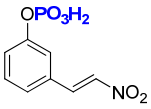	308	**1.79**	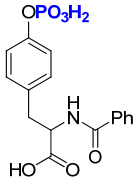	1239	**1.118**	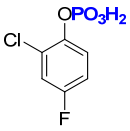	>9500
1.40	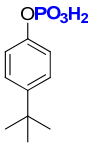	338	**1.80**	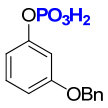	1311	**1.119**	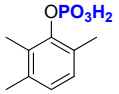	>9500
1.41	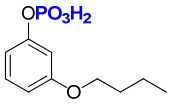	343	**1.7**	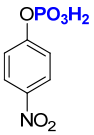	1336	**1.120**	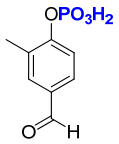	>9500
1.42	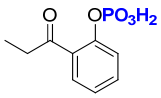	346	**1.81**	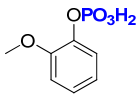	1342	**1.121**	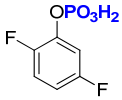	>9500

1.43	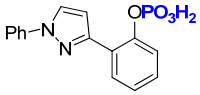	351	**1.82**	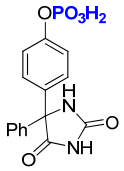	1580	**1.122**	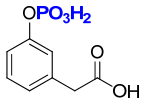	>9500
1.44	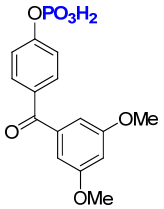	352	**1.83**	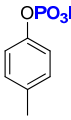	1634	**1.123**	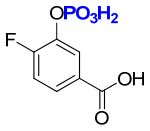	>9500
1.45	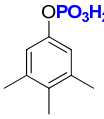	355	**1.84**	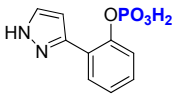	1648	**1.124**	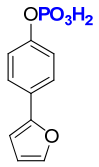	>9500
1.46	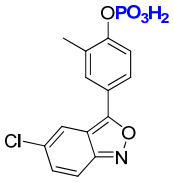	362	**1.85**	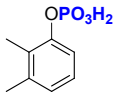	1758	**1.125**	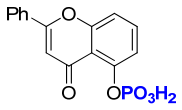	>9500
1.47	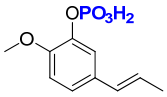	386	**1.86**	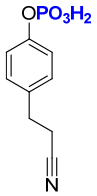	1752	**1.126**	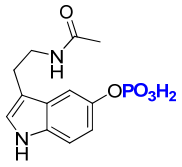	>9500
1.48	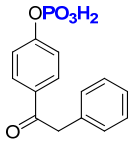	422	**1.87**	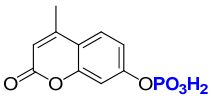	1823	**1.127**	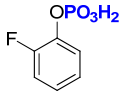	>9500
1.49	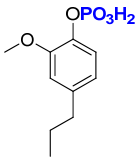	425	**1.88**	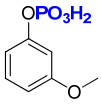	1840	**1.128**	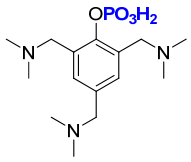	>9500

Substrate Optimization

With lead biphenyl substrate **1.13** identified, optimization was then carried out at the substrate stage, before conversion to more synthetically challenging inhibitors. For this step of the method, a small library of biphenyl phosphate substrates (25 compounds total) was synthesized and evaluated versus PtpB to investigate SAR and determine functionality necessary to improve turnover. Biphenyl substrates **1.132** were synthesized using standard Suzuki cross-coupling methods to couple the appropriate phenol (**1.129**) with a variety of aryl boronic acids (**1.130**) to afford the biphenyl alcohol (**1.131**), followed by treatment with phosphorous oxylchloride, water quench, and RP-HPLC purification (Scheme 1.4).

Scheme 1.4. Synthesis of biphenyl *O*-aryl phosphate substrates

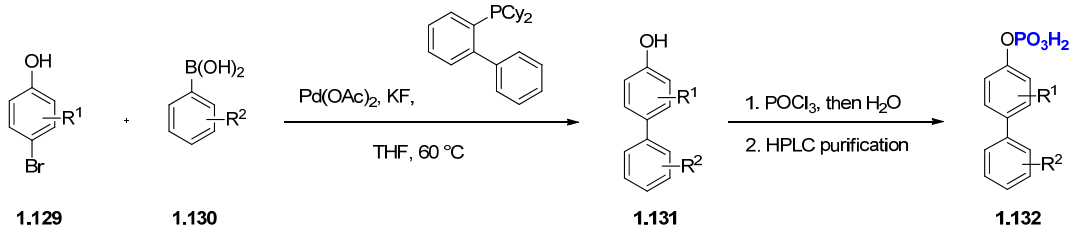

1.129 1.130 1.131 1.132

Following synthesis and purification, the focused biphenyl library was screened versus PtpB to investigate SAR (Table 1.4, see Figure 1.4 for K_M and k_{cat}/K_M values for selected substrates). Compared to the initial biphenyl lead substrate **1.13** (K_M = 86 μM), compounds **1.133**-**1.153** all were found to have improved turnover. Fluoro and trifluoromethyl substituents both proved beneficial, and in particular, the *p*-fluoro substituted derivative **1.146** conferred a ~2-fold decrease in K_M relative to biphenyl substrate **1.13**, while the *m*-trifluoromethyl substituted biphenyl phosphate **1.138** showed a >4-fold decrease in K_M. Gratifyingly, merging these two substituents provided substrate **1.135** with >6-fold improvement in K_M. Finally, the 2-isopropyl substituted substrate **1.153** was merged with biphenyl **1.138** to provide substrate **1.133** with >14-fold improved affinity versus **1.13**, as predicted from the initial fragment library (**1.9**, Figure 1.3). Because merged substrate **1.133** approached the limit of assay detection, further investigation of SAR at the substrate stage was halted in favor of conversion to inhibitors.

Table 1.4. Biphenyl substrate screen versus PtpB

#	Structure	K_M (μM)	#	Structure	K_M (μM)	#	Structure	K_M (μM)
1.13	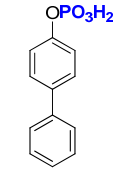	86.0	**1.141**	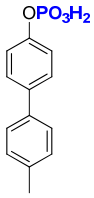	31.0	**1.150**	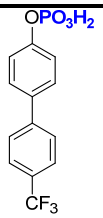	59.0
1.133	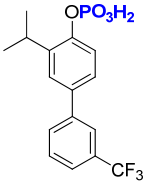	6.0	**1.142**	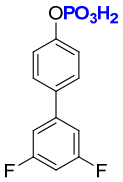	33.0	**1.151**	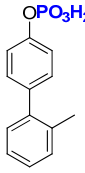	64.0
1.134	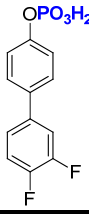	13.0	**1.143**	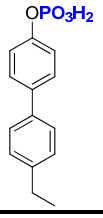	35.0	**1.152**	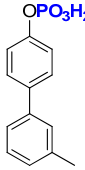	66.0

1.135	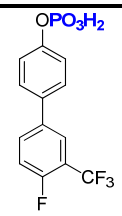	13.0	**1.144**	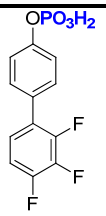	36.0	**1.153**	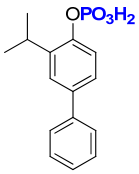	67.0
1.136	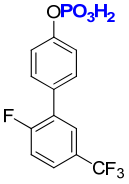	15.0	**1.145**	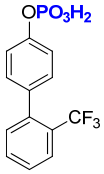	42.0	**1.154**	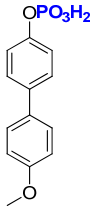	103
1.137	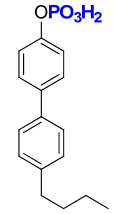	16.0	**1.146**	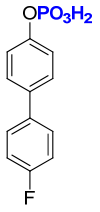	45.0	**1.155**	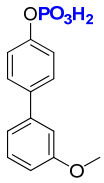	113
1.138	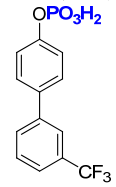	19.0	**1.147**	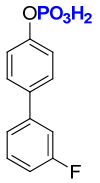	49.0	**1.156**	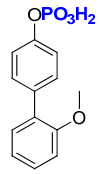	130
1.139	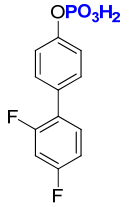	20.0	**1.148**	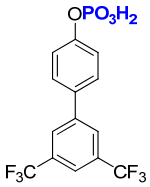	56.0	**1.157**	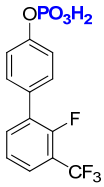	138
1.140	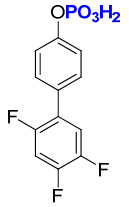	27.0	**1.149**	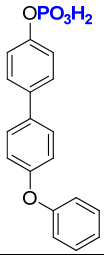	57.0			

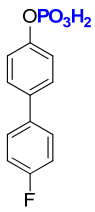
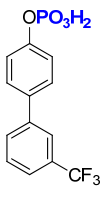
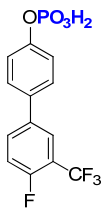
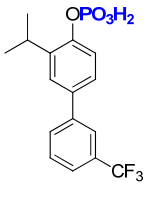

Substrate	**1.146**	**1.138**	**1.135**	**1.133**
K_M, μM (PtpB)	45	19	13	6.2
rel. k_{cat}/K_M	51.5	63.5	49.1	43.4

Figure 1.4. Complete kinetic data for selected biphenyl phosphate substrates.

Conversion of Substrates to Inhibitors

The final step of the SAS method involves conversion of substrates to inhibitors by replacement of the phosphate group with known, non-hydrolyzeable phosphate mimetics. Introducing the phosphate isostere at this later stage greatly facilitates optimization efforts because phosphate substrates are inherently more straightforward to prepare than the corresponding inhibitors. A variety of phosphate isosteres have been reported and could be introduced,[30] but many contain at least two acidic sites and lead to inhibitors with poor cellular permeability.[31] We therefore selected two promising monoacidic phosphate isosteres, the isothiazolidinone[32] and the isoxazole carboxylic acid,[33] which have been effectively used in inhibitors of PTP1B, a human phosphatase targeted for diabetes treatment, with good cell permeability and activity.

Isoxazole Carboxylic Acid Inhibitor Synthesis

Isoxazole carboxylic acid inhibitors were synthesized by modified literature procedures, beginning with Suzuki coupling between the appropriate 4-bromophenol (**1.158**)[34] and a variety of aryl boronic acids (**1.159**) to arrive at biphenyl phenols **1.160**. Triflation was then followed by Sonogashira coupling with trimethylsilyl acetylene,[35] and removal of the silyl group to afford **1.162**. Copper-mediated formal 1,3-dipolar cycloaddition with ethyl-2-chloro-2-(hydroximino)acetate was then followed by saponfication to give the desired isoxazole inhibitors **1.164**. This method was used to synthesize inhibitors **1.170-1.173** (Table 1.5), using 4-bromo-2-isopropylphenol, 4-bromo-2-cyclohexylphenol, or 4-bromophenol as starting materials.

Scheme 1.5. General method for the synthesis of isoxazole inhibitors

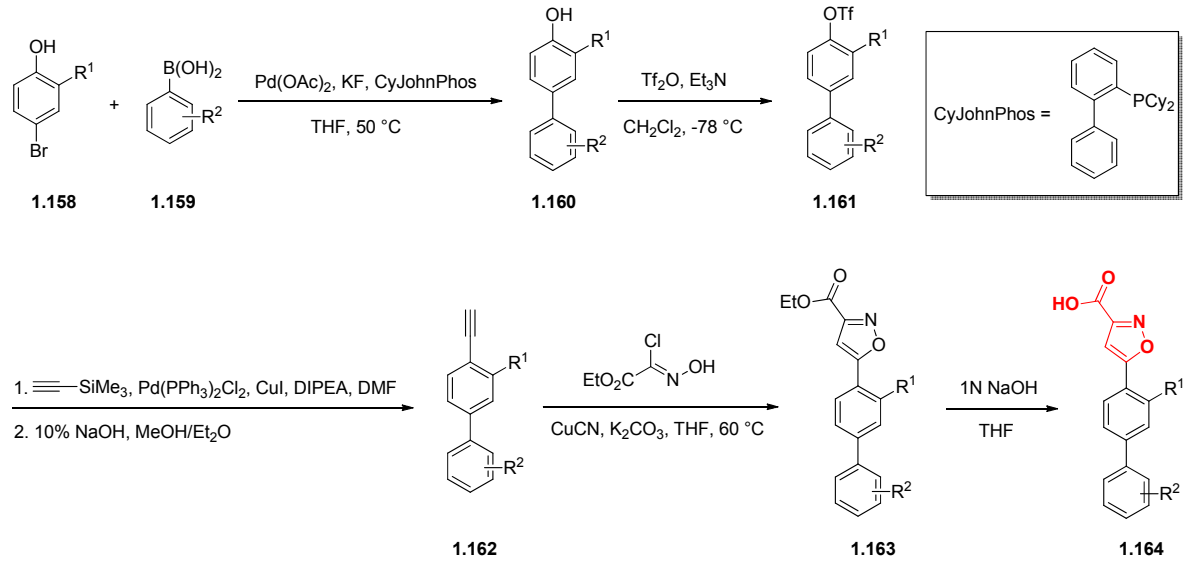

Isothiazolidinone Inhibitor Synthesis

Isothiazolidinone inhibitor synthesis began with construction of compound **1.165** as described previously.[36] Suzuki coupling of compound **1.165** with the appropriate aryl boronic

acid **1.166** then provided **1.167** (Scheme 1.6). This method was used to synthesize compound **1.169** (Table 1.5) for comparison to the isoxazole carboxylic acid analogs.

Scheme 1.6. General method for the synthesis of isothiazolidinone inhibitors

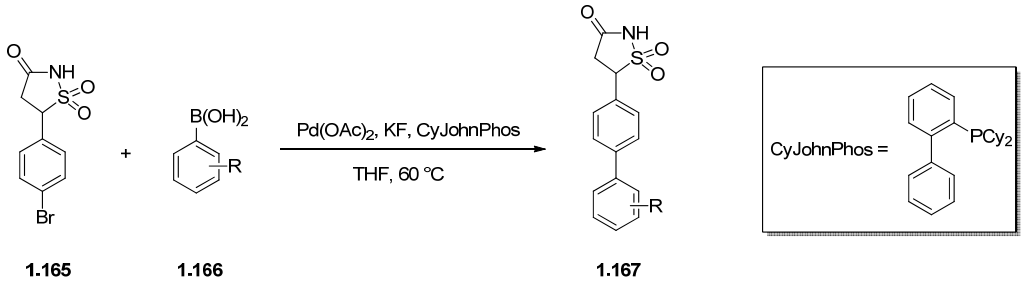

Inhibitor Assay Method

After preparation of a series of inhibitors, K_i values against PtpB were determined using a standard inhibition assay for phosphatases with *p*-nitrophenyl phosphate (pNPP) as the chromogenic substrate (Scheme 1.7).[37] In this competitive inhibition assay, the absorbance of **1.168** is continuously monitored at 410 nm as pNPP is turned over by the phosphatase of interest. The concentration of pNPP is held constant while the concentration of inhibitor is varied, resulting in sigmoidal dose-response curves from which K_i values can be determined. Assays were performed with 0.005% Triton X-100 detergent to prevent non-specific aggregation-based inhibition of the enzyme. Inhibition was found to be independent of both enzyme and detergent concentrations, indicating that inhibitors are binding productively in the active site rather than forming micelle aggregates.

Scheme 1.7. Assay method for PTP inhibitors

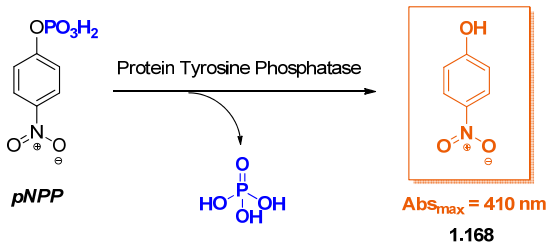

The results of the inhibitor screen versus PtpB are shown in Table 1.5. Isothiazolidinone **1.169** has a K_i of 8.8 μM as a racemic mixture, while isoxazole carboxylic acid **1.170** has a K_i of 2.5 μM. Due to the modest increase in potency and ease of synthesis compared to the isothiazolidinone, the isoxazole carboxylic acid isostere was initially chosen for the synthesis of additional inhibitor analogs. Addition of the isopropyl group at R^2, which was observed to be a favorable element for binding in substrate **1.9** as determined by K_M analysis, provided inhibitor **1.171** with a K_i of 850 nM. Notably, k_{cat}/K_M values for substrates **1.138** and **1.133** (63.5 and 43.4, respectively) would predict a loss of activity for inhibitor **1.171** as compared to **1.170** rather than the observed gain, which is consistent with the observation that phosphate mimetics are substrate and not transition state analogs (vide supra). Inhibitor **1.172** with a fluoro group at

R^3 was prepared based upon K_M SAR obtained from the small, focused biphenyl substrate library (Table 1.4) and showed further increased potency, with a K_i of 500 nM. Finally, replacement of the isopropyl group of **1.172** with a cyclohexyl group decreased the K_i to 220 nM (compound **1.173**), as predicted from K_M analysis of substrate **1.14** (Figure 1.3). The increase in potency observed for inhibitor **1.173** is best predicted by comparison of K_M values for corresponding substrates **1.9** and **1.14**, rather than k_{cat}/K_M values (13.0 and 10.8, respectively), which would predict a decrease in activity for replacing the *ortho* isopropyl group in inhibitor **1.172** with the *ortho* cyclohexyl group in **1.173**. The structure of compound **1.173** is also significant because the use of *ortho* alkyl groups has not been previously explored in phosphatase inhibitor development. Additionally, inhibitor **1.173** represents the most potent small molecule inhibitor of PtpB currently known in the literature.[25e,38]

Table 1.5. Inhibitor screen versus PtpB

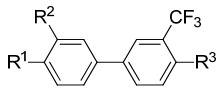

#	R^1	R^2	R^3	K_i (μM)[a]
1.169	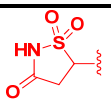	H	H	8.80 ± 0.11
1.170	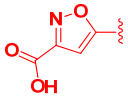	H	H	2.50 ± 0.26
1.171	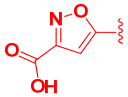		H	0.85 ± 0.09
1.172	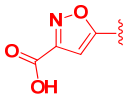		F	0.50 ± 0.02
1.173	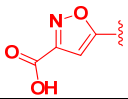		F	0.22 ± 0.03

[a]Compounds were assayed in duplicate, and repeated in triplicate.

Inhibitor Selectivity

Compound **1.173** was also evaluated against a panel of mycobacterial and human PTPs to test for selectivity (Table 1.6). Interfering with human phosphatase activity may have undesired side-effects and thus selectivity is desireable, and in some cases essential; T-cell PTP (TC-Ptp) knockout mice, for example, show severe side effects that ultimately cause lethality.[39] Human dual-specificity and classical tyrosine phosphatases such as VHR, TC-Ptp, CD45, and LAR are highly homologous and thus achieving selectivity for human phosphatase targets can be challenging. PtpB, on the other hand, is a mycobacterial target that has no directly related human homologue. Selectivity over human PTPs is therefore predicted to be attainable, and in fact inhibitor **1.173** was found to be highly selective over all human PTPs tested (Table 1.6). This compound was additionally selective over the other phosphatase expressed and secreted by

Mtb, PtpA. This is significant, since it provides a chemical tool for further exploring the biochemical role of PtpB without affecting the activity of PtpA.

Table 1.6. Selectivity panel for inhibitor **1.173**

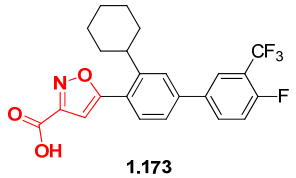

1.173

	Mtb PTPs		Human PTPs			
	PtpB	**PtpA**	**VHR**	**TC-Ptp**	**CD45**	**LAR**
K_i (μM)	0.22 ± 0.03	>50	>50	>50	7.70 ± 0.31	21.4 ± 0.78
Selectivity	--	>225	>225	>225	35	98

Conclusions

Potent and selective inhibitors of PtpB have been identified using the SAS method, a novel fragment-based approach for inhibitor identification. The envisioned three step SAS method was successfully applied beginning with *O*-aryl phosphate substrates, which are the simplest mimics of natural PTP substrates, as a starting point for fragment lead identification. Optimization at the substrate stage afforded quick and facile access to a library of compounds for SAR exploration, which were rapidly evaluated against PtpB using a continuous coupled assay, then converted to inhibitors by replacement of the phosphate group with known, non-hydrolyzeable phosphate mimetics. This led to the identification of inhibitors with novel structural motifs not previously used for phosphatase inhibitor development.

The most potent of these inhibitors (**1.173**, K_i = 220 nM) was shown to be highly selective over human and mycobacterial phosphatases, providing a chemical tool for further dissection of the biochemical role of PtpB. Moreover, compound **1.173** is nonpeptidic and low molecular weight (MW = 433 Da), leaving room for additional modifications to further improve potency, selectivity, and/or physicochemical properties. Structural characterization and biological evaluation of inhibitor **1.173** in TB-infected cells is currently in progress (in collaboration with Prof. Tom Alber at UCB, and Dr. Christoph Grundner at Seattle Biomedical Research Institute). This is the first successful demonstration of the SAS method for phosphatases, and builds upon previous applications of the method to protease targets.[25a-d] This method represents an important alternative to commonly used high throughput screening and fragment based methods, especially for phosphatases, which have proven to be particularly difficult drug targets.

Experimental

General Synthetic Methods

Unless otherwise noted, all reagents were obtained from commercial suppliers and used without further purification. Tetrahydrofuran (THF), dichloromethane (CH_2Cl_2), toluene, and

diethyl ether (Et_2O) were dried over alumina under a nitrogen atmosphere. Solvents used for reactions set up in a nitrogen-filled Braun inert atmosphere box, including THF and toluene, were additionally degassed with three consecutive freeze pump thaw cycles and stored over 3Å molecular sieves. Methanol was dried over calcium hydride under a nitrogen atmosphere. All reactions, unless otherwise stated, were performed under inert atmosphere using syringe, cannula, and Schlenk techniques, or set up in a nitrogen-filled Braun inert atmosphere box, with flame or oven-dried glassware. All ^{1}H, ^{13}C, ^{19}F, and ^{31}P NMR spectra were measured with a Bruker DRX-500, AVB-400, AVQ-400 or AV-300 spectrometer. NMR chemical shifts are reported in ppm relative to 1,2-difluorobenzene (-138.9) for ^{19}F NMR and trimethylphosphate (3.0) for ^{31}P NMR. Mass spectrometry (HRMS) was carried out by the University of California, Berkeley Mass Spectrometry Facility.

Synthesis of *O*-Aryl Phosphate Substrates

General Synthesis of O-*Aryl Phosphate Substrates (**1.2**) from Commercially Available Phenols*

The desired phenol (1.0 mmol) and CH_2Cl_2 (3 mL) were added to an 18 mm x 150 mm test tube. The resulting solution was cooled to 0 °C and pyridine (21 mmol) was added. Phosphorus oxychloride (10 mmol) in CH_2Cl_2 (3 mL) was then added dropwise with stirring at 0 °C over 10 minutes. The reaction mixture was then stirred for 2 h under N_2 at 0 °C. The reaction was quenched by dropwise addition of 1:1 acetone:water (6 mL). Volatile solvents were then removed under reduced pressure, and the resulting oil was dissolved in water (2 mL) and purified via preparative scale reversed-phase HPLC on a C18 column.

Analytical Data for Selected O-*Aryl Phosphates*

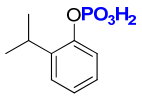

Phosphate 1.9. ^{1}H NMR (400 MHz, CD_3OD): δ 7.24-7.34 (m, 2H), 7.06-7.17 (m, 2H), 3.41 (sept, 1H), 1.22 (d, J = 6.9 Hz, 6H); ^{13}C NMR (126 MHz, CD_3OD): δ 150.24 (d, J = 6.8 Hz), 141.04 (d, J = 6.5 Hz), 127.81, 127.69, 126.00, 121.10, 121.08, 28.05, 23.52; ^{31}P NMR (162 MHz, CD_3OD): δ -5.25; mp 90-91 °C; HRMS-FAB (*m/z*): $[M + H]^+$ calcd for $C_9H_{14}O_4P$, 217.0624; found, 217.0635.

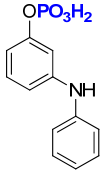

Phosphate 1.11. ^{1}H NMR (400 MHz, CD_3OD): δ 7.19-7.26 (m, 2H), 7.06-7.18 (m, 3H), 6.95 (s, 1H), 6.81-6.90 (m, 2H), 6.65 (d, J = 8.1 Hz, 1H); ^{13}C NMR (126 MHz, CD_3OD): δ 153.74 (d, J = 6.6 Hz), 147.01, 144.55, 131.04, 130.32, 121.97, 119.27, 114.16, 112.48 (d, J = 4.5 Hz), 109.48 (d, J = 4.9 Hz); ^{31}P NMR (162 MHz, CD_3OD): δ -5.18; mp 172-173 °C; HRMS-FAB (*m/z*): $[M + H]^+$ calcd for $C_{12}H_{12}NO_4P$, 265.0504; found, 265.0500.

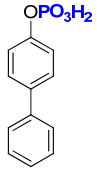

Phosphate 1.13. ^{1}H NMR (400 MHz, CD_3OD): δ 7.53-7.62 (m, 4H), 7.37-7.44 (m, 2H), 7.24-7.34 (m, 3H); ^{13}C NMR (126 MHz, CD_3OD): δ 150.54 (d, J = 6.7 Hz), 141.77, 139.11, 130.02, 129.25, 128.42, 128.00, 121.85 (d, J = 4.6 Hz); ^{31}P NMR (162 MHz, CD_3OD): δ -5.08; mp 178-180 °C; HRMS-FAB (*m/z*): $[M + H]^+$ calcd for $C_{12}H_{11}O_4P$, 250.0395; found, 250.0391.

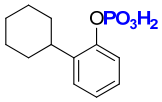

Phosphate 1.14. ^{1}H NMR (400 MHz, CD_3OD): δ 7.20-7.30 (m, 2H), 7.07-7.13 (m, 2H), 2.30-3.09 (m, 4H), 1.71-1.79 (m, 1H), 1.35-1.52 (m, 4H), 1.24-1.35 (m, 1H); ^{13}C NMR (126 MHz, CD_3OD): δ 150.28 (d, J = 7.0 Hz), 140.28 (d, J = 6.3 Hz), 128.47, 127.61, 125.94, 121.15 (d, J = 2.3 Hz), 38.37, 34.68, 28.18, 27.52; ^{31}P NMR (162 MHz, CD_3OD): δ -5.25; mp 143-145 °C; HRMS-FAB (*m/z*): $[M + H]^+$ calcd for $C_{12}H_{18}O_4P$, 257.0937; found, 257.0950.

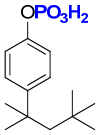

Phosphate 1.17. ^{1}H NMR (400 MHz, CD_3OD): δ 7.35 (d, J = 8.2 Hz, 2H), 7.11 (d, J = 8.1 Hz, 2H), 1.76 (s, 1H), 1.35 (s, 1H), 0.72 (s, 1H); ^{13}C NMR (126 MHz, CD_3OD): δ 150.57 (d, J = 6.7 Hz), 147.60, 128.46, 120.64 (d, J = 4.7 Hz), 58.02, 39.32, 33.29, 32.46, 32.43; ^{31}P NMR (162 MHz, CD_3OD): δ -5.05; mp 116-118 °C; HRMS-FAB (*m/z*): $[M + H]^+$ calcd for $C_{14}H_{24}O_4P$, 287.1407; found, 287.1418.

General Synthesis of Biphenyl O*-Aryl Phosphate Substrates*

The appropriate 4-bromophenol (1.0 mmol) was added to a flame-dried flask that was flushed with N_2. The required boronic acid (1.5 mmol) was then added, followed by potassium fluoride (174 mg, 3.00 mmol), palladium acetate (11.5 mg, 0.0500 mmol), 2-(dicyclohexylphosphino)biphenyl (35 mg, 0.10 mmol), and THF (4 mL). The flask was then sealed under a N_2 atmosphere and the reaction mixture was heated to 60 °C with stirring for 18 h. The reaction was then quenched by addition of H_2O (5 mL), and the crude product was extracted with EtOAc (4 × 10 mL), dried over anhydrous $MgSO_4$ (s), and filtered. The solvent was removed under reduced pressure to provide the desired biphenyl phenol. The resulting biphenyl phenol (1.0 mmol) and CH_2Cl_2 (3 mL) were then added to an 18 mm x 150 mm test tube. The resulting solution was cooled to 0 °C and pyridine (21 mmol) was added. Phosphorus oxychloride (10 mmol) in CH_2Cl_2 (3 mL) was then added dropwise with stirring at 0 °C over 10 minutes. After addition of phosphorus oxychloride, the reaction mixture was stirred for 2 h under N_2 at 0 °C. The reaction was then quenched by dropwise addition of 1:1 acetone:water (6 mL). Volatile solvents were then removed under reduced pressure, and the resulting oil was dissolved in water (2 mL) and purified via preparative scale reversed-phase HPLC on a C18 column.

Analytical Data for Selected Biphenyl O*-Aryl Phosphates*

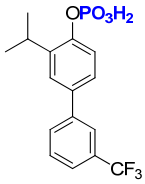

Biphenyl Phosphate 1.133. ^{1}H NMR (400 MHz, CD_3OD): δ 7.79-7.72 (m, 2H), 7.59-7.26 (m, 6H), 3.46 (sept, *J* = 7.0 Hz, 1H), 1.27 (d, *J* = 6.9 Hz, 6H); ^{19}F NMR (376 MHz, CD_3OD): δ -63.19; ^{31}P NMR (162 MHz, CD_3OD): δ -5.25; mp 202-203 °C; HRMS-FAB (*m/z*): $[M + H]^+$ calcd for $C_{16}H_{16}F_3O_4P$, 360.0738; found, 360.0744.

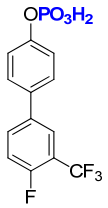

Biphenyl Phosphate 1.135. ^{1}H NMR (400 MHz, CD_3OD): δ 7.99-7.78 (m, 3H), 7.58 (m, 1H), 7.39-7.22 (m, 3H); ^{19}F NMR (376 MHz, CD_3OD): δ -62.095, -114.23; ^{31}P NMR (162 MHz, CD_3OD): δ -5.23; mp 190-191 °C; HRMS-FAB (*m/z*): $[M + H]^+$ calcd for $C_{13}H_9F_4O_4P$, 336.0175; found, 336.0173.

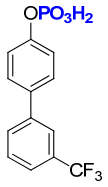

Biphenyl Phosphate 1.138. ^{1}H NMR (400 MHz, CD_3OD): δ 7.81-7.88 (m, 2H), 7.59-7.67 (m, 4H), 7.29-7.36 (m, 2H); ^{19}F NMR (376 MHz, CD_3OD): δ -63.34; ^{31}P NMR (162 MHz, CD_3OD): δ -5.06; mp 186-188 °C; HRMS-FAB (*m/z*): $[M + H]^+$ calcd for $C_{13}H_{10}F_3O_4P$, 318.0269; found, 318.0268.

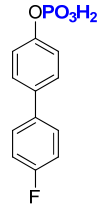

Biphenyl Phosphate 1.146. ^{1}H NMR (400 MHz, CD_3OD): δ 7.51-7.61 (m, 4H), 7.23-7.30 (m, 2H), 7.09-7.18 (m, 2H); ^{19}F NMR (376 MHz, CD_3OD): δ -117.38; ^{31}P NMR (162 MHz, CD_3OD): δ -5.05; mp 182-183 °C; HRMS-FAB (*m/z*): $[M + H]^+$ calcd for $C_{12}H_{10}FO_4P$, 268.0301; found, 268.0296.

Synthesis of Isothiazolidinone Inhibitor 1.169

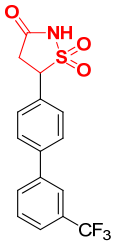

Compound 1.169. Compound **1.165** (20 mg, 0.070 mmol) was added to a flame-dried flask that was flushed with N_2. 3-(trifluoromethyl)-phenylboronic acid (27 mg, 0.14 mmol) was then added, followed by potassium fluoride (16 mg, 0.28 mmol), palladium acetate (2.3 mg, 0.0035 mmol), 2-(dicyclohexylphosphino)biphenyl (2.5 mg, 0.0070 mmol), and THF (0.5 mL). The flask was then sealed under a N_2 atmosphere and the reaction mixture was heated to 60 °C with stirring for 18 h. The reaction was then quenched by addition of H_2O (9 mL), and the crude product was extracted with EtOAc (4 × 10 mL), dried over anhydrous $MgSO_4$ (s), and filtered. The solvent was then removed under reduced pressure to provide crude **x.x**. The crude product was purified via reversed-phase chromatography (linear gradient of 5-100% CH_3CN in H_2O) to give compound **1.169** as a white solid (21 mg, 84% yield). **Analytical data.** ^{1}H NMR (400 MHz, $CDCl_3$): δ 7.93-7.91 (m, 2H), 7.72-7.66 (m, 4H), 7.58-7.55 (m, 2H), 5.51 (s, 1H), 4.87 (m, 1H), 3.24 (m, 2H); ^{19}F NMR (376 MHz, CD_3OD): δ -63.30; HRMS-FAB (*m/z*): $[M + H]^+$ calcd for $C_{16}H_{12}F_3NO_3S$, 355.0490; found, 355.0486.

Synthesis of Isoxazole Inhibitors 1.170-1.173

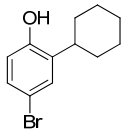

1.174

Compound 1.174. Compound **1.174** was synthesized from commercially available 2-cyclohexylphenol by modification of literature procedures.[34] 2-Cyclohexylphenol (25.0 g, 0.14 mol) was added to a flame-dried flask that was flushed with N_2 and dissolved in acetic acid (187 mL, 3.27 mol). A 48% solution of HBr in H_2O (95 mL, 0.84 mol) was then added, followed by dropwise addition of dimethylsulfoxide (95 mL, 1.34 mol) via addition funnel. The reaction was stirred at room temperature for 5 minutes, then quenched carefully, open to the atmosphere, with 10 N NaOH until neutral pH. The aqueous layer was extracted with Et_2O (3 x 300 mL), the organic layer washed with brine (1 x 600 mL), dried over anhydrous Na_2SO_4 (s) and filtered. The solvent was removed under reduced pressure to provide crude product which was purified using a silica gel plug, eluting with 6:1 hexanes:EtOAc, to give pure **1.174** as a beige oil (36.23 g, 99% yield). **Analytical data.** ^{1}H NMR (400 MHz, $CDCl_3$): δ 7.27 (s, 1H), 7.15 (dd, J = 8.5, 2.4 Hz, 1H), 6.63 (d, J = 8.5 Hz, 1H), 4.66 (bs, 1H), 2.81-2.71 (m, 1H), 1.91-1.71 (m, 5H), 1.50-1.30 (m, 5H); MS-ESI (*m/z*): $[M + H]^+$ calcd for $C_{12}H_{16}BrO$, 255.0306; found 254.0 and 256.0; HRMS-EI (*m/z*): $[M + H]^+$ calcd for $C_{12}H_{16}BrO$, 255.0301; found 255.0306.

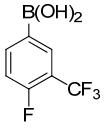

1.175

Compound 1.175. Compound **1.175** was synthesized by modified literature procedures.[40] Activated magnesium turnings (2.7 g, 0.11 mol) were added to a flame-dried round-bottomed flask under N_2 and covered with ether (16 mL). A speck of iodine was added to initiate the reaction, followed by dropwise addition of a solution of 5-bromo-2-fluorobenzotrifluoride (10.4 mL, 0.07 mol) in ether (74 mL) via addition funnel. The reaction mixture was heated periodically during addition in an oil bath set at 70 ºC to maintain reflux. In a separate flask, trimethoxyborane (44 mL, 0.38 mol) was dissolved in ether (326 mL) and cooled to -78 ºC. The grignard solution was transferred to the trimethoxyborane solution via cannula while maintaining the reaction temperature at -78 ºC. The reaction was stirred at -78 ºC and allowed to come to ambient temperature overnight. The reaction was quenched by addition of 3M HCl (250 mL) and stirred for 10 minutes at ambient temperature. The organic layer was separated, then the aqueous was extracted ether (2 x 250 mL). The combined organics were washed with water (2 x 500 mL), then the combined aqueous layer was filtered to provide a white solid that was recrystallized from H_2O (300 mL), hot filtering once to remove brown byproducts before cooling and filtering off the resulting white fluffy solid **1.175** (11.28 g, 74% yield). **Analytical data.** Analytical data was found to match that reported in the literature.[40b] ^{1}H NMR (400 MHz, CD_3OD): δ 8.15 – 7.85 (m, 2H), 7.42 – 7.16 (m, 1H); ^{19}F NMR (376 MHz, CD_3OD): δ -62.75 (d, J = 12.4 Hz), -115.14 (s).

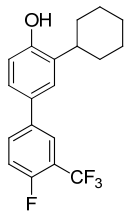

1.176

Compound 1.176. Compound **1.174** (2.47 g, 9.68 mmol) was added to a flame-dried flask that was flushed with N_2. 3-(trifluoromethyl)-4-fluoro-phenylboronic acid **1.175** (3.02 g, 14.5 mmol) was then added, followed by potassium fluoride (1.68 g, 29.0 mmol), palladium acetate (65 mg, 0.10 mmol), 2-(dicyclohexylphosphino)biphenyl (68 mg, 0.20 mmol), and THF (10 mL). The flask was then sealed under a N_2 atmosphere and the reaction mixture was heated to 60 °C with stirring for 18 h. The reaction was then quenched by addition of H_2O (15 mL), and the aqueous layer was extracted with EtOAc (4 × 50 mL). The organic layer was dried over anhydrous Na_2SO_4 (s) and filtered. The solvent was removed under reduced pressure to provide crude product which was purified via automated silica gel chromatography (linear gradient of 0-10% EtOAc in hexanes) to yield compound **1.176** as a white solid (2.95 g, 90% yield). **Analytical data.** ^{1}H NMR (400 MHz, $CDCl_3$): δ 7.79-7.69 (m, 2H), 7.38 (m, 1H), 7.32-7.17 (m, 2H), 6.90-6.67 (m, 1H), 4.83 (bs, 1H), 2.97-2.79 (m, 1H) 2.01-1.77 (m, 5H), 1.59-1.36 (m, 5H); ^{19}F NMR (376 MHz, $CDCl_3$): δ -60.51 (d, J = 15.1), -117.76 (m); mp 75-78 °C; HRMS-FAB (*m/z*): $[M + H]^+$ calcd for $C_{19}H_{18}F_4O$, 338.1294; found, 338.1290.

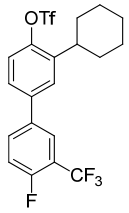

1.177

Compound 1.177. Compound **1.176** (3.40 g, 10.0 mmol) was added to a flask and dissolved in CH_2Cl_2 (100 mL) under N_2. The resulting solution was then cooled to -78 °C, and Et_3N was added, followed by dropwise addition of a solution of triflic anhydride (3.38 mL, 20.0 mmol) in CH_2Cl_2 (40 mL). Once addition of triflic anhydride was complete, the reaction was stirred for 1.5 h at -78 °C. The reaction was then quenched carefully with H_2O (100 mL) open to air. The aqueous layer was then extracted with CH_2Cl_2 (3 x 100 mL). The combined organics were then washed with aqueous saturated $NaHCO_3$ (1 × 300 mL), and brine (1 x 300 mL). The organic layer was dried over anhydrous Na_2SO_4 (s) and filtered. The solvent was removed under reduced pressure to provide crude **1.177**, which was purified via silica gel chromatography (hexanes) to yield compound **1.177** as a white solid (3.78 g, 80% yield). **Analytical data.** ^{1}H NMR (400 MHz, $CDCl_3$): δ 7.81-7.71 (m, 2H), 7.53 (m, 1H), 7.46-7.27 (m, 3H), 2.94 (m, 1H), 1.99-1.78 (m, 5H), 1.57-1.27 (m, 5H); ^{19}F NMR (376 MHz, $CDCl_3$): δ -60.60 (d, J = 12.6 Hz), -73.00, -115.30 (m); mp 69-72 °C; HRMS-FAB (*m/z*): $[M + H]^+$ calcd for $C_{20}H_{17}F_7O_3S$, 470.0787; found, 470.0782.

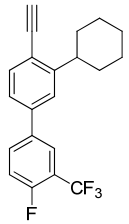

1.178

Compound 1.178. $Pd(PPh_3)_2Cl_2$ (400 mg, 0.600 mmol) and CuI (120 mg, 0.600 mmol) were added to a flask equipped with a stir bar and placed under a N_2 atmosphere. Compound **1.177** (2.80 g, 5.95 mmol) and diisopropyl ethyl amine (4.10 mL, 20.8 mmol) were added to a separate flask and dissolved in DMF (25 mL) under a N_2 atmosphere. This resulting solution was then added by cannula to the flask containing $Pd(PPh_3)_2Cl_2$ and CuI. Trimethylsilyl acetylene (1.3 g, 13 mmol) was then added by cannula as a solution in DMF (25 mL). The flask was then heated to 45 °C, and reaction mixture was stirred for 48 h. The reaction was quenched by addition of H_2O (25 mL) and hexanes (25 mL). The resulting suspension was then filtered, and the organic layer was separated. The organic layer was then dried over anhydrous $MgSO_4$ (s) and filtered, and the solvent was removed under reduced pressure to provide protected **1.178**. The silyl-protected **1.178** was dissolved in Et_2O (40 mL) and 10% (w/v) NaOH (20 mL) was added followed by MeOH (50 mL). The resulting reaction mixture was stirred for 18 h. The organic layer was then separated and washed with 10% (v/v) HCl (2 × 50 mL). The organic layer was dried over anhydrous $MgSO_4$ (s) and filtered, and the solvent was removed under reduced pressure to provide crude **1.178**. The product was purified via silica gel chromatography (hexanes) to yield compound **1.178** as a brown oil (1.26 g, 61% yield). **Analytical data.** ^{1}H NMR (400 MHz, $CDCl_3$): δ 7.83-7.74 (m, 2H), 7.60 (m, 1H), 7.43 (m, 1H), 7.37-7.29 (m, 2H), 3.38 (s, 1H), 3.18 (m, 1H), 2.02-1.80 (m, 5H), 1.65-1.40 (m, 5H); ^{19}F NMR (376 MHz, $CDCl_3$):

δ -60.54, -115.93 (m); mp 98-99 °C; HRMS-FAB (*m/z*): $[M + H]^+$ calcd for $C_{21}H_{18}F_4$, 346.1345; found, 346.1342.

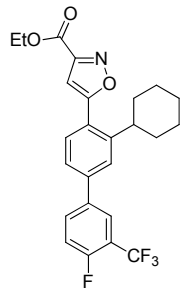

1.179

Compound 1.179. Compound **1.178** (693 mg, 2.00 mmol) and ethyl chlorooximidoacetate (303 mg, 2.00 mmol) were dissolved in *t*-BuOH (6 mL). To the resulting solution, H_2O (6 mL) was added, followed by sodium ascorbate (200 µL of a 1M solution), copper sulfate (5.4 mg in 200 µL), and finally $KHCO_3$ (866 mg, 8.66 mmol). The reaction mixture was stirred at 50 °C for 24 h at which point EtOAc (50 mL) and H_2O (50 mL) were added. The organic layer was then separated, dried over anhydrous $MgSO_4$ (s) and filtered, and the solvent was removed under reduced pressure to yield crude **1.179**. The product was purified by automated silica gel chromatography (linear gradient of 10 → 40% ethyl acetate in hexanes) to yield **1.179** as a white solid (73 mg, 8% yield). **Analytical data.** ^{1}H NMR (400 MHz, $CDCl_3$): δ 7.82-7.73 (m, 2 H), 7.64-7.43 (m, 3 H), 7.30 (m, 1 H), 6.79 (s, 1 H), 4.49 (q, J = 7.0 Hz, 2H), 3.41 (m, 1H), 1.94-1.73 (m, 5H), 1.46 (t, J = 6.9 Hz, 3H), 1.61-1.32 (m, 5H); ^{19}F NMR (376 MHz, $CDCl_3$): δ -60.72, -115.25 (m); mp 207-208 °C; HRMS-FAB (*m/z*): $[M + H]^+$ calcd for $C_{21}H_{18}F_4$, 461.1614; found, 461.1610.

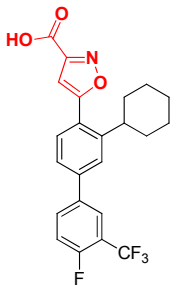

1.173

Compound 1.173. Compound **1.179** (20 mg, 0.040 mmol) was added to a flask and dissolved in THF (1 mL). NaOH (1N solution, 1 mL) was then added. The reaction mixture was stirred at ambient temperature for 2 h. The solvent was removed under reduced pressure, and EtOAc (10 mL) and HCl (2N, 10 mL) were added. The organic layer was separated and washed with 2N HCl (4 × 10 mL) and brine (1 × 10 mL). The organic layer was then dried over anhydrous $MgSO_4$ (s) and filtered, and the solvent was removed under reduced pressure to yield **1.173** as a white solid (16 mg, 94% yield). **Analytical data.** ^{1}H NMR (400 MHz, 1:1 $CDCl_3$:CD_3OD): δ 7.87-7.85 (m, 2H), 7.69-7.65 (m, 2H), 7.54-7.47 (m, 2H), 6.89 (s, 1H), 2.94 (m, 1H), 1.99-1.78 (m, 5H), 1.57-1.27 (m, 5H); ^{19}F NMR (376 MHz, $CDCl_3$): δ -62.02 (d, J = 13 Hz), -117.89 (m); mp 211-213 °C; HRMS-FAB (*m/z*): $[M + H]^+$ calcd for $C_{23}H_{19}F_4NO_3$, 433.1301; found, 433.1305.

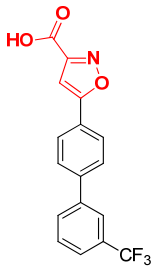

1.170

Compound 1.170. Isoxazole **1.170** was synthesized using procedures analogous to those reported for compound **1.173** (vide supra). **Analytical data.** ^{1}H NMR (400 MHz, 1:1 $CDCl_3$:CD_3OD): δ 7.99-7.96 (m, 2H), 7.90-7.87 (m, 2H), 7.80-7.78 (m, 2H), 7.68-7.65 (m, 2H), 7.10 (s, 1H); ^{19}F NMR (376 MHz, CD_3OD): δ -62.46; mp 194-195 °C; HRMS-FAB (*m/z*): $[M + H]^+$ calcd for $C_{17}H_{10}F_3NO_3$, 376.0613; found, 376.0610.

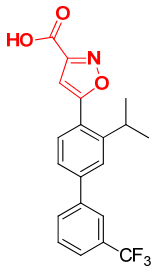

1.171

Compound 1.171. Isoxazole **1.171** was synthesized using procedures analogous to those reported for compound **1.173** (vide supra). **Analytical data.** ^{1}H NMR (400 MHz, 1:1 $CDCl_3$:CD_3OD): δ 7.80-7.77 (m, 2H), 7.62-7.48 (m, 5H), 6.81 (s, 1H), 3.32 (sept, J = 7.0 Hz, 1H), 1.29 (d, J = 6.9 Hz, 6H); ^{19}F NMR (376 MHz, CD_3OD): δ -63.17; mp 206-207 °C; HRMS-FAB (*m/z*): $[M + H]^+$ calcd for $C_{20}H_{16}F_3NO_3$, 375.1082; found, 375.1084.

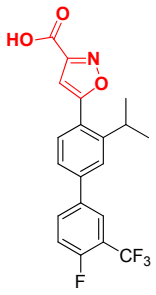

1.172

Compound 1.172. Isoxazole **1.172** was synthesized using procedures analogous to those reported for compound **1.173** (vide supra). **Analytical data.** ^{1}H NMR (400 MHz, 1:1 $CDCl_3$:CD_3OD): δ 7.87-7.85 (m, 2 H), 7.69-7.65 (m, 2 H), 7.54-7.47 (m, 2 H), 6.89 (s, 1H), 3.38 (sept, J = 7.0 Hz, 1H), 1.37 (d, J = 6.9 Hz, 6H); ^{19}F NMR (376 MHz, CD_3OD): δ -62.02 (d, J = 13 Hz), -117.89 (m); mp 204-205 °C; HRMS-FAB (*m/z*): $[M + H]^+$ calcd for $C_{20}H_{16}F_4NO_3$, 394.1066; found, 394.1058.

Assay Procedures

Determination of Substrate K_M

96-well plates were used with reaction volumes of 100 μL per well. 30 μL of water was added to each well, followed by 5 μL of buffer (stock solution: 1.0 M Tris-HCl, 20 mM $MgCl_2$, pH 7.5, 0.1% Triton X-100), 40 μL of 2-amino-6-mercapto-7-methylpurine riboside (MESG) solution (1 mM), and 10 μL of purine nucleotide phosphorylase (PNP) solution (0.01 U/mL). 5 μL of the appropriate substrate dilution, serially diluted 2.5-fold for a total of 8 different concentrations in DMSO, was then added to the wells. The coupled assay was started by addition of 10 μL of 1 μM PtpB, and the reaction progress was monitored at 360 nm at ambient temperature. The initial rate data collected was used for Michaelis-Menton kinetic analysis, where the K_M and relative k_{cat}/K_M could be obtained. K_M and V_{max} were determined using nonlinear regression analysis on the substrate-velocity data with the equation $v = V_{max}*[S]/(K_M+[S])$.

Determination of Inhibitor K_i

96-well plates were used to run K_i assays, with reaction volumes of 100 μL per well. 45 μL of water was added to each well, followed by 20 μL of sodium citrate buffer (stock solution: 100 mM sodium citrate, pH 6.2, 0.02% Triton X-100), 5 μL of 20 mM ethylenediamine tetraacetic acid (EDTA) stock solution, 5 μL of 20 mM DL-dithiothreitol (DTT) stock solution, and 10 μL of 1 μM PtpB stock solution. Then 5 μL of the appropriate inhibitor stock solutions, serially diluted 2-fold for a total of 10 different concentrations in DMSO, plus one blank well as a control (DMSO only) was added to the wells and the plate was incubated at room temperature for 5 minutes. The reaction was started by addition of 10 μL of 2 mM pNPP substrate stock, and reaction progress was monitored at 405 nm with continued incubation at ambient temperature. The initial rate data collected was used for the determination of K_i values. The kinetic values were obtained from nonlinear regression of substrate-velocity curves in the presence of various concentrations of inhibitor using the equation $v = V_{max}*[S]/(K_M((1+[I])/ K_i)+[S])$.

References

1. Barford, D., *et al. Annu. Rev. Biophys. Biomol. Struct.* **1998**, *27*, 133-164.
2. Ramponi, G.; Stefani, M. *International Journal of Biochemistry and Cell Biology* **1997**, *29*, 279-292.
3. Zhang, Z., *et al. Pharmacology and Therapeutics* **2002**, *93*, 307-317.
4. (a) Zhang, S.; Zhang, Z.-Y. *Drug Disc.Today* **2007**, *12*, 373-381; (b) Nichols, A., *et al. Drug Dev. Res.* **2006**, *67*, 559; (c) van Huijsduijnen, R., *et al. J. Med. Chem* **2004**, *47*, 4142-4146; (d) Zhang, Z.-Y.; Lee, S.-Y. *Expert Opin. Invest. Drugs* **2003**, *12*, 223-233.
5. Combs, A. P. *J. Med. Chem.* **2009**, *53*, 2333-2344.
6. World Health Organization, Global Tuberculosis Report 2009: http://www.who.int/tb/publications/global_report/2009/pdf/full_report.pdf
7. (a) For a review of currently used TB therapeutics and compounds in development, see: ; (b) Janin, Y. *Bioorg. Med. Chem. Lett.* **2007**, *15*, 2479-2513.
8. Brennan, P.; Nikaido, H. *Annu. Rev. Biochem.* **1995**, *64*, 29-63.
9. (a) Singh, R., *et al. Mol. Microbiol.* **2003**, *50*, 751-762; (b) Castandet, J., *et al. Res. Microbiol.* **2005**, *156*, 1005-1013; (c) Cowley, S. C., *et al. Res. Microbiol.* **2002**, *153*, 233-241; (d) Beresford, N., *et al. Biochem. J.* **2007**, *406*, 13-18; (e) Singh, R., *et al. Tuberculosis* **2005**, *85*, 325-335.
10. Koul, A., *et al. J. Bacteriol.* **2000**, *182*, 5425.
11. Bach, H., *et al. Cell Host Microbe* **2008**, *3*, 316-322.
12. Grundner, C., *et al. FEMS Microbiol. Lett.* **2008**, *287*, 181-184.
13. Louw, G., *et al. Antimicrob. Agents Chemother.* **2009**, *53*, 3181.
14. Grundner, C., *et al. Structure* **2005**, *13*, 1625-1634.
15. Grundner, C., *et al. Structure* **2007**, *15*, 499-509.
16. Zhou, B., *et al. Proc. Natl. Acad. Sci. U.S.A.* **2010**.
17. Walters, W.; Namchuk, M. *Nat. Rev. Drug Discovery* **2003**, *2*, 259-266.
18. Coan, K., *et al. J. Med. Chem* **2009**, *52*, 2067-2075.
19. Denu, J.; Dixon, J. *Curr. Opin. Chem. Biol.* **1998**, *2*, 633-641.
20. Moretto, A., *et al. Bioorg. Med. Chem. Lett.* **2006**, *14*, 2162-2177.
21. (a) Hajduk, P. J.; Greer, J. *Nat. Rev. Drug Discovery* **2007**, *6*, 211-219; (b) Carr, R. A. E., *et al. Drug Disc.Today* **2005**, *10*, 987-992; (c) Erlanson, D. A., *et al. J. Med. Chem.* **2004**, *47*, 3463-3482.
22. (a) Liu, G., *et al. J. Med. Chem.* **2003**, *46*, 4232-4235; (b) Szczepankiewicz, B., *et al. J. Am. Chem. Soc* **2003**, *125*, 4087-4096; (c) Shuker, S., *et al. Science* **1996**, *274*, 1531.
23. (a) Lepre, C., *et al. Chem. Rev* **2004**, *104*, 3641-3676; (b) Meyer, B.; Peters, T. *Angewandte Chemie-International Edition* **2003**, *42*, 864-891.
24. Hartshorn, M., *et al. J. Med. Chem* **2005**, *48*, 403-413.
25. (a) Inagaki, H., *et al. J. Med. Chem.* **2007**, *50*, 2693-2699; (b) Salisbury, C. M.; Ellman, J. A. *ChemBioChem* **2006**, *7*, 1034-1037; (c) Patterson, A. W., *et al. J. Med. Chem.* **2006**, *49*, 6298-6307; (d) Wood, W. J. L., *et al. J. Am. Chem. Soc.* **2005**, *127*, 15521-15527; (e) Soellner, M. B., *et al. J. Am. Chem. Soc.* **2007**, *129*, 9613-9615.
26. Developed and distributed by SciTegic, C. D., Suite 401, San Diego, CA 92123-1365; http://www.scitegic.com.

27. (a) Webb, M. R. *Proc. Natl. Acad. Sci. U. S. A.* **1992**, *89*, 4884-7; (b) Assay kit containing necessary reagents was purchased from Invitrogen: http://www.invitrogen.com/site/us/en/home.html
28. (a) Valizadeh, M.*, et al. Arch. Biochem. Biophys.* **2004**, *424*, 154-162; (b) Iyer, S.*, et al. Bioorg. Med. Chem. Lett.* **2004**, *14*, 5931-5935; (c) Hiriyanna, K. T.*, et al. Anal. Biochem.* **1994**, *223*, 51-58; (d) Lazarus, R.*, et al. Arch. Biochem. Biophys.* **1979**, *197*, 218-225; (e) Hussain, M.*, et al. Bioorg. Med. Chem. Lett.* **2008**, *16*, 6764-6777.
29. (a) Horton, D. A.*, et al. Chem. Rev.* **2003**, *103*, 893-930; (b) Hajduk, P. J.*, et al. J. Med. Chem.* **2000**, *43*, 3443-3447.
30. (a) Rye, C. S.; Baell, J. B. *Curr. Med. Chem.* **2005**, *12*, 3127-3141; (b) Zhang, Z.-Y. *Annu. Rev. Pharmacol. Toxicol.* **2002**, *42*, 209-234; (c) Kotoris, C. C.*, et al. Bioorg. Med. Chem. Lett.* **1998**, *8*, 3275-3280.
31. Hu, X. *Bioorg. Med. Chem. Lett.* **2006**, *16*, 6321-6327.
32. (a) Sparks, R. B.*, et al. Bioorg. Med. Chem. Lett.* **2007**, *17*, 736-740; (b) Combs Andrew, P.*, et al. Org. Lett.* **2007**, *9*, 1279-82; (c) Yue, E. W.*, et al. Bioorg. Med. Chem. Lett.* **2006**, *14*, 5833-5849; (d) Combs, A. P.*, et al. J. Med. Chem.* **2006**, *49*, 3774-3789; (e) Ala, P. J.*, et al. J. Biol. Chem.* **2006**, *281*, 32784-32795; (f) Ala, P. J.*, et al. J. Biol. Chem.* **2006**, *281*, 38013-38021; (g) Combs, A. P.*, et al. J. Med. Chem.* **2005**, *48*, 6544-6548.
33. Liu, G.*, et al. J. Med. Chem* **2003**, *46*, 4232-4235.
34. Klarmann, E.*, et al. J. Am. Chem. Soc.* **1933**, *55*, 4657-4662.
35. (a) Hosokawa, S.*, et al. Tetrahedron Lett.* **2007**, *48*, 7305-7308; (b) Takemura, I.*, et al. Tetrahedron Lett.* **2006**, *47*, 6673-6676; (c) Zbinden, K.*, et al. Bioorg. Med. Chem. Lett.* **2005**, *15*, 5344-5352.
36. Crawley, M.*, et al. Org. Lett* **2005**, *7*, 5067-5069.
37. Montalibet, J.*, et al. Methods* **2005**, *35*, 2-8.
38. (a) Noeren-Mueller, A.*, et al. Angew. Chem., Int. Ed. Engl.* **2008**, *47*, 5973-5977; (b) Correa, I. R., Jr.*, et al. Chem.--Asian J.* **2007**, *2*, 1109-1126.
39. Tiganis, T.; Bennett, A. *Biochem. J.* **2007**, *402*, 1.
40. (a) Rosen, B. M.*, et al. J. Am. Chem. Soc.* **2009**, *131*, 17500-17521; (b) Liaw, B. R.*, et al. Polymer* **2007**, *48*, 7087-7097.

Chapter 2. Design and Synthesis of New Inhibitor Analogs for the *Mycobacterium tuberculosis* Phosphatase PtpB

Abstract: *In this chapter, the design and synthesis of new inhibitor analogs for the Mycobacterium tuberculosis (Mtb) phosphatase PtpB is described. Analogs were synthesized by replacement of the isoxazole phosphate mimetic described in Chapter 1 with other common and effective phosphate mimetics, namely the isothiazolidinone (IZD) and difluoromethylphosphonic acid (DFMP). The basic scaffold of the inhibitor was identified from structure-activity relationships established for the isoxazole inhibitor, while the phosphate mimetics were chosen based on their proven cell permeability and activity when incorporated into previously reported inhibitors for the phosphatase PTP1B. The inhibitory activity of each compound was evaluated, and the full panel is currently undergoing testing in TB-infected macrophages.*

Authorship

This work was conducted in collaboration with Dr. Christoph Grundner, who provided enzyme for inhibitor assays and is conducting all cell-based assays.

Introduction

Mycobacterium tuberculosis (*Mtb*) PtpB is a secreted virulence factor that functions within human macrophages, and has been shown to interfere with host macrophage apoptosis as a mechanism of survival in the host.[1] PtpB is attractive as a therapeutic target due to its localization outside of the unusually thick mycobacterial cell wall, which is difficult to penetrate and leads to long treatment times for tuberculosis (TB). In Chapter 1, the development of isoxazole carboxylic acid inhibitor **1.173** for PtpB was described, using the substrate activity screening (SAS) method, a novel fragment-based approach for the identification of phosphatase inhibitors. Initial screening of the *O*-aryl phosphate substrate library described in Chapter 1 revealed that *ortho* substituents are preferred for optimal PtpB binding, with the cyclohexyl group providing the most favorable enzyme interactions. Isoxazole inhibitor **1.173** was found to be the most potent inhibitor of PtpB, with a K_i of 220 nM (Figure 2.1).[2]

In order to compare binding affinity and cell activity, we desired a route to analogous inhibitors **2.1** and **2.2** incorporating other commonly used phosphate mimetics. A variety of phosphate isosteres have been reported and could be introduced in place of the isoxazole,[3] but many contain at least two acidic sites and lead to inhibitors with poor cellular permeability.[4] We therefore chose two phosphate mimetics that have been effectively used in inhibitors of PTP1B, a human phosphatase targeted for diabetes treatment, with good cell permeability and activity, including the isothiazolidinone (IZD) and difluoromethylphosphonic acid (DFMP) (Figure 2.1). The monoanionic IZD[5] phosphate mimetic was developed by Incyte through rational structure-based design,[5g] while the DFMP pharmacophore is a commonly used phosphate mimetic that has been investigated extensively in the literature.[6] Despite being dianionic, the DFMP isostere has recently been shown by Merck to be cell permeable and orally bioavailable in animals when incorporated into nonpeptidic inhibitors of PTP1B.[7]

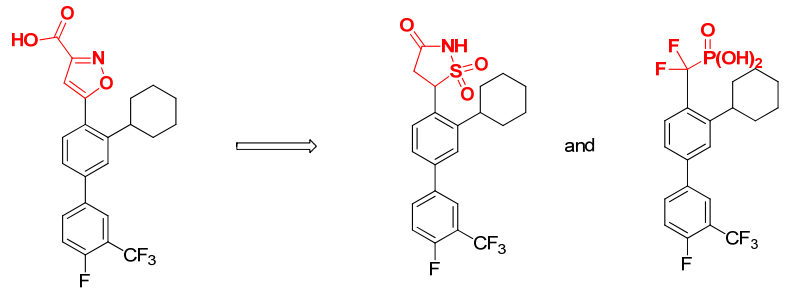

Figure 2.1. Inhibitor analogs of isoxazole carboxylic acid **1.173** (Chapter 1).

Isothiazolidinone Inhibitor Analog

Isothiazolidinone Inhibitor Synthesis

Several syntheses have been reported for the IZD isostere,[5a,5c-e] with the most recent providing access to each enantiomer of the final inhibitor,[5b] albeit with the use of chiral preparatory chromatography. Due to considerable steric interactions introduced by the cyclohexyl group positioned *ortho* to the isostere, the synthesis of IZD inhibitor **2.1** poses a significant challenge. The racemic synthesis of this compound begins with construction of heterocycle **2.6** (Scheme 2.1) using modified literature procedures.[5c,8] Commercially available carboxylic acid **2.3** is first coupled with *tert*-butyl amine to afford amide **2.4**. The resulting amide is then cyclized with sulfuryl chloride to afford heterocycle **2.5**, which is then elaborated to the final racemic coupling partner **2.6** via ruthenium-catalyzed oxidation.

Scheme 2.1. Synthesis of heterocycle **2.6**

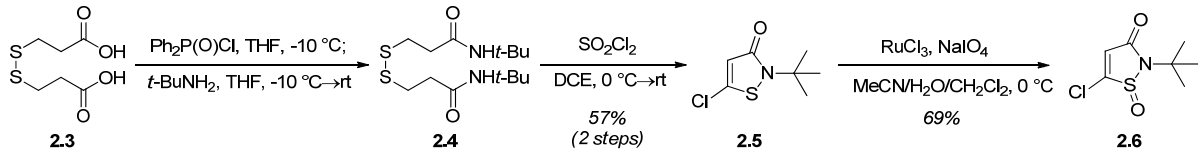

Synthesis of boronic ester **2.12** for coupling with heterocycle **2.6** begins with quantitative bromination of *o*-cyclohexyl phenol **2.7**, followed by Suzuki coupling with 4-fluoro-3-trifluoromethyl boronic acid **2.9** to afford biphenyl compound **2.10** (Scheme 2.2). Treatment with triflic anhydride under basic conditions then affords triflate **2.11**, which can be coupled with bis(pinacolato)diboron to provide boronic ester **2.12**.[9] This coupling step required significant optimization due to the presence of the sterically encumbered *ortho* cyclohexyl group, which has not been previously reported as a partner in Suzuki couplings.

Scheme 2.2. Synthesis of boronic ester **2.12**

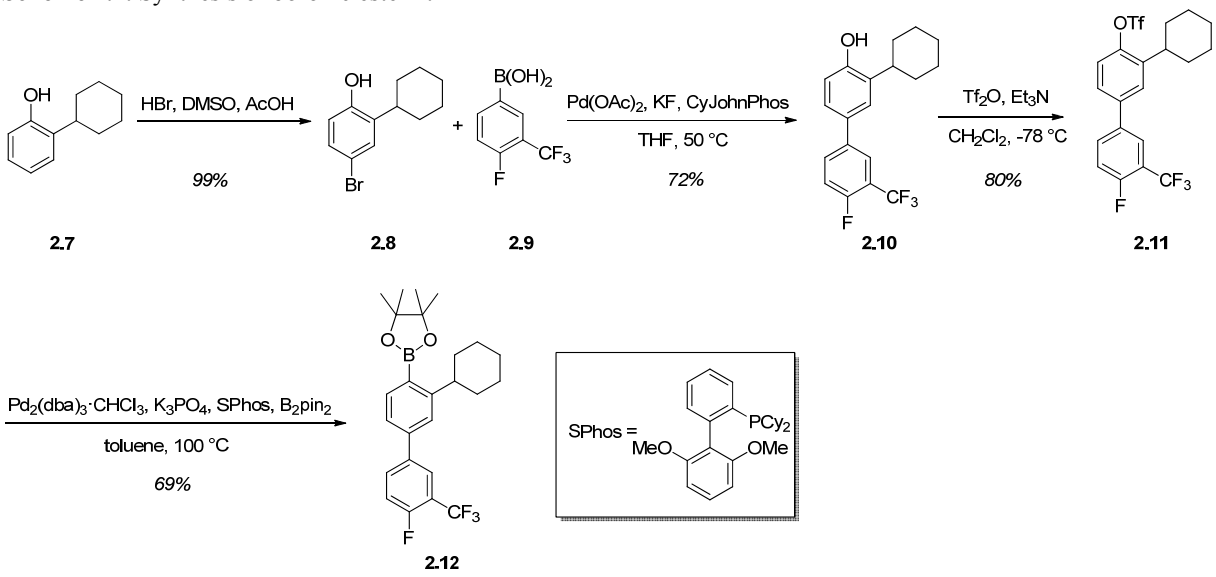

To determine optimal conditions for boration of hindered triflate **2.11**, we first screened conditions using the biphenyl model substrate **2.13** (Table 2.1). Standard Suzuki conditions for coupling with bis(pinacolato)diboron failed to produce product (entry 1), as did standard

Buchwald conditions using cyclohexyl JohnPhos as the ligand (entry 2). Similarly, all attempts to couple with pinacol borane gave no reaction (entries 3-4). Finally, inclusion of the Buchwald ligand SPhos[9-10] afforded product, albeit in low yield (entry 5). Increasing the temperature to 130 °C decreased the yield, likely due to protodeborylation of the product (entry 6), but switching to $Pd_2(dba)_3$ in addition to reversed-phase purification of the somewhat unstable boronic ester improved the yield significantly to 66% (entry 7). Upon applying the same conditions to the desired triflate **2.11**, the pinacol ester **2.12** was obtained in 69% yield (Scheme 2.2).

Table 2.1. Coupling of model triflate **2.13** to afford model boronic ester **2.14**

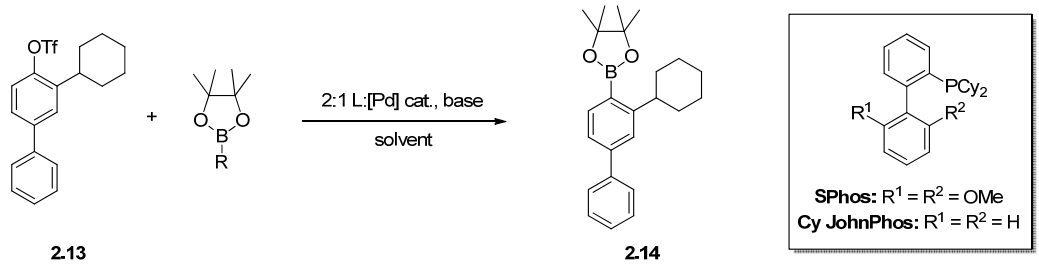

2.13 **2.14**

Entry	R	[Pd] cat.	Ligand	Base	Solvent	Temp (°C)	Time (h)	%Yield[a]
1	Bpin	$Pd(dppf)Cl_2$	--	KOAc	dioxane	80	26	0%
2	Bpin	$Pd(OAc)_2$	Cy JohnPhos	KF	toluene	100	17	0%
3	H	$Pd(PPh_3)_4$	--	Et_3N	dioxane	80	4	0%
4	H	$Pd(dppf)Cl_2$	--	Et_3N	dioxane	70	27	0%
5	Bpin	$Pd(OAc)_2$	SPhos	K_3PO_4	toluene	100	15	28%
6	Bpin	$Pd(OAc)_2$	SPhos	K_3PO_4	toluene	130	16	14%
7	Bpin	$Pd_2(dba)_3 \cdot CHCl_3$	SPhos	K_3PO_4	toluene	110	17	66%

[a]Yield was determined by mass balance after silica gel column chromatography.

The next step, coupling between boronic ester **2.12** and heterocycle **2.6**, also required optimization to overcome the unfavorable steric interactions of the bulky *ortho* cyclohexyl group (Scheme 2.3). Table 2.2 shows some of the conditions attempted for this coupling, beginning with the same conditions used to synthesize boronic ester **2.12** (entry 1). These conditions did produce product, but in low yield (15%), in this case due to competitive formation of decomposition byproducts, likely through ring opening of either the heterocycle and/or coupled product, as determined by NMR analysis. We observed similar decomposition byproducts when using an amination catalyst developed by Hartwig (entries 2-3), which was designed to increase the rate of oxidative addition, a step that is often rate-limiting in the Suzuki catalytic cycle.[11] Ultimately, we found that inclusion of catalytic water enabled formation of product at reduced temperatures, which minimized the formation of undesired ring-opened byproducts (entry 4). Increasing the amount of catalytic water and the reaction time ultimately gave the coupled product in 69% yield (entry 5). To complete the synthesis, the resulting coupled product **2.15** was then reduced with sodium borohydride, followed by oxidation to sulfone **2.17** with *m*-CPBA (Scheme 2.3). Final TFA deprotection then gave the desired isothiazolidinone inhibitor **2.1** in racemic form.

Table 2.2. Optimization of the coupling reaction between boronic ester **2.12** and heterocycle **2.6**

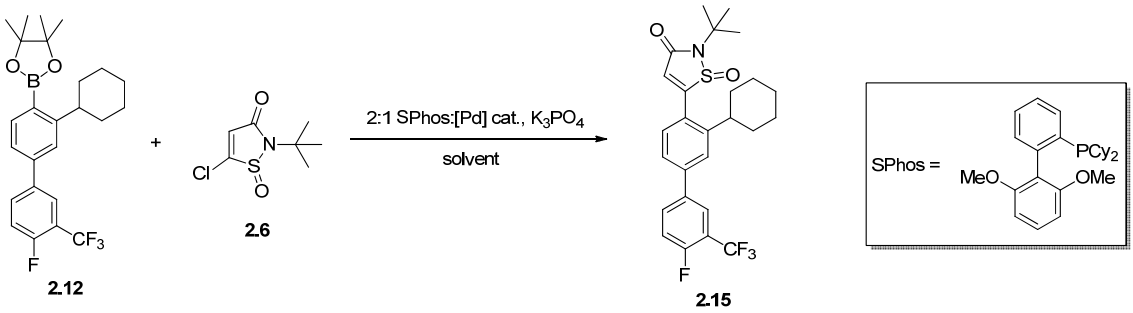

2.12 + **2.6** → **2.15**

Entry	[Pd] cat.	Solvent	Temp (°C)	Time (h)	%Yield[a]
1	$Pd_2(dba)_3 \cdot CHCl_3$	toluene	100	20	15%
2	$Pd[P(o\text{-}tol)_3]_2$	toluene	60	20	15%
3	$Pd[P(o\text{-}tol)_3]_2$	toluene	100	23	28%
4	$Pd(OAc)_2$	THF, 1 mol% H_2O	60	20	54%
5	$Pd(OAc)_2$	THF, 10 mol% H_2O	60	24	69%

[a]Yield was determined by mass balance after silica gel column chromatography.

Scheme 2.3. Final steps of the IZD synthesis

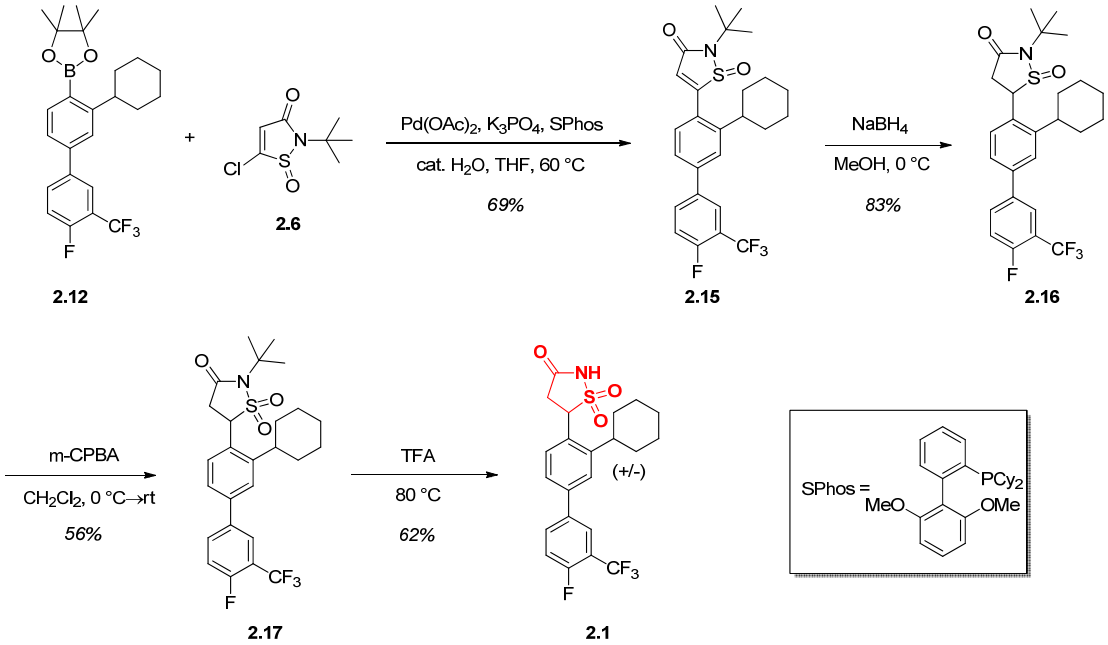

2.12 + **2.6** → **2.15** → **2.16**; **2.16** → **2.17** → **2.1**

Isolation and Evaluation of Enantiomerically Pure Isothiazolidinone Inhibitors

Based on previous studies of IZD inhibitors for PTP1B,[5a,5c-g] we reasoned that PtpB should bind one IZD enantiomer preferentially, and we therefore isolated the two enantiomers **2.20** and **2.21** to compare binding affinity (Figure 2.2). Isolation was achieved by subjecting compound **2.17** to chiral preparatory chromatography,[12] followed by the same TFA treatment

described above to remove the *tert*-butyl protecting group from compounds **2.18** and **2.19**. Compounds **2.18** and **2.19** were found to have >99% ee and >99% purity after separation and isolation.

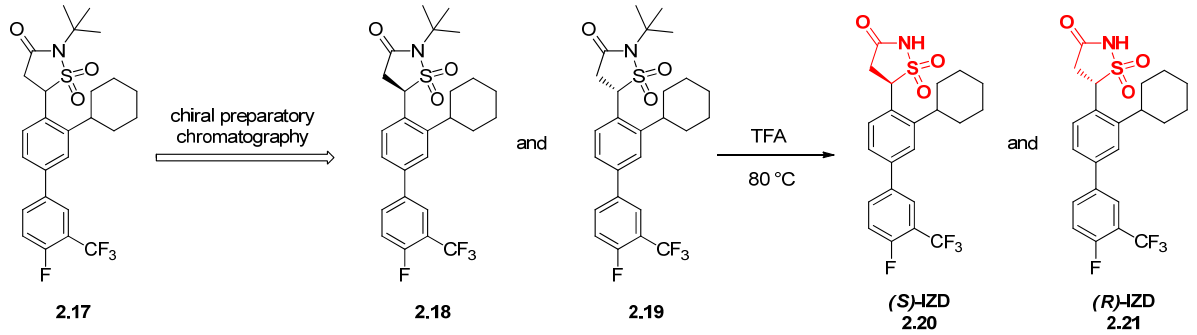

Figure 2.2. Isolation of enantiomerically pure IZD compounds **2.20** and **2.21**.

Following isolation, each compound was assayed versus PtpB along with racemic IZD **2.1** as a control (Table 2.3 – note that the absolute configuration of each compound has not been established; repeated attempts at crystallization failed to produce crystals sufficient for X-Ray analysis, likely due to the inability of these compounds to pack with the necessary co-solvents). In this case, only modest discrimination was found for the two enantiomers (K_i = 2.5 and 8.2 μM for **2.20** and **2.21**, versus 3.8 μM for racemic IZD **2.1**), despite previous reports of large discrimination for inhibitors of PTP1B.[5e,5g] Though PTP active sites are generally highly homologous, there is no directly related human homologue of PtpB, and the active site may be sufficiently different from that of PTP1B such that it can accommodate both IZD enantiomers. Unfortunately, due to the unusually high flexibility of PtpB, modeling studies would be unlikely to provide meaningful depictions of interactions between our compounds and the PtpB active site. This scaffold is still of general interest, however, because inhibitors that incorporate this scaffold will have different physicochemical properties from the corresponding inhibitors incorporating the isoxazole pharmacophore, which will impact important factors that contribute to compound efficacy such as cell permeability, protein binding, oral bioavailability, and clearance rates.

Table 2.3. Assay of racemic and enantiomerically pure IZD inhibitors versus PtpB

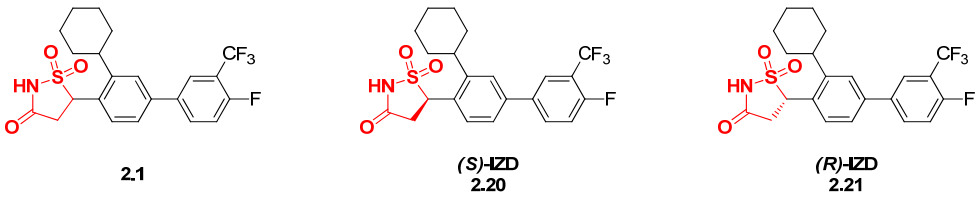

Compound	K_i (μM)[a]
2.1	3.8 ± 2.0
2.20 or **2.21**	2.5 ± 0.0
2.20 or **2.21**	8.2 ± 0.4

[a]Compounds were assayed in duplicate.

Enantioselective Sulfoxidation Studies

Because the IZD pharmacophore continues to be of interest to our inhibitor development efforts including development of inhibitors for other PTPs, we elected to investigate more efficient methods for the enantioselective synthesis of these compounds. Although enantiomerically pure isothiazolidinone inhibitors can be isolated via chiral preparatory chromatography, we desired a more general synthetic route to these compounds that could not only be applied to a variety of scaffolds, but could also ultimately be applied on production scale. Asymmetric reduction of isothiazolines such as **2.15** (Scheme 2.3) is one possible approach for accomplishing an asymmetric synthesis of inhibitors of this class; however, researchers at Incyte extensively investigated enantioselective reduction catalysts and found that none of the reductants examined reduced isothiazolines to isothiazolidines with sufficient selectivity and yield,[5b] and so we sought to develop a different approach. Enantioselective sulfoxidation is an alternative method that may be used to access IZD enantiomers (vide infra). This approach is attractive because it can potentially be used at different steps in the synthetic sequence, and because there are a variety of catalysts available for this transformation.

In 2007, Incyte reported that isothiazolidinone inhibitors could be made as single enantiomers by taking advantage of a stereoselective reduction of enantiomerically pure sulfinamides with sodium borohydride (as exemplified by sulfinamide **2.22** in Scheme 2.4).[5b] In this reduction, the borohydride attacks the sulfinamide from the less sterically and electronically hindered face where the lone pair resides, thereby resulting in product **2.23** with >99:1 dr. Subsequent oxidation of the sulfinamide to the sulfonamide followed by removal of the *tert*-butyl protecting group then provides the desired isothiazolidinone inhibitors. Though the reduction is selective, this transformation requires the preparation of enantiomerically pure sulfonamides (*e.g.* **2.22**), which can be accomplished by chiral preparatory chromatography as reported by Incyte and described above (vide supra), or more generally by enantioselective sulfoxidation of sulfenamide **2.24** (Scheme 2.5) using a chiral catalyst and oxidant. The resulting enantiomerically pure sulfinamide **2.25** can then be reduced using Incyte's stereoselective reduction process to produce diastereomerically pure products **2.26** that can be elaborated to the final enantiomerically pure inhibitors **2.27** as described for the racemic IZD inhibitor **2.1** (Scheme 2.3).

Scheme 2.4. Stereoselective $NaBH_4$ reduction reported by Incyte[5b]

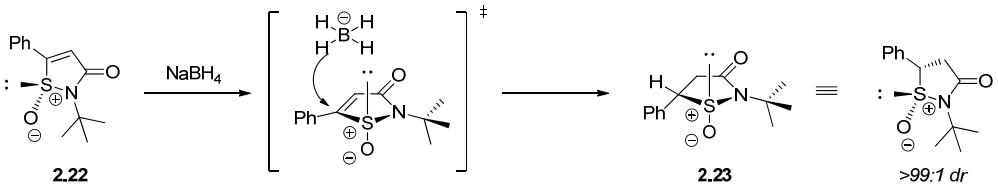

Scheme 2.5. Enantioselective sulfoxidation strategy for isolation of enantiomerically pure IZD inhibitors

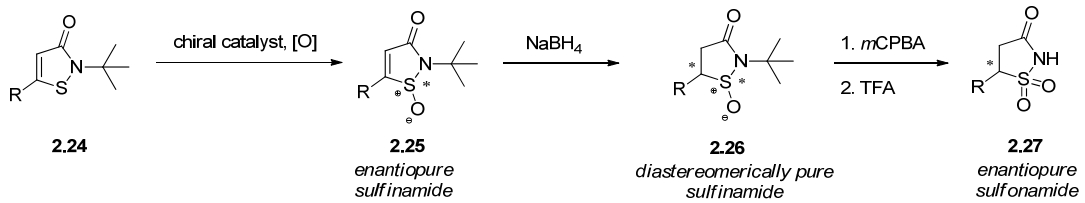

To test the feasibility of enantioselective sulfoxidation on the IZD scaffold, we chose to first evaluate the asymmetric oxidation of heterocyclic sulfenamide **2.5** (Table 2.4), which via Suzuki cross-coupling reactions could serve as an extremely versatile intermediate in the synthesis of IZD-based inhibitors. A variety of enantioselective sulfoxidation conditions commonly reported in the literature were evaluated,[13] and in all cases, the frequently reported substrate thioanisole was used as a control to ensure that the conditions were correctly implemented (data not shown). An enzymatic method using chloroperoxidase and hydrogen peroxide in the presence of aqueous pH 5.0 buffer failed to turn over substrate **2.5** (entry 1). The popular commercially available Davis oxaziridine reagent, **2.29**, also failed to produce product (entry 2), as did Kagan conditions using titanium/diethyl tartrate **2.30** complexes, in the presence of both cumene hydroperoxide and *tert*-butyl hydroperoxide (entries 3-4). The lack of conversion observed for each of these catalysts likely results from the more electron-deficient character of the sulfur in the heterocyclic sulfenamides relative to standard thioether substrates. While Bolm's conditions using complexes between vanadium and ligands **2.31** or **2.32** did produce product, only modest yields and enantioselectivity were observed (entries 5-6). Jacobsen's catalyst **2.33** in the presence of iodosobenzene gave the most promising results, with 74% yield and with 55% ee (entry 7).

Table 2.4. Enantioselective sulfoxidation of heterocycle **2.5**

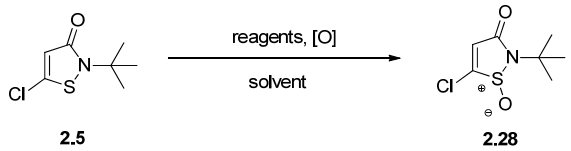

2.5 **2.28**

Entry	Reagents	Oxidant	Solvent	Temp (°C)	%Yield[c]	%ee[d]
1	chloroperoxidase	H_2O_2	aq. acetate buffer	rt	0%	--
2	**2.29**	--	CH_3CN	rt	0%	--
3	**2.30**, Ti(O*i*-Pr)$_4$, *i*-PrOH	CHP[a]	CH_2Cl_2	-20	0%	--
4	**2.30**, Ti(O*i*-Pr)$_4$, H_2O	TBHP[b]	CH_2Cl_2	-20	0%	--
5	**2.31**, $VO(acac)_2$	H_2O_2	acetone	0	50%	20%
6	**2.32**, $VO(acac)_2$	H_2O_2	CH_2Cl_2	rt	20%	20%
7	**2.33**	PhIO	CH_3CN	0 → rt	74%	55%

[a]CHP = cumene hydroperoxide. [b]TBHP = *tert*-butyl hydroperoxide. [c]Yield was determined by mass balance after silica gel column chromatography. [d]Enantiomeric excess was determined by chiral HPLC.

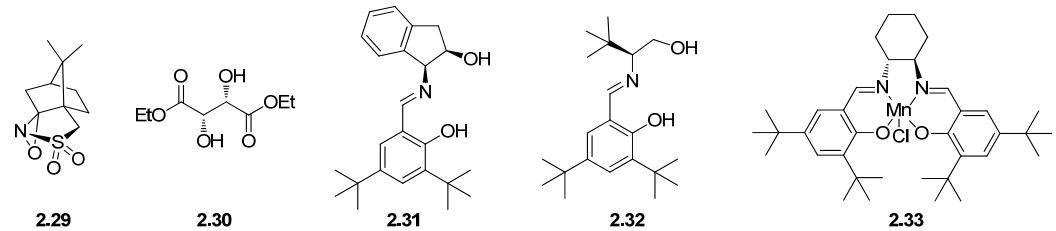

2.29 **2.30** **2.31** **2.32** **2.33**

Enantioselective sulfoxidation methods rely on the chiral catalyst discriminating between the two prochiral lone pairs on sulfur as the catalyst interacts with the two groups directly adjacent to the sulfur. This interaction is also dictated by the orientation of the chiral metal-oxo

complex formed *in situ*, which depends on the substituents surrounding the metal. To see if the initial enantioselectivity obtained with heterocycle **2.5** (55% ee for product **2.28**) could be improved upon, bulkier Katsuki catalysts previously reported to give high enantioselectivity in sulfoxidation reactions with aryl-alkyl sulfide substrates[14] were investigated. In addition to increasing bulk around the metal center, these salen scaffolds allow for flexibility in reaction conditions, as they can be reacted with a variety of metals and oxidants to produce the active catalyst, either before reaction or *in situ* (Scheme 2.6).

Salen catalysts **2.39** and **2.40** were synthesized according to minor modification of literature procedures (Scheme 2.6).[14] The synthesis of the required chiral aldehyde **2.38** began with monotriflation of *(R)*-BINOL, followed by Kumada coupling of **2.34** with phenyl magnesium bromide, MOM protection (**2.36**), directed formylation (**2.37**), and final deprotection to afford chiral aldehyde **2.38**. This aldehyde was then condensed with the chiral diamine (1*R*)-*trans*-1,2-cyclohexanediamine and reacted with manganese acetate, followed by salt exchange to arrive at catalyst **2.39**. Alternatively, chiral aldehyde **2.38** could be condensed with (1*R*)-*trans*-1,2-cyclohexanediamine to afford salen scaffold **2.40**, which can be used with a metal source and oxidant to generate the active catalyst *in situ*.

Scheme 2.6. Synthesis of Katsuki salen catalysts

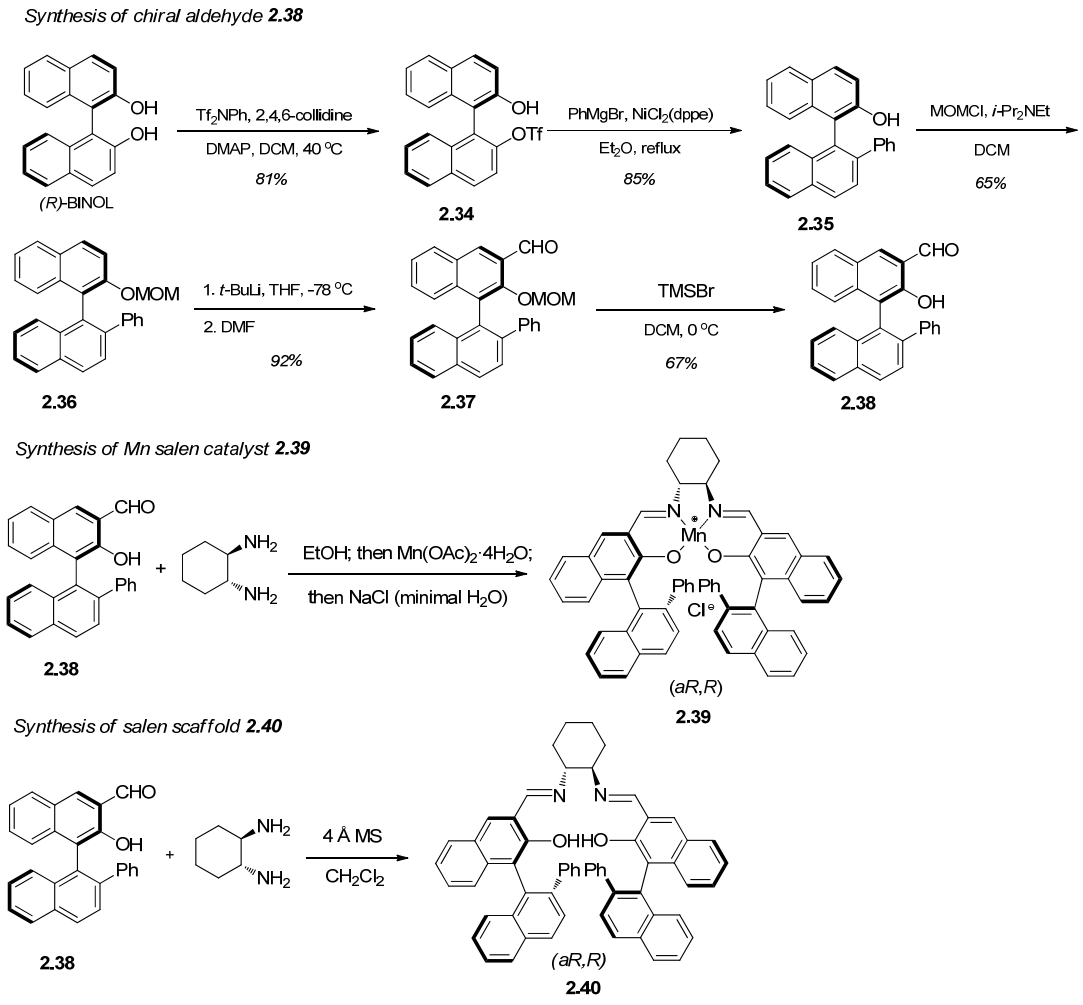

Table 2.5 shows the results of enantioselective sulfoxidation attempts on heterocyclic substrates **2.5**, **2.41**, and **2.42** with Jacobsen catalysts **2.33**, **2.43**, and **2.44** and Katsuki salen catalysts **2.39** and **2.40**. Thioanisole was used as a control for all reactions (data not shown). Compared to the initial result with Jacobsen's catalyst **2.33** (entry 1), manganese catalyst **2.43**, which is the analogous hexafluorophosphate salt, provided similar enantioselectivity (48% ee), but a lower yield (entry 2). Similarly, the manganese Katsuki catalyst **2.39** afforded product in ~50% yield with comparable 51% ee (entry 3). Unfortunately, *in situ* formation of the niobium catalyst with either the Jacobsen or Katsuki scaffolds **2.44** and **2.40**, respectively, failed to provide product in either case (entries 4-5).

Because improvements in the enantioselectivity for the oxidation of chloro heterocycle **2.5** seemed unlikely without significant catalyst optimization, the same oxidation conditions were also attempted on model phenyl substrate **2.41** to evaluate whether sulfoxidation could be carried out at a later stage in the inhibitor synthesis (Scheme 2.3). Interestingly, the enantioselectivity for phenyl model substrate **2.41** was greatly improved to 80% with catalyst **2.33** (entry 6). This is likely due to the increased ability of the chiral catalyst to discriminate between the two groups flanking the sulfur atom (aryl-alkyl instead of halogen-alkyl). Unfortunately, however, attempting the same oxidation on the desired cyclohexyl substrate **2.42** resulted in an enantioselectivity of 50%, similar to heterocycle **2.5** (entry 7). Although the cyclohexyl group improves the size difference between the two substituents attached to sulfur, it may also prevent close approach to the catalyst and may change the conformation of the sulfenamide such that interactions with the catalyst are altered, resulting in lowered enantioselectivities. Other parameters that could still be explored to improve on this result include solvent, oxidant, and temperature screens, as well as the synthesis of other Katsuki complexes to explore the effect of different phenyl ring substituents or chiral diamine pieces. Finally, other metals could be explored, including titanium, which is commonly used in these transformations.

Table 2.5. Enantioselective sulfoxidation with Katsuki and Jacobsen catalysts

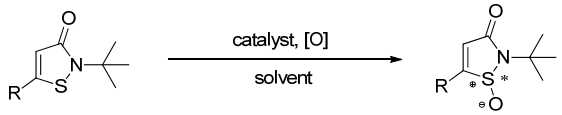

Entry	#	R	Catalyst	Oxidant	Solvent	Temp (°C)	%Yield[a]	%ee[b]
1	**2.5**	Cl	**2.33**	PhIO	CH_3CN	0 → rt	74%	55%
2	**2.5**	Cl	**2.43**	PhIO	CH_3CN	0 → rt	46%	48%
3	**2.5**	Cl	**2.39**	PhIO	CH_3CN	0 → rt	47%	-51%
4	**2.5**	Cl	**2.44**, $NbCl_3$(dme)	UHP	CH_2Cl_2	-10	0%	--
5	**2.5**	Cl	**2.40**, $NbCl_3$(dme)	UHP	CH_2Cl_2	rt	0%	--
6	**2.41**		**2.33**	PhIO	CH_3CN	0 → rt	66%	80%
7	**2.42**	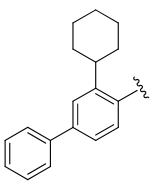	**2.33**	PhIO	CH_3CN	0 → rt	38%	55%

[a]Yield was determined by mass balance after silica gel column chromatography. [b]Enantiomeric excess was determined by chiral HPLC.

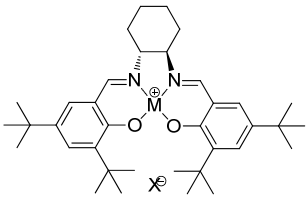

2.33: M = Mn, X = Cl
2.43: M = Mn, X = PF_6
2.44: No metal

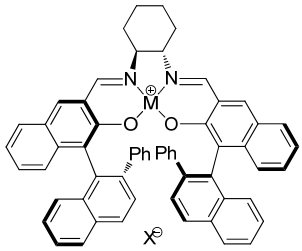

2.39: M = Mn, X = Cl
2.40: No metal

Difluoromethylphosphonic Acid Analog

To complete the PtpB inhibitor panel and provide further comparison of phosphate mimetics in terms of PtpB binding affinity, we also developed a route to the DFMP analog. Several synthetic approaches have been reported for installation of the DFMP isostere and could be used in the synthesis of the DFMP compound.[15] We chose a relatively mild and straightforward cross coupling approach between aryl iodide **2.46** and a commercially available diethyl phosphonate (Scheme 2.7),[15c] since this strategy is compatible with a variety of functional groups, and allows for early or late stage incorporation of the DFMP warhead. Synthesis of DFMP analog **2.2** began by coupling bis(neoglycolato)diboron with triflate intermediate **2.11** used in the synthesis of the IZD inhibitor. This was followed by iodination with *in situ*-generated ICl to form the aryl iodide **2.46**, then copper and zinc-mediated coupling with diethyl(bromodifluoromethyl)phosphonate to afford the aryl phosphonate **2.47**. Final deprotection then afforded the desired DFMP inhibitor **2.2**.

Scheme 2.7. Synthesis of DFMP inhibitor **2.2**

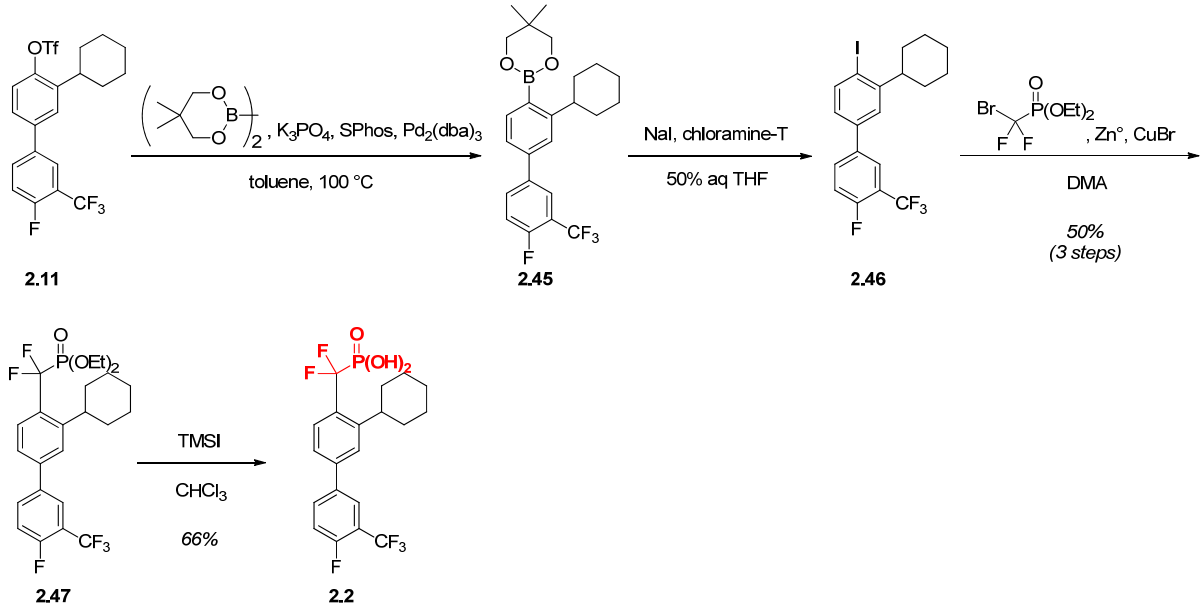

Activity of the Inhibitor Panel versus PtpB

The IZD compound **2.1** was found to have a K_i of 3.8 μM versus PtpB as a racemic mixture, comparable to the isoxazole scaffold **1.173**, while the enantiomerically pure IZD compounds **2.20** and **2.21** were found to have a K_i of 2.5 and 8.2 μM. The DFMP compound **2.2** was found to have a K_i of 0.68 μM versus PtpB, comparable to the isoxazole scaffold (Table 2.6). All together, the isoxazole, IZD, and DFMP inhibitors represent a complete set of compounds that can be used to further dissect the biochemical role of PtpB in TB infection. Each compound is being evaluated in TB-infected cells to determine differences in cell permeability, and may additionally be evaluated in animal infection models.

Table 2.6. Activity of full panel of inhibitors versus PtpB

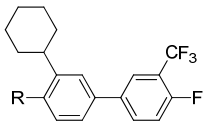

#	R	K_i (μM)[a]
1.173	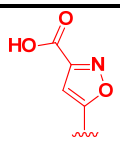	0.22 ± 0.03
2.1	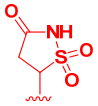	3.8 ± 2.0
2.2	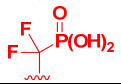	0.68 ± 0.30

[a]Compounds were assayed in duplicate, and repeated in triplicate.

Conclusions

Two new inhibitor analogs for *Mtb* PtpB have been identified. Each of these compounds contains the optimal scaffold identified in Chapter 1 by using the SAS method, a novel fragment-based approach for phosphatase inhibitor development. Inhibitors **2.1** and **2.2** incorporate the IZD and DFMP phosphate mimetics, respectively, in place of the isoxazole carboxylic acid warhead developed for compound **1.173** (Chapter 1). These mimetics were chosen based on previous incorporation into inhibitors of the phosphatase PTP1B, an enzyme targeted for diabetes treatment. Each enantiomer of the IZD inhibitor **2.1** was isolated via chiral preparatory chromatography, and X-ray analysis of these compounds is in progress. Enantioselective sulfoxidation was preliminarily explored as a more general method to access enantiomerically pure IZD inhibitors, and initially promising results were achieved with Katsuki salen catalysts. Although the IZD and DFMP analogs are comparable to the isoxazole inhibitor in terms of binding affinity, they are expected to vary in terms of cell permeability and activity. The entire panel of inhibitor analogs is therefore currently being evaluated in TB-infected cells and, if found to be cell permeable, will be further evaluated in animal infection models.

Experimental

General Synthetic Methods

Unless otherwise noted, all reagents were obtained from commercial suppliers and used without further purification. Tetrahydrofuran (THF), dichloromethane (CH_2Cl_2), toluene, and diethyl ether (Et_2O) were dried over alumina under a nitrogen atmosphere. Solvents used for reactions set up in a nitrogen-filled Braun inert atmosphere box, including THF and toluene, were additionally degassed with three consecutive freeze pump thaw cycles and stored over 3Å molecular sieves. Methanol was dried over calcium hydride under a nitrogen atmosphere. All reactions, unless otherwise stated, were performed under inert atmosphere using syringe, cannula, and Schlenk techniques, or set up in a nitrogen-filled Braun inert atmosphere box, with flame or oven-dried glassware. All ^{1}H, ^{13}C, ^{19}F, and ^{31}P NMR spectra were measured with a Bruker DRX-500, AVB-400, AVQ-400 or AV-300 spectrometer. NMR chemical shifts are reported in ppm relative to 1,2-difluorobenzene (-138.9) for ^{19}F NMR and trimethylphosphate (3.0) for ^{31}P NMR. Mass spectrometry (HRMS) was carried out by the University of California, Berkeley Mass Spectrometry Facility.

*Synthesis of Isothiazolidinone Inhibitor **2.1***

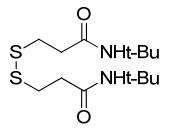

2.4

Compound 2.4. Compound **2.4** was synthesized via modified literature procedures,[5c] beginning with commercially available dithiopropionic acid. Dithiopropionic acid (20.0 g, 0.950 mol) was added to a flame-dried 3-necked flask that was flushed with N_2 and equipped with a mechanical stirrer. THF (240 mL) was added and the solution was cooled to -10 °C in an ice/acetone bath. *N*-methylmorpholine (40 mL, 2.1 mol) was then added at -10 °C via addition funnel, followed by diphenylphosphinic chloride (46 mL, 4.2 mol), also via addition funnel. The resulting solution was stirred for 30 min at -10 °C, followed by cannula addition of a solution of *tert*-butylamine (40 mL, 3.8 mol) in THF (240 mL). The resulting slurry was allowed to warm to ambient temperature and stirred for 26 h. The reaction was quenched by dilution with Et_2O (1.0 L), and extraction with 1N NaOH (2.0 L). The organic layer was separated and washed with 10% HCl (1 x 1.0 L), and brine (1 x 1.0 L). The combined organic layer was dried over anhydrous Na_2SO_4(s) and filtered. The solvent was removed under reduced pressure to provide crude **2.4**, which was purified via silica gel chromatography (gradient of 4:1→1:2 hexanes:EtOAc), to give **2.4** as an orange solid (12.7 g, 97% pure by NMR) that was taken on without further purification. **Analytical data.** Analytical data was found to match that of previous literature reports[5c,8b,16]: ^{1}H NMR (400 MHz, $CDCl_3$) δ 2.95 (t, *J* = 7.0 Hz, 4H), 2.52 (t, *J* = 7.0 Hz, 4H), 1.36 (s, 18H).

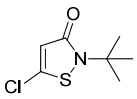

2.5

Compound 2.5. Compound **2.5** was synthesized from **2.4** via modified literature procedures.[5c,5g] Compound **2.4** (11.1 g, 35.0 mmol) was added to a flame-dried flask that was fitted with a stirbar and flushed with N_2, and then dichloroethane (174 mL) was added. The resulting solution was cooled to 0 °C, followed by dropwise addition of sulfuryl chloride (8.4 mL, 104 mmol) via syringe pump (10 mL syringe, 0.89 mL/min addition rate). The resulting solution was allowed to warm to ambient temperature and was stirred for 2.5 h. The reaction was quenched by dropwise addition of ice water (200 mL). The organic layer was separated and extracted with dichloromethane (3 x 200 mL), dried over anhydrous Na_2SO_4(s), and filtered. The solvent was removed under reduced pressure to provide crude **2.5**, which was purified using a silica gel plug (eluent 6:1 hexanes:EtOAc) to give **2.5** as a low melting orange solid, which was taken on without further purification (2.65 g, 93% pure by NMR). **Analytical data.** Analytical data was found to match that of previous literature reports[5c,5g,8a,16]: ^{1}H NMR (400 MHz, $CDCl_3$) δ 6.19 (s, 1H), 1.61 (s, 9H); ^{13}C NMR (126 MHz, $CDCl_3$) δ 166.82, 143.89, 116.68, 59.11, 28.21.

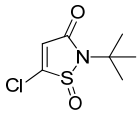

2.6

Compound 2.6. Compound **2.6** was synthesized from **2.5** via modified literature procedures.[5b,5g] Compound **2.5** (2.7 g, 13.8 mmol) was added to a flame-dried flask that was fitted with a stirbar. After flushing with N_2, acetonitrile (42 mL), dichloromethane (42 mL), and H_2O (63 mL) were added. The mixture was cooled to 0 °C, and sodium periodate (4.4 g, 20.8 mmol) was added portionwise, followed by $RuCl_3$ (29 mg, 1.0 mol%). The resulting mixture was stirred vigorously at 0 °C for 1 h, and was then diluted with dichloromethane (100 mL). The organic layer was separated, then washed with brine (3 x 100 mL), dried over anhydrous Na_2SO_4(s), and filtered. The solvent was removed under reduced pressure to provide crude **2.6**, which was purified via automated silica gel chromatography (linear gradient of 5-25% EtOAc/hexanes) to afford **2.6** as an offwhite solid (2.28 g, 7% yield over 3 steps). **Analytical data.** Analytical data was found to match that of previous literature reports[5b,5g]: ^{1}H NMR (400 MHz, $CDCl_3$) δ 6.55 (s, 1H), 1.64 (s, 9H).

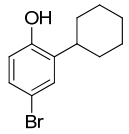

2.8

Compound 2.8. Compound **2.8** was synthesized as described in Chapter 1 (compound **1.174**).

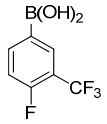

2.9

Compound 2.9. Compound **2.9** was synthesized as described in Chapter 1 (compound **1.175**).

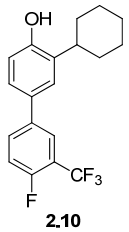

2.10

Compound 2.10. Compound **2.10** was synthesized as described in Chapter 1 (compound **1.176**).

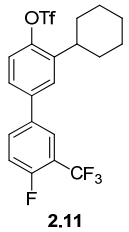

2.11

Compound 2.11. Compound **2.11** was synthesized as described in Chapter 1 (compound **1.177**).

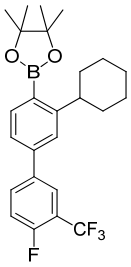

2.12

Compound 2.12. To a 10 mL Schlenk tube fitted with a stirbar in a nitrogen-filled Braun inert atmosphere box was added compound **2.11** (0.72 g, 1.53 mmol), followed by bis(pinacolato)diboron (1.16 g, 4.59 mmol), K_3PO_4 (0.97 g, 4.59 mmol), tris(dibenzylideneacetone)dipalladium-chloroform adduct (47 mg, 0.04 mmol, 3.0 mol%), and 2-dicyclohexylphosphino-2',6'-dimethoxybiphenyl (SPhos, 38 mg, 0.08 mmol, 6.0 mol%). Toluene (3.06 mL) was then added and the reaction tube was closed under N_2 atmosphere. The resulting mixture was then heated with stirring in an oil bath at 110 °C for 22 hours. The reaction mixture was then diluted with Et_2O and passed through a pad of Celite. The solvent was removed under reduced pressure to provide crude **2.12**, which was purified via automated reversed-phase C18 chromatography (linear gradient of 80 to 95% acetonitrile in H_2O) to yield compound **2.12** as an off-white solid (0.47 g, 69% yield). **Analytical data.** ^{1}H NMR (400 MHz, $CDCl_3$): δ 7.82-7.73 (m, 3H), 7.41 (m, 1H), 7.33 (dd, J = 7.7, 1.6 Hz, 1H), 7.28-7.24 (m, 1H), 3.38-3.29 (m, 1H), 1.91-1.75 (m, 5H), 1.53-1.43 (m, 5H), 1.37 (s, 12H); ^{19}F NMR (376 MHz, $CDCl_3$): δ -60.51 (d, J = 6.3 Hz), -116.51 (m); HRMS-EI (*m/z*): $[M + H]^+$ calcd for $C_{25}H_{29}BF_4O_2$, 448.2189; found, 448.2197.

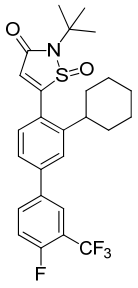

2.15

Compound 2.15. To a 1 mL Schlenk tube fitted with a stirbar in a nitrogen-filled Braun inert atmosphere box was added compound **2.12** (34 mg, 0.10 mmol), followed by compound **2.6** (41 mg, 0.15 mmol), K_3PO_4 (127 mg, 0.600 mmol), palladium acetate (3.4 mg, 0.02 mmol, 15 mol%), and 2-dicyclohexylphosphino-2',6'-dimethoxybiphenyl (SPhos, 12 mg, 0.04 mmol, 30 mol%). A 100:1 H_2O:THF solution (0.20 mL) was then added and the reaction tube was closed under N_2 atmosphere. The resulting mixture was then heated with stirring in an oil bath at 60 °C for 24 h. The reaction mixture was then diluted with Et_2O and passed through a pad of Celite. The solvent was removed under reduced pressure to provide crude **2.15**, which was purified via automated silica gel chromatography (linear gradient of 2 to 15% EtOAc in hexanes) to yield compound **2.15** as a yellow solid (34 mg, 69% yield). **Analytical data.** ^{1}H NMR (400 MHz, $CDCl_3$): δ 7.79-7.77 (m, 2H), 7.54 (m, 1H), 7.45 (m, 2H), 7.33-7.30 (m, 1H), 6.48 (s, 1H), 2.80-2.70 (m, 1H), 1.95-1.73 (m, 5H), 1.72 (s, 9H), 1.55-1.30 (m, 5H); ^{19}F NMR (376 MHz, $CDCl_3$): δ -60.57 (d, J = 12.6 Hz), -115.18 (m); HRMS-EI (*m/z*): $[M + H]^+$ calcd for $C_{26}H_{28}F_4NO_2S$, 494.1772; found, 494.1777.

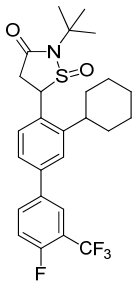

2.16

Compound 2.16. To a 10 mL flask fitted with a stirbar under N_2 was added compound **2.15** (263 mg, 0.530 mmol) and MeOH (1.77 mL), followed by cooling to 0 °C. Sodium borohydride (40 mg, 1.07 mmol) was then added and the resulting slurry was stirred at 0 °C for 2 h. The reaction was quenched at 0 °C by dropwise addition of a 10% solution of acetic acid in THF, with the flask open to the atmosphere. The mixture was concentrated to remove MeOH to give crude **2.16**, which was purified by recrystallization from EtOAc/MeOH to give compound **2.16** as an off-white solid (219 mg, 83% yield). **Analytical data.** ^{1}H NMR (400 MHz, $CDCl_3$): δ 7.90-7.68 (m, 2H), 7.55 (d, J = 8.2 Hz, 1H), 7.47 (d, J = 1.7 Hz, 1H), 7.42 (dd, J = 8.1, 1.8 Hz, 1H), 7.31-7.24 (m, 1H), 7.31-7.24 (m, 1H), 4.64 (dd, J = 12.0, 7.1 Hz, 1H), 3.57 (dd, J = 17.1, 12.0, 1H), 3.02 (dd, J = 17.0, 7.1 Hz, 1H), 2.84-2.79 (m, 1H), 1.98-1.77 (m, 5H), 1.65 (s, 9H), 1.63-1.50 (m, 5H); ^{19}F NMR (376 MHz, $CDCl_3$): δ -60.50 (d, J = 12.4 Hz), -115.96 (m); HRMS-ESI (*m/z*): $[M + H]^+$ calcd for $C_{26}H_{30}F_4NO_2S$, 496.1855; found, 496.1928.

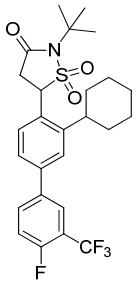

2.17

Compound 2.17. Compound **2.16** (219 mg, 0.44 mmol) was added to a flask under N_2, dissolved in chloroform (5.5 mL), and cooled to 0 °C. 3-Chloroperoxybenzoic acid (>77%, 197 mg, 0.88 mmol) was added at 0 °C, and the reaction was allowed to warm to ambient temperature and stirred for 18 h. The reaction was quenched at 0 °C by dropwise addition of aqueous saturated $NaHCO_3$, follwed by extraction with $NaHCO_3$ (5 x 5 mL), and washing with brine (1 x 5 mL). The organic layer was dried over anhydrous Na_2SO_4(s) and filtered. The solvent was removed under reduced pressure to provide crude **2.17**, which was purified via automated silica gel chromatography (linear gradient of 5-20% EtOAc in hexanes) to yield compound **2.17** as a white solid (117 mg, 56% yield). **Analytical data.** ^{1}H NMR (400 MHz, $CDCl_3$): δ 7.80-7.70 (m, 2H), 7.51 (d, J = 1.3 Hz, 1H), 7.48-7.40 (m, 2H), 7.33-7.26 (m, 1H), 5.24 (dd, J = 8.3 Hz, 1H), 3.31 (dd, J = 17.2, 8.6 Hz, 1H), 3.20 (dd, J = 17.1, 7.9 Hz, 1H), 2.95-2.82 (m, 1H), 2.05-1.75 (m, 5H), 1.68 (s, 9H), 1.65-1.40 (m, 5H); ^{19}F NMR (376 MHz, $CDCl_3$) δ -60.56 (d, J = 15.1 Hz), -115.56 (m); MS-FAB (*m/z*): $[M + H]^+$ calcd for $C_{26}H_{30}F_4NO_3S$, 512.1804; found, 512.0; HRMS-EI (*m/z*): $[M + H]^+$ calcd for $C_{26}H_{29}F_4NO_3S$, 511.1803; found, 511.1804.

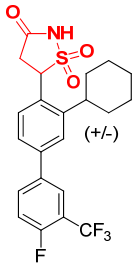

2.1

Compound 2.1. To a J-Young tube was added compound **2.1** (21 mg, 0.04 mmol) as a solution in d_4-TFA (0.55 mL), which was sealed and heated to 80 °C in an oil bath. The reaction was monitored by NMR until complete conversion of starting material was observed. The resulting mixture was concentrated to give crude **2.1**, which was dissolved in a minimal volume of dimethylsulfoxide (1.0 mL) and purified via automated reversed-phase C18 column chromatography (linear gradient of 15 to 95% acetonitrile in H_2O with 0.1% trifluoroacetic acid) to give pure **2.1** as a white powder (12 mg, 62% yield). **Analytical data.** ^{1}H NMR (400 MHz, CD_3OD): δ 7.86-7.75 (m, 2H), 7.53-7.47 (m, 2H), 7.44 (dd, J = 4.1, 1.8 Hz, 1H), 7.33 (t, J = 9.6 Hz, 1H), 5.55 (t, J = 8.4 Hz, 1H), 3.33 (dd, J = 17.4, 8.2 Hz, 1H), 3.27 (dd, J = 17.4, 8.2 Hz, 1H), 2.99-2.90 (m, 1H), 1.90-1.66 (m, 5H), 1.59-1.22 (m, 5H); ^{19}F NMR (376 MHz, CD_3OD) δ -62.06 (d, J = 12.8 Hz), -118.48 (m); MS-ESI (*m/z*): $[M - H]^-$ calcd for $C_{22}H_{20}F_4NO_3S$, 454.1178; found, 454.0; HRMS-FAB (*m/z*): $[M - H]^-$ calcd for $C_{22}H_{20}F_4NO_3S$, 454.1106; found, 454.1091.

*Chiral Separation of Compound **2.1***

Compound **2.1** was separated into enantiomerically pure isothiazolidinones **2.20** and **2.21** with >99% chemical purity and >99% ee by Lotus Separations, LLC using chiral preparatory supercritical fluid chromatography. The racemic compound was loaded as a 7 mg/mL solution in methanol, with an injection volume of 0.7 mL, onto a Chiralpak AD-H column (2 x 15 cm), and eluted with 35% isopropanol/CO_2 at 100 bar, with a flowrate of 65 mL/min. Peaks were visualized using UV at 220 nm. Analytical chromatograms (Scheme 2.8-2.6) were obtained by injecting compound solutions onto a Chiralpak AD-H column (25 x 0.46 cm), followed by elution with 35% isopropanol/CO_2 at a flowrate of 3 mL/min.

Scheme 2.8. HPLC trace of racemic **2.1**

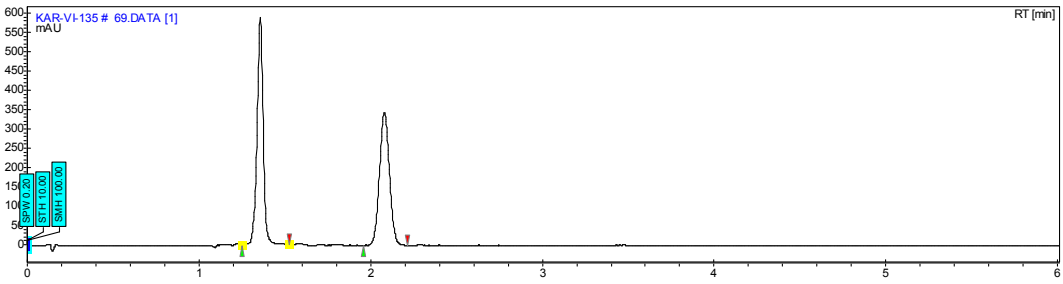

Scheme 2.9. HPLC trace of enantiomerically pure **2.20** or **2.21** ("peak 1")

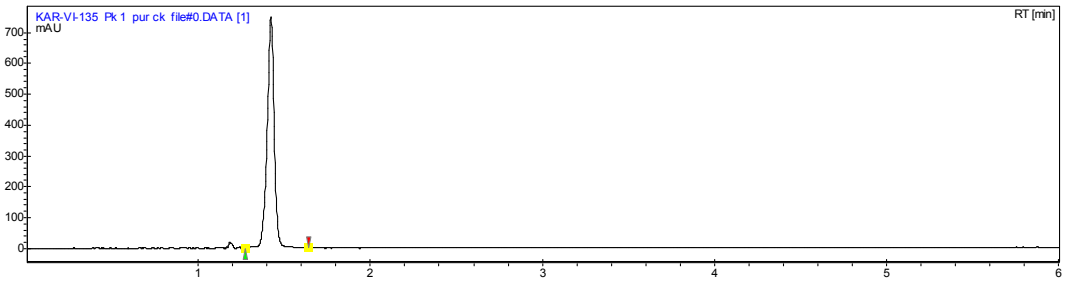

Scheme 2.10. HPLC trace of enantiomerically pure **2.20** or **2.21** ("peak 2")

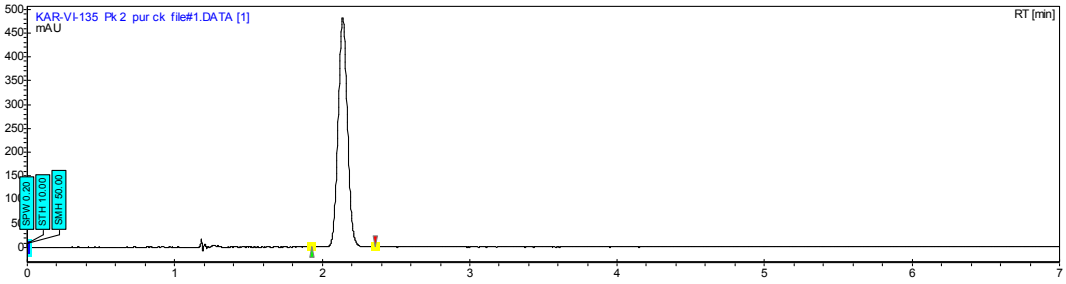

*Synthesis of Difluoromethylphosphonic Acid Inhibitor **2.2***

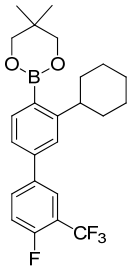

2.45

Compound 2.45. To a 5 mL Schlenk tube fitted with a stirbar in a nitrogen-filled Braun inert atmosphere box was added compound **2.11** (100 mg, 0.21 mmol), followed by bis(neopentylglycolato)diboron (96 mg, 0.43 mmol), K_3PO_4 (90 mg, 0.43 mmol), tris(dibenzylideneacetone)dipalladium-chloroform adduct (13 mg, 0.01 mmol, 6.0 mol%), and 2-dicyclohexylphosphino-2',6'-dimethoxybiphenyl (SPhos, 11 mg, 0.02 mmol, 12.0 mol%). Toluene (0.43 mL) was added, and the reaction tube was closed under an N_2 atmosphere. The resulting mixture was then heated with stirring in an oil bath at 100 °C for 26 h. The reaction mixture was diluted with Et_2O and passed through a pad of Celite. The solvent was removed under reduced pressure to provide crude **2.45**, which was purified via automated silica gel chromatography (linear gradient of 5 to 20% EtOAc in hexanes) to yield compound **2.45** as a yellow-orange solid (63 mg, 92% pure by NMR), which was taken on without further purification. **Analytical data.** ^{1}H NMR (400 MHz, $CDCl_3$): δ 7.81-7.71 (m, 3H), 7.42-7.40 (m, 1H), 7.32 (dd, J = 7.7, 1.8 Hz, 1H), 7.28-7.22 (m, 1H), 3.80 (s, 4H), 3.33-3.23 (m, 1H), 1.96-1.73 (m, 5H), 1.53-1.36 (m, 5H), 1.07 (s, 6H); ^{19}F NMR (376 MHz, $CDCl_3$): δ -60.50 (d, J = 12.5 Hz), -116.83 (m).

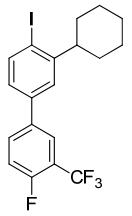

2.46

Compound 2.46. Compound **2.45** (416 mg, 0.96 mmol) was added to a flask under N_2 and dissolved in THF (4.8 mL). Sodium iodide was then added as a 1.0 N solution in water (1.2 mL) followed by chloramine-T (541 mg, 1.92 mmol). The resulting mixture was stirred vigorously for 15 min at room temperature. The reaction was quenched by addition of H_2O, and the aqueous layer extracted with Et_2O (3 x 5 mL). The organic layer was dried over anhydrous Na_2SO_4(s) and filtered. The solvent was removed under reduced pressure to provide crude **2.46**, which was purified via automated silica gel chromatography (linear gradient of 3-10% EtOAc in hexanes) to yield compound **2.46** as a white solid (188 mg, 71% pure by NMR), which was taken on without further purification. **Analytical data.** ^{1}H NMR (400 MHz, $CDCl_3$): δ 7.90 (d, J = 8.1 Hz, 1H), 7.78-7.66 (m, 2H), 7.35-7.23 (m, 2H), 7.04 (dd, J = 8.1, 2.2 Hz, 1H), 2.85-2.80 (m, 1H), 2.02-1.75 (m, 5H), 1.58-1.32 (m, 5H); ^{19}F NMR (376 MHz, $CDCl_3$): δ -60.55 (d, J = 12.5 Hz), -115.90 (m).

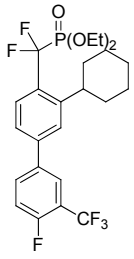

2.47

Compound 2.47. To a 25 mL flame-dried flask fitted with a stirbar under an N_2 atmosphere was added activated zinc dust (500 mg, 7.65 mmol), followed by *N,N*-dimethylacetamide (3.8 mL). The resulting mixture was heated to 60 °C in an oil bath with stirring. In a separate flask under an N_2 atmosphere, diethyl(bromodifluoromethyl)phosphonate (1.36 mL, 7.65 mmol) was dissolved in *N,N*-dimethylacetamide (3.8 mL), and this solution was added to the zinc mixture dropwise at 60 °C. The resulting mixture was stirred for 10 min at 60 °C, followed by stirring at ambient temperature for 4 h. In a separate 10 mL flask fitted with a stirbar under an N_2 atmosphere, compound **2.46** (135 mg, 0.30 mmol) and CuBr (86 mg, 0.60 mmol) were dissolved in *N,N*-dimethylacetamide (0.1 mL), followed by stirring for 30 min at ambient temperature. This solution was then added dropwise to the zinc solution, and the resulting mixture was sonicated for 12 h at ambient temperature. The reaction was quenched by addition of H_2O (10 mL), and the resulting mixture was diluted with Et_2O (15 mL), and filtered through Celite. The aqueous layer was extracted with Et_2O (3 x 15 mL), and the organic layer was washed with brine (1 x 75 mL), dried over anhydrous Na_2SO_4(s) and filtered. The solvent was removed under reduced pressure to provide crude **2.47**, which was purified via automated silica gel chromatography (linear gradient of 6-25% EtOAc in hexanes) to yield compound **2.47** as a white solid (77 mg, 50% yield). **Analytical data.** ^{1}H NMR (400 MHz, $CDCl_3$): δ 7.81-7.70 (m, 2H), 7.63-7.58 (m, 1H), 7.57-7.53 (m, 1H), 7.43-7.38 (m, 1H), 7.32-7.26 (m, 1H), 4.32-4.12 (m, 4H), 3.28-3.17 (m, 1H), 1.96-1.73 (m, 5H), 1.56-1.38 (m, 5H), 1.35 (t, J = 7.1 Hz, 6H); ^{19}F NMR (376 MHz, $CDCl_3$): δ -60.57 (d, J = 12.6 Hz), -100.766 (d, J_{FP} = 116.3 Hz), -115.51 (m); ^{31}P NMR (162 MHz, CD_3OD): δ 6.29 (t, J_{PF} = 116.2 Hz). MS-ESI (*m/z*): $[M + H]^+$ calcd for $C_{24}H_{28}F_6O_3P$, 509.1602; found, 509.0; HRMS-EI (*m/z*): $[M + H]^+$ calcd for $C_{24}H_{28}F_6O_3P$, 509.1690; found, 509.1680.

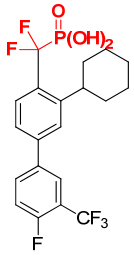

2.2

Compound 2.2. To a 5 mL flame-dried flask fitted with a stirbar under an N_2 atmosphere was added compound **2.47** (72 mg, 0.14 mmol) and $CHCl_3$ (0.24 mL). To the resulting solution was added iodotrimethylsilane (61 µL, 0.43 mmol) dropwise by syringe. The resulting solution was stirred at ambient temperature for 14 h, and then the solvent was removed under reduced pressure to give crude **2.2** as an orange oil. The crude oil was dissolved in a minimal amount of dimethylsulfoxide (1.0 mL) which was purified by automated reversed-phase

C18 column chromatography (linear gradient of 5 to 95% acetonitrile in H_2O with 0.1% trifluoroacetic acid) to give compound **2.2** as a white powder (42 mg, 66% yield). **Analytical data.** ^{1}H NMR (400 MHz, CD_3COCD_3): δ 8.08-7.96 (m, 2H), 7.83-7.77 (m, 1H), 7.65-7.47 (m, 2H), 6.61 (br s, 2H), 3.41-3.29 (m, 1H), 1.93-1.23 (m, 10H); ^{19}F NMR (376 MHz, CD_3COCD_3): δ -61.03 (d, J = 12.6 Hz), -102.52 (d, J_{FP} = 113.7 Hz), -118.01 (m); ^{31}P NMR (162 MHz, CD_3COCD_3): δ 5.96 (t, J_{PF} = 113.6 Hz). MS-ESI (*m/z*): $[M + H]^+$ calcd for $C_{20}H_{20}F_6O_3P$, 453.0976; found, 453.0; HRMS-EI (*m/z*): $[M + H]^+$ calcd for $C_{20}H_{19}F_6O_3PNa$, 475.0873; found, 475.0874.

Assay Procedures

Determination of Inhibitor K_i

96-well plates were used to run K_i assays, with reaction volumes of 100 µL per well. 45 µL of water was added to each well, followed by 20 µL of sodium citrate buffer (stock solution: 100 mM sodium citrate, pH 6.2, 0.02% Triton X-100), 5 µL of 20 mM ethylenediamine tetraacetic acid (EDTA) stock solution, 5 µL of 20 mM DL-dithiothreitol (DTT) stock solution, and 10 µL of 1 µM PtpB stock solution. Then 5 µL of the appropriate inhibitor stock solutions, serially diluted 2-fold for a total of 10 different concentrations in DMSO, plus one blank well as a control (DMSO only) was added to the wells and the plate was incubated at room temperature for 5 minutes. The reaction was started by addition of 10 µL of 2 mM pNPP substrate stock, and reaction progress was monitored at 405 nm with continued incubation at ambient temperature. The initial rate data collected was used for the determination of K_i values. The kinetic values were obtained from nonlinear regression of substrate-velocity curves in the presence of various concentrations of inhibitor using the equation $v = V_{max}*[S]/(K_M((1+[I])/ K_i)+[S])$.

References

1. (a) Zhou, B.*, et al. Proc. Natl. Acad. Sci. U.S.A.* **2010**; (b) Beresford, N.*, et al. Biochem. J.* **2007**, *406*, 13-18; (c) Grundner, C.*, et al. Structure* **2005**, *13*, 1625-1634; (d) Singh, R.*, et al. Mol. Microbiol.* **2003**, *50*, 751-762.
2. Soellner, M. B.*, et al. J. Am. Chem. Soc.* **2007**, *129*, 9613-9615.
3. (a) Rye, C. S.; Baell, J. B. *Curr. Med. Chem.* **2005**, *12*, 3127-3141; (b) Zhang, Z.-Y. *Annu. Rev. Pharmacol. Toxicol.* **2002**, *42*, 209-234; (c) Kotoris, C. C.*, et al. Bioorg. Med. Chem. Lett.* **1998**, *8*, 3275-3280.
4. Hu, X. *Bioorg. Med. Chem. Lett.* **2006**, *16*, 6321-6327.
5. (a) Sparks, R. B.*, et al. Bioorg. Med. Chem. Lett.* **2007**, *17*, 736-740; (b) Combs Andrew, P.*, et al. Org. Lett.* **2007**, *9*, 1279-82; (c) Yue, E. W.*, et al. Bioorg. Med. Chem. Lett.* **2006**, *14*, 5833-5849; (d) Combs, A. P.*, et al. J. Med. Chem.* **2006**, *49*, 3774-3789; (e) Ala, P. J.*, et al. J. Biol. Chem.* **2006**, *281*, 32784-32795; (f) Ala, P. J.*, et al. J. Biol. Chem.* **2006**, *281*, 38013-38021; (g) Combs, A. P.*, et al. J. Med. Chem.* **2005**, *48*, 6544-6548.
6. (a) Sun, J.-P.*, et al. J. Biol. Chem.* **2003**, *278*, 12406-12414; (b) Shen, K.*, et al. J. Biol. Chem.* **2001**, *276*, 47311-47319; (c) Sarmiento, M.*, et al. J. Med. Chem.* **2000**, *43*, 146-155; (d) Taing, M.*, et al. Biochemistry* **1999**, *38*, 3793-3803; (e) Yao, Z.-J.*, et al. Bioorg. Med. Chem. Lett.* **1998**, *6*, 1799-1810; (f) Puius, Y. A.*, et al. Proc. Natl. Acad. Sci. U. S. A.* **1997**, *94*, 13420-13425.
7. Han, Y.*, et al. Bioorg. Med. Chem. Lett.* **2008**, *18*, 3200-3205.
8. (a) Miller, G.*, et al. J. Heterocycl. Chem.* **1971**, *8*; (b) Lewis, S.*, et al. J. Heterocycl. Chem.* **1971**, *8*.
9. Billingsley, K.; Buchwald, S. L. *J. Am. Chem. Soc.* **2007**, *129*, 3358-3366.
10. (a) Barder, T. E.*, et al. J. Am. Chem. Soc.* **2005**, *127*, 4685-4696; (b) Barder, T. E.; Buchwald, S. L. *Org. Lett.* **2004**, *6*, 2649-2652.
11. Ogata, T.; Hartwig, J. F. *J. Am. Chem. Soc.* **2008**, *130*, 13848-9.
12. Chiral separation was performed by Lotus Separations, LLC, Washington Road, Frick Lab, Room 201, Princeton, NJ 08544-0000: http://www.lotussep.com/
13. Fernandez, I.; Khiar, N. *Chem. Rev* **2003**, *103*, 3651-3706.
14. (a) Kokubo, C.; Katsuki, T. *Tetrahedron* **1996**, *52*, 13895-13900; (b) Sasaki, H.*, et al. Tetrahedron* **1994**, *50*, 11827-11838; (c) Noda, K.*, et al. Tetrahedron Lett.* **1994**, *35*; (d) Noda, K.*, et al. Tetrahedron* **1994**, *50*, 9609-9618.
15. (a) Hussain, M.*, et al. Bioorg. Med. Chem. Lett.* **2008**, *16*, 6764-6777; (b) Ibrahimi, O. A.*, et al. Bioorg. Med. Chem. Lett.* **2000**, *10*, 457-460; (c) Yokomatsu, T.*, et al. Tetrahedron* **1997**, *53*, 815-822; (d) Solas, D.*, et al. J. Org. Chem* **1996**, *61*, 1537-1539.
16. Baldwin, J. E.*, et al. Tetrahedron* **1981**, *37*, 2181-2189.

Chapter 3. Development of Inhibitors of the *Mycobacterium tuberculosis* Phosphatase PtpA

Abstract: *In this chapter, the design and synthesis of difluoromethylphosphonic acid (DFMP) inhibitor analogs for the Mycobacterium tuberculosis (Mtb) phosphatase PtpA is described. The basic scaffold of the inhibitor was identified from structure-activity relationships established by assaying the O-aryl phosphate substrate library described in Chapter 1, while the phosphate mimetic was chosen based on activity versus PtpA and established cell permeability and activity when incorporated into previously reported inhibitors for the phosphatase PTP1B. The inhibitory activity of each compound was evaluated, and the most potent compound is currently undergoing testing in TB-infected macrophages. This compound was also found to be selective over many common human phosphatases, including reasonable selectivity over a highly homologous human low molecular weight enzyme. Selectivity was also achieved over the other Mtb phosphatase PtpB, providing a chemical tool for further dissection of the biochemical role of PtpA. The majority of this work has been published (Rawls, K. A.; Lang, P. T.; Takeuchi, J.; Imamura, S.; Baguley, T. D.; Grundner, C.; Alber, T.; Ellman, J. A., Bioorg. Med. Chem. Lett.* ***2009****, 19, 6851-6854).*

Authorship

This work was conducted in collaboration with Dr. Jun Takeuchi, Dr. Shinichi Imamura, Dr. P. Therese Lang, Dr. Christoph Grundner, and Tyler Baguley. The inhibitor library was made by Dr. Takeuchi, Dr. Imamura, Tyler Baguley and myself. I performed all substrate and inhibitor assays, Dr. Lang performed all modeling studies and structural overlays, and Dr. Christoph Grundner provided enzyme for inhibitor assays.

Introduction

Mtb PtpA, like PtpB (Chapter 1), is a secreted virulence factor that functions within human macrophages.[1] PtpA has been reported to inhibit phagocytosis and increase actin polymerization in macrophages,[2] and may be a promising target for therapeutic applications. Importantly, this target resides outside the mycobacterial cell wall, which is unusually thick and difficult to penetrate. Due to the cell wall complexity, current antibiotics must be used in tandem, with four or more drugs typically administered simultaneously, and take up to a year to eradicate TB infection. This lengthy treatment time has in turn lead to significant antibacterial resistance, prompting the need for new drugs to both shorten treatment time and address the spread of antibiotic resistance associated with these treatments. Targeting PtpA is a novel strategy that in theory would reduce the ability of TB bacteria to grow and survive in the infected host, thus reducing treatment time. Very few PtpA inhibitors have been reported in the literature thus far, and the novel inhibitors described in this chapter represent some of the most potent and selective compounds reported to date.[3]

Inhibitor Scaffold Identification

Development of inhibitors for PtpA began by screening the same *O*-aryl phosphate library synthesized for PtpB (Chapter 1). Notably, the hit substrates obtained from this screen were distinct from those obtained for PtpB, with substitution not tolerated *ortho* or *meta* to the phosphate group (Figure 3.1). In particular, the biphenyl substrate **3.4**, which was optimized for PtpB, had weak activity versus PtpA (K_M = 2450 μM versus 86 μM for PtpB). Due to its amenability to modification versus compound **3.8** and its improved water solubility compared to compound **3.7**, substrate **3.6** was chosen as the initial focus of further optimization. Because of the modular synthesis of benzamide inhibitor scaffolds, further optimization was carried out at the inhibitor stage.

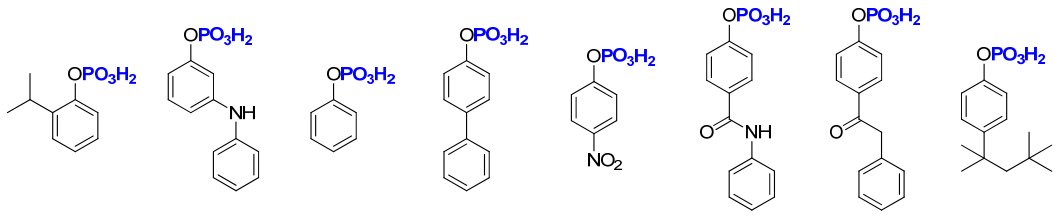

	3.1	3.2	3.3	3.4	3.5	3.6	3.7	3.8
K_M, μM (PtpA)	>4000	>4000	3439	2450	1336	246	219	178

Figure 3.1. Selected hits from the initial *O*-aryl phosphate substrate screen versus PtpA.

Initial Inhibitor Library Synthesis and Evaluation

The isoxazole carboxylic acid inhibitor analog of compound **3.6** was prepared, but found not to inhibit PtpA. Therefore, we turned our attention to the difluoromethylphosphonic acid (DFMP) isostere, which has been investigated extensively in the literature.[4] Despite being dianionic, this isostere has recently been shown to be cell permeable and orally bioavailable in animals when incorporated into nonpeptidic PTP1B inhibitors.[5] Additionally, this isostere is easily synthesized and allows for access to compounds with sufficient potency for X-ray crystallographic analysis. A series of DFMP inhibitors was prepared via modified literature procedures[6] and evaluated against PtpA for initial SAR investigation.

The synthesis of benzamide DFMP inhibitors began with benzyl protection of commercially available 4-iodobenzoic acid **3.9**, followed by zinc and copper-mediated coupling with diethyl(bromodifluoromethyl)phosphonate to afford **3.11**, and hydrogenolysis to remove the benzyl protecting group (Scheme 3.1).[7] A number of amines were incorporated at this stage, followed by deprotection to afford the desired compounds (**3.14**). Using this general method, compounds incorporating a variety of functionality were synthesized for initial SAR investigation.

Scheme 3.1. Synthesis of DFMP benzamide inhibitors

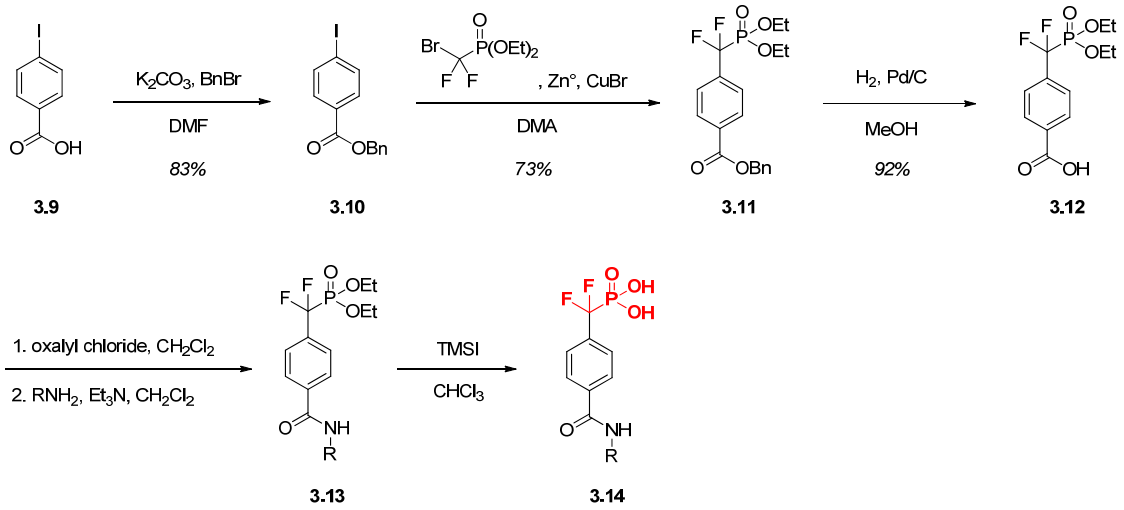

Compounds with other substitution patterns were also investigated for comparison to the benzamide scaffold and to further flush out initial SAR (Scheme 3.2 - Scheme 3.7). Each of these compounds was synthesized via coupling and deprotection strategies similar to that shown in Scheme 3.1, but with different starting materials and coupling partners. Compound **3.17**, for example, was synthesized by coupling 1-bromo-4-iodobenzene with diethyl(bromodifluoromethyl)phosphonate to install the phosphonate ester, followed by deprotection (Scheme 3.2). Alternatively, intermediate **3.16** could be coupled with commercially available 1-methylpyrazole-4-boronic acid pinacol ester, followed by deprotection to arrive at **3.19**.

Scheme 3.2. Synthesis of DFMP inhibitors **3.17** and **3.19**

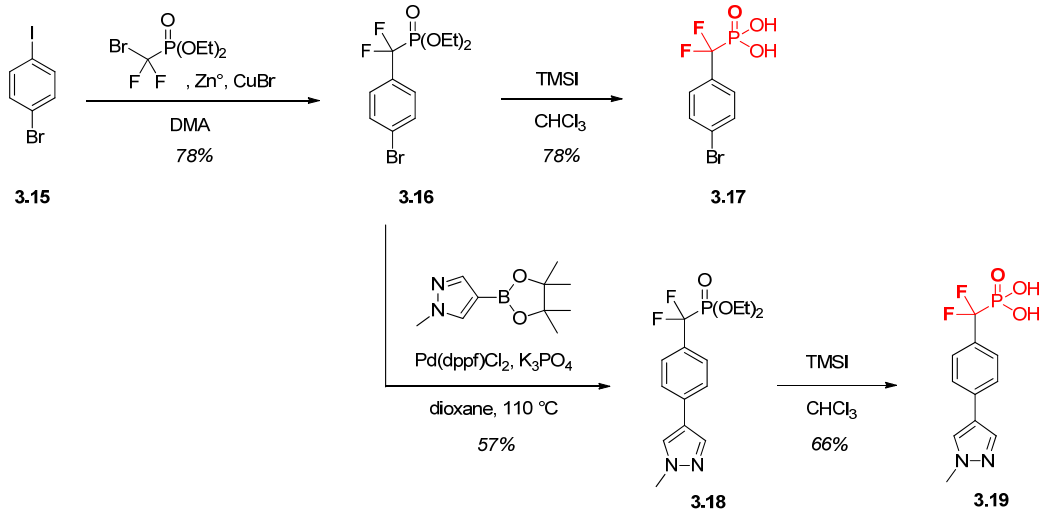

Inhibitor **3.22** was synthesized starting from commercially available 4-iodobiphenyl **3.20** (Scheme 3.3). This compound was first coupled with diethyl(bromodifluoromethyl)phosphonate to afford **3.21**, followed by deprotection to afford the desired inhibitor. Similarly, reverse amide compound **3.26** was synthesized starting by coupling commercially available 1-iodo-4-nitrobenzene **3.23** with diethyl(bromodifluoromethyl)phosphonate, followed by hydrogenation to afford amine **3.25**, addition of benzoyl chloride, and final deprotection to arrive at **3.26** (Scheme 3.4). Alternatively, intermediate **3.24** could be deprotected to afford nitro compound **3.27** (Scheme 3.4). The *meta* substituted benzanilide **3.31** and the extended analog **3.35** were made by coupling commercially available acid chlorides **3.28** or **3.32** with aniline, followed by the same coupling and deprotection sequence used for the other inhibitors (Scheme 3.5 and Scheme 3.6).

Scheme 3.3. Synthesis of DFMP inhibitor **3.22**

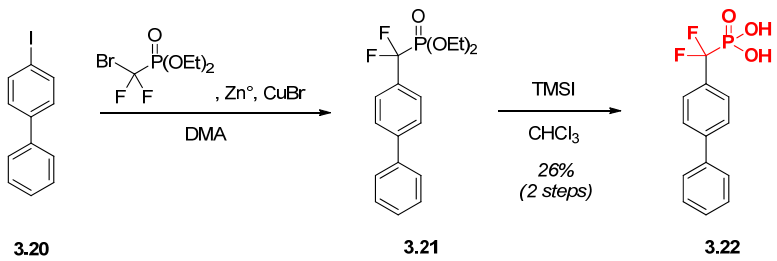

Scheme 3.4. Synthesis of DFMP inhibitors **3.26** and **3.27**

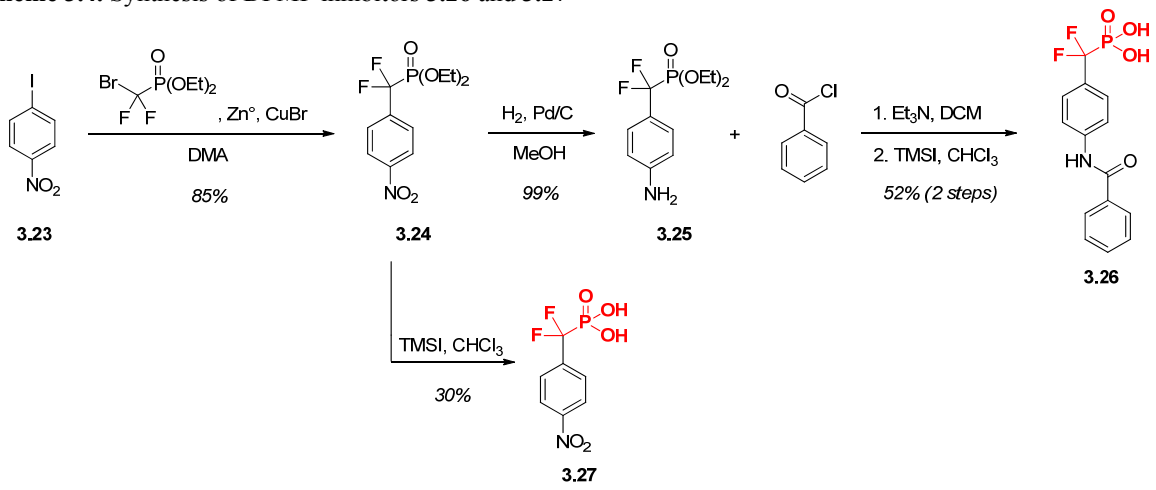

Scheme 3.5. Synthesis of DFMP inhibitor **3.31**

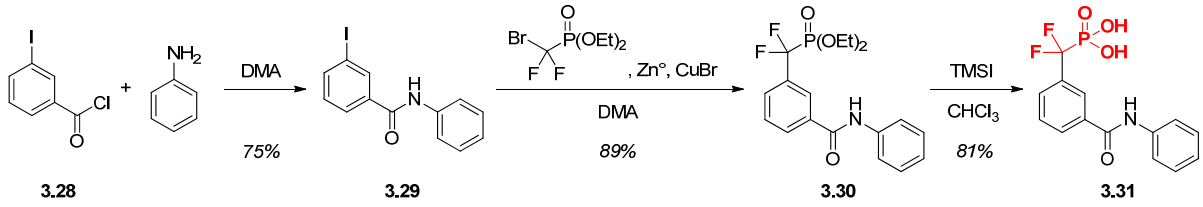

Scheme 3.6. Synthesis of DFMP inhibitor **3.35**

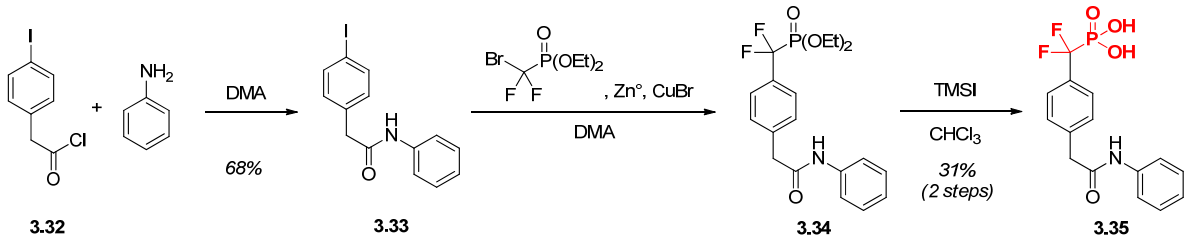

Inhibitors **3.43** and **3.44** were synthesized from common intermediate **3.38** (Scheme 3.7). This intermediate was made by performing a Balz-Schiemann reaction on commercially available **3.36**, followed by fusion of the heterocycle to arrive at **3.38**. Upon treatment of **3.38** with benzyl bromide, the constitutional isomers **3.39** and **3.40** were formed. These compounds were separated via silica gel chromatography and each coupled with diethyl(bromodifluoromethyl)phosphonate, followed by deprotection to arrive at inhibitors **3.43** and **3.44**.

Scheme 3.7. Synthesis of DFMP inhibitors **3.43** and **3.44**

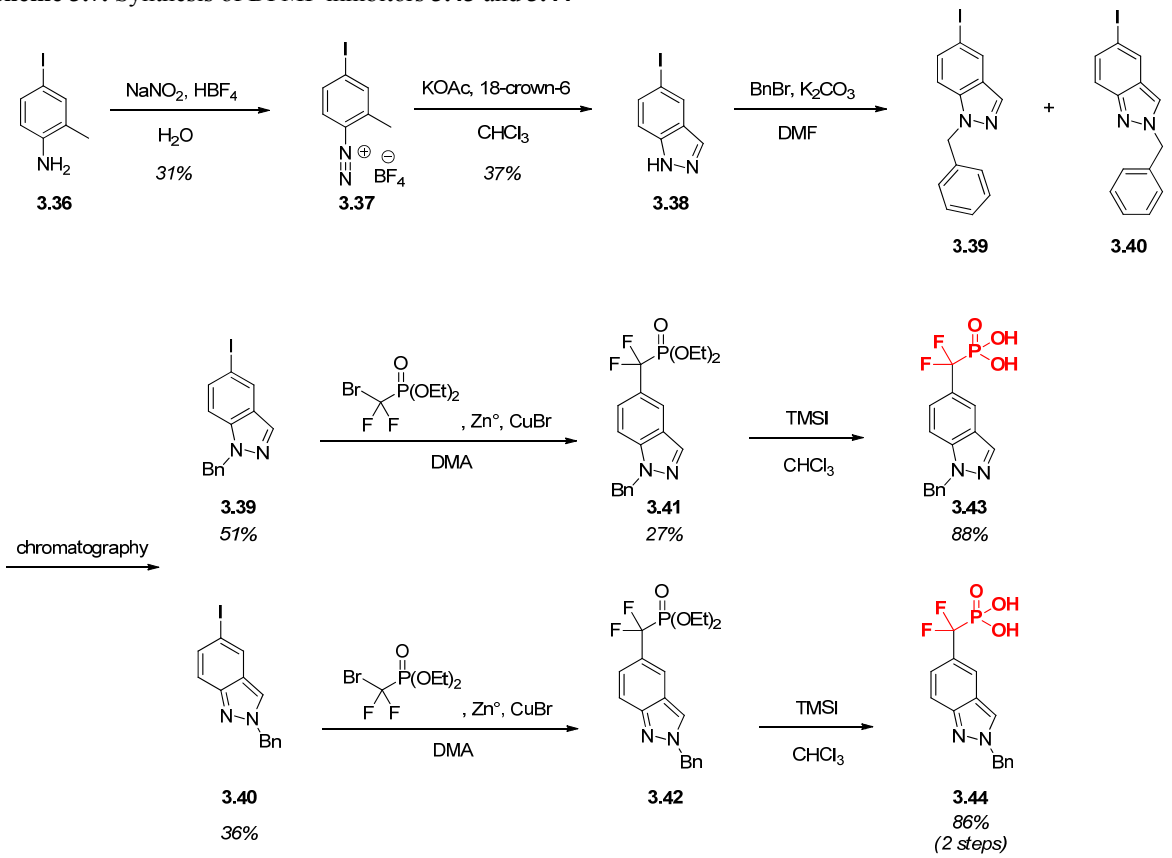

Upon assaying the initial library of DFMP compounds versus PtpA (Table 3.1 and Figure 3.2), benzanilide **3.55**, the direct analog of initial substrate hit **3.6** (Figure 3.1), was identified as the most potent compound (K_i = 24.0 μM). Alkyl substituted benzamide compounds **3.46-3.50** showed minimal inhibitory activity; only alkyl compound **3.52** showed modest affinity, potentially due to the increased acidity of the amide NH as compared to the other alkyl analogs. Electron withdrawing substituents also resulted in compounds with minimal inhibitory activity (**3.45**, **3.17**, and **3.27**), suggesting that the presence of the amide and/or aromatic functionality is important for activity.

The conformation and position of the amide bond and aromatic ring also proved to be important, as evidenced by the minimal inhibitory activity of extended analog **3.35** (K_i >100 μM) and increase in K_i for reverse amide **3.26** (K_i = 65.5 μM) as compared to benzanilide **3.55**. *N*-Heteroaryl benzamide **3.54** (K_i = 33.0 μM), on the other hand, had affinity comparable to **3.55**, while *N*-benzyl substituted **3.53** was about half as potent as **3.55** (K_i = 43.1 μM), likely due to the differing placement of the aromatic ring. Compounds **3.22** and **3.19**, which contain aromatic groups but lack amide functionality, both had poor binding affinity, likely because these compounds are more structurally rigid than **3.55** and additionally lack hydrogen bonding sites. As predicted from the initial substrate library (Figure 3.1), *meta* substituted benzanilide **3.31** and fused compounds **3.43** and **3.44** did not bind efficiently to the enzyme (Figure 3.2). Due to its amenability to further modification versus compound **3.54**, which also bound with reasonable affinity (K_i = 33.0 μM), the benzanilide scaffold **3.55** (K_i = 24.0 μM) was chosen as the focus of further optimization.

Table 3.1. Initial inhibitor screen versus PtpA – *para* substituted analogs

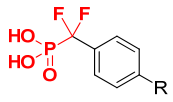

#	R	K_i (μM)	#	R	K_i (μM)	#	R	K_i (μM)
3.45		>100	**3.48**		>100	**3.51**	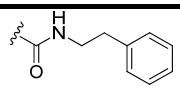	63.6
3.35	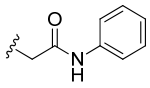	>100	**3.49**	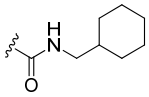	>100	**3.52**	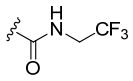	49.7
3.22		>100	**3.17**		92.3	**3.53**	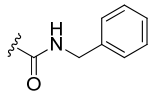	43.1
3.19	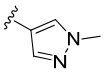	>100	**3.27**		75.4	**3.54**	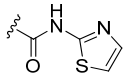	33.0
3.46	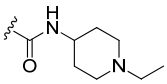	>100	**3.50**	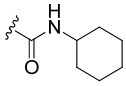	72.4	**3.55**	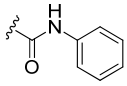	24.0
3.47	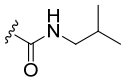	>100	**3.26**	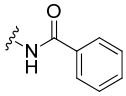	65.5			

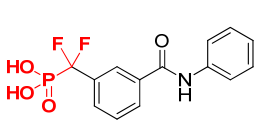

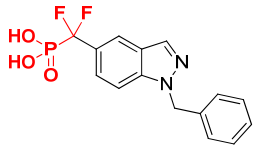

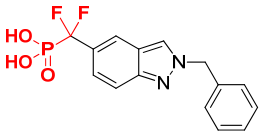

	3.31	**3.43**	**3.44**
K_i, μM (PtpA)	>100	>100	84.4

Figure 3.2. Initial inhibitor screen versus PtpA – other analogs.

Benzanilide Scaffold Optimization and Evaluation

With benzanilide **3.55** (K_i = 24.0 μM) identified as the most potent compound in the initial screen versus PtpA, a focused benzanilide library was synthesized to further flesh out SAR and improve potency (Table 3.2). All focused library members were synthesized via the route previously described for benzamide compounds (Scheme 3.1) using commercially available substituted anilines. Both electron donating and electron withdrawing groups were investigated, but analogs incorporating electron withdrawing groups generally provided more potent compounds (Table 3.2). Substitution at the *meta* and *para* positions (**3.62**, **3.64**, **3.66-3.67**, **3.69**, **3.72-3.75**, and **3.78-3.80**) generally resulted in compounds with a more substantial improvement in affinity than substitution at the *ortho* position (**3.56-3.58**, **3.60-3.61**, and **3.63**), with electron withdrawing substituents resulting in the highest affinity inhibitors (**3.69**, **3.72-3.75**, **3.78-3.79**). Combining favorable elements resulted in compounds **3.68**, **3.70-3.71**, **3.77**, and **3.81-3.88**, all with improved affinity compared to the lead benzanilide **3.55** (K_i = 24.0 μM). The most potent of these compounds, **3.88**, had a K_i of 3.4 ± 0.3 μM.

Table 3.2. Focused benzanilide library screen versus PtpA

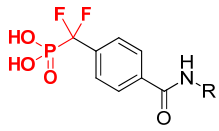

#	R	K_i (μM)	#	R	K_i (μM)	#	R	K_i (μM)
3.56	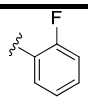	>100	**3.55**		24.0	**3.79**	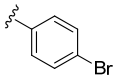	10.3
3.57		92.7	**3.68**	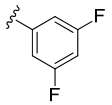	23.6	**3.80**	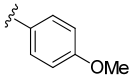	9.9
3.58		93.4	**3.69**	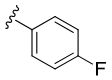	22.7	**3.81**	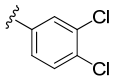	6.7
3.59	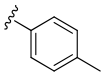	64.6	**3.70**	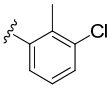	22.3	**3.82**	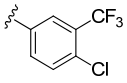	6.0
3.60		62.0	**3.71**	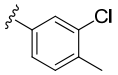	19.4	**3.83**	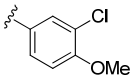	5.5
3.61	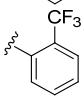	54.8	**3.72**	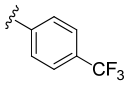	18.5	**3.84**	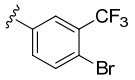	4.9
3.62	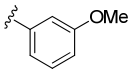	54.4	**3.73**	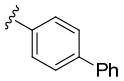	18.5	**3.85**	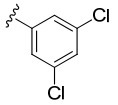	4.7
3.63		44.6	**3.74**	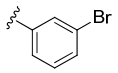	18.2	**3.86**	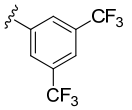	3.4
3.64	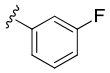	43.8	**3.75**	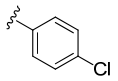	16.9	**3.87**	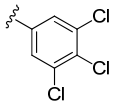	3.0
3.65	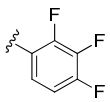	39.5	**3.76**	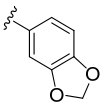	12.7	**3.88**	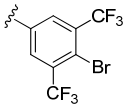	3.4
3.66	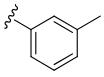	36.0	**3.77**	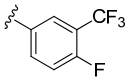	13.4			
3.67	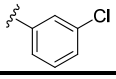	34.5	**3.78**	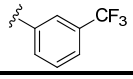	10.7			

To rule out non-specific aggregation-based inhibition,[8] compound **3.88** was tested with two different concentrations of enzyme (300 and 600 nM) and the detergent Triton X-100 (0.004% and 0.01%, Figure 3.3). Gratifyingly, the K_i values remained constant (within experimental error) for each of the parameters examined. Additionally, the inhibition curves for compound **3.88** were found to have a Hill coefficient of h = -1.0 ± 0.1, indicating that the K_i values found were due to inhibitor binding in a single enzyme site rather than non-specific aggregation.

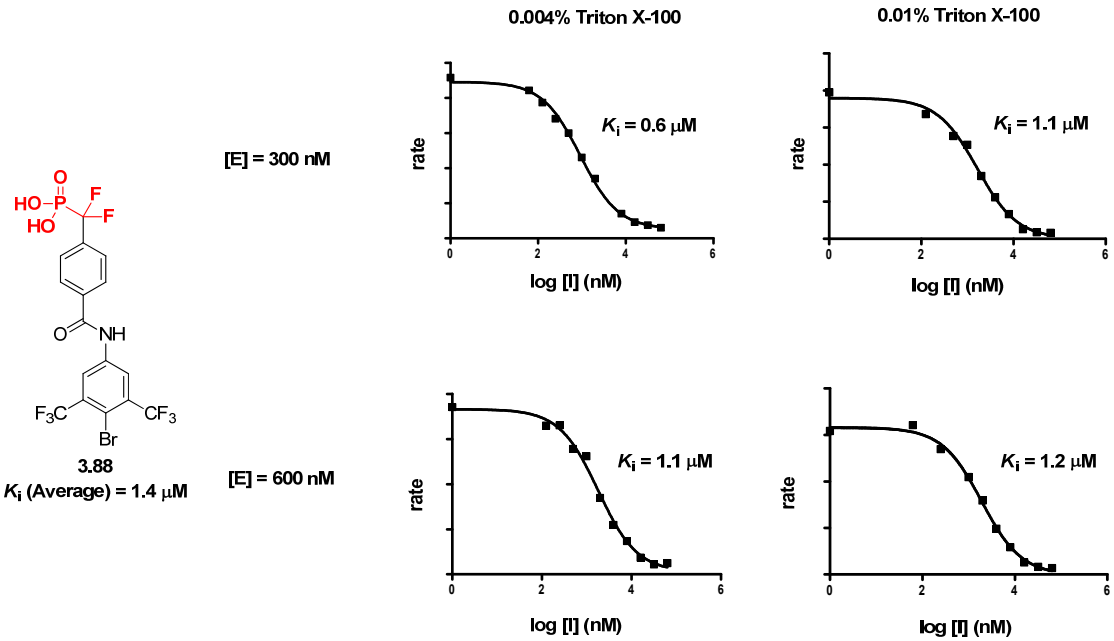

Figure 3.3. K_i values of inhibitor **3.88** at two concentrations of PtpA and Triton X-100 detergent. K_i values were found to be independent of each of these factors, indicating that inhibition is not aggregation-based.

Amide Replacement Analog Synthesis and Evaluation

To investigate the importance of the amide moiety, we synthesized several amide replacement analogs (Scheme 3.8). We reasoned that the position of the amide as well as the availability of a hydrogen bond donor and acceptor may play an important role in binding affinity. We therefore examined removal of the carbonyl (**3.91**), replacement of the nitrogen with other heteroatoms (**3.94**), methylation of the amide nitrogen (**3.96**), replacement of the carbonyl with a sulfonamide moiety (**3.100**), and replacement of the amide with a urea group (**3.102**). Each of these analogs was synthesized in a fashion similar to the benzanilide library (Scheme 3.1), but with different coupling partners. The amide analog **3.91**, for example, was synthesized by reductive amination between 4-iodobenzladehyde and aniline, followed by coupling and deprotection, while the ether analog **3.94** was synthesized by Mitsunobu coupling of 4-iodobenzylalcohol and phenol, followed by the same coupling and deprotection sequence. The methylated analog **3.96** was synthesized by coupling previously described intermediate **3.12** with *N*-methylaniline, followed by deprotection. The requisite iodine compound **3.98** for synthesis of the sulfonamide analog **3.100** was made by coupling commercially available 4-iodobenzenesulfonyl chloride **3.97** with aniline. Finally, the urea derivative was synthesized by addition of previously described amine **3.25** to isocyanate **3.101**, followed by deprotection.

Scheme 3.8. Synthesis of amide replacement analogs **3.91**, **3.94**, **3.96**, **3.100**, and **3.102**

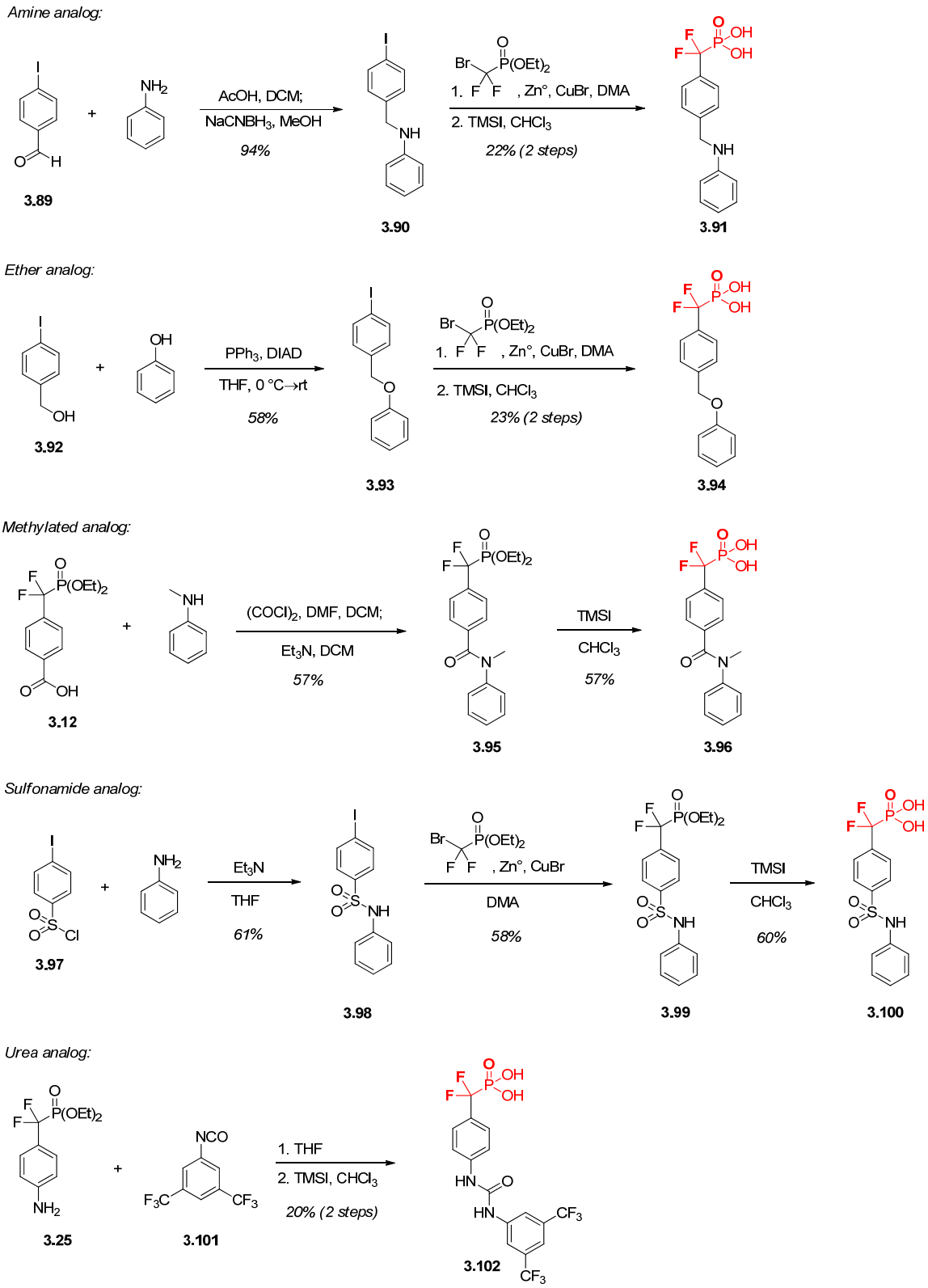

Upon evaluation of each inhibitor versus PtpA (Table 3.3), it was found that methylating the nitrogen (**3.96**), removing the carbonyl (**3.91**), replacing the nitrogen with oxygen in addition to carbonyl removal (**3.94**), and replacing the amide with a sulfonamide moiety (**3.100**) all resulted in loss of activity. This could be due to a loss of hydrogen bonding interactions at either the site of the carbonyl or amide NH, or to changes in entropic penalties of binding associated with increasing the number of rotatable bonds (**3.91** and **3.94**). Interestingly, however, replacing the amide moiety with a urea group resulted in compound **3.102** (K_i = 3.1 μM), with affinity similar to amide analog **3.86** (K_i = 3.3 μM). Although this compound has a different conformation than the amide, it contains additional sites for potential hydrogen bonding, which may explain its similar binding affinity. To further rationalize our *in vitro* SAR, molecular modeling of our PtpA inhibitors was investigated.

Table 3.3. Evaluation of amide replacement analogs versus PtpA

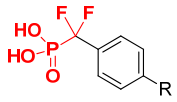

#	R	K_i (μM)	#	R	K_i (μM)
3.91	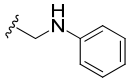	>100	**3.102**	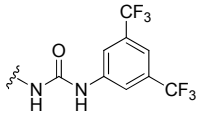	3.1
3.94	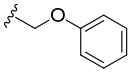	>100	**3.86**	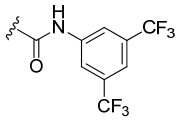	3.3
3.96	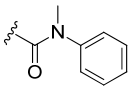	>100	**3.88**	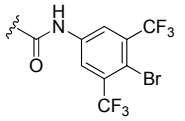	3.4
3.100	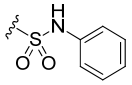	>100			

Modeling Studies

Using AMBER 9[9] and DOCK 6.4,[10] a molecular model of all PtpA inhibitors bound in the active site of a previously published apo crystal structure of PtpA (PDB ID 1U2P)[11] was generated (Figure 3.4). The published crystal structure of apo-PtpA was first relaxed using molecular dynamics in AMBER,[12] followed by docking the compounds into the PtpA active site with DOCK 6.4. Each of the compounds, including the initial lead benzanilide **3.55**, optimized inhibitor **3.88**, and urea inhibitor **3.102**, docked such that the DFMP warhead was in direct contact with the catalytic residues of the protein. Additionally, the scoring function of the docking program ranked the compounds in the same general order observed experimentally (data not shown), indicating that our model is reasonably accurate.

Each of the docked compounds exhibited significant hydrogen bonding interactions with PtpA (Figure 3.4). Nine hydrogen bonds were found between compound **3.55** and PtpA active-site residues, versus seven for compound **3.88** and ten for compound **3.102**. The carbonyl of the urea group of **3.102** is positioned opposite that of **3.55** and **3.88**, allowing for formation of an

additional hydrogen bond with His49 not observed with the other inhibitors. This model of inhibitor-enzyme interactions also predicted varying degrees of pi-stacking with Trp48, the effectiveness of which depended on the orientation of the aryl ring and its resulting ability to overlap with the indole ring of Trp48. This binding mode was not unexpected, since Trp pi-stacking has been previously observed in inhibitor-enzyme complexes.[13] Further development of SAR around the urea scaffold could lead to compounds with improved affinity compared to benzanilide **3.88**. Modifications to further improve potency could include introduction of functionality that takes advantage of hydrogen bonding with His49 while also improving pi-stacking efficiency with Trp48, as well as introduction of functionality off of the pendant anilide ring to extend into an adjacent unfilled enzyme pocket (Figure 3.5).

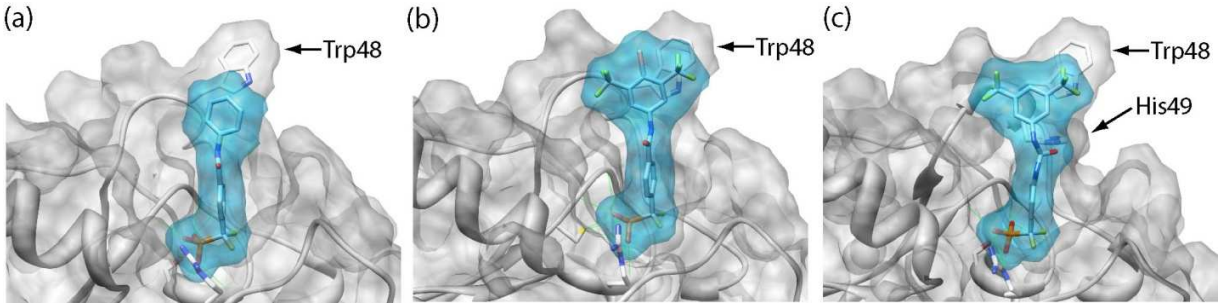

Figure 3.4. Model of (a) parent benzanilide **3.55**, (b) optimized benzanilide **3.88**, and (c) extended urea inhibitor **3.102** docked in the active site of PtpA (PDB ID 1U2P)[11] using DOCK 6.4.[10] Hydrogen bonds (green lines) between each inhibitor and active site residues are shown. His49 is emphasized to show H-bonding with compound **3.102**, and Trp48 is emphasized to show pi-stacking interactions with each inhibitor.

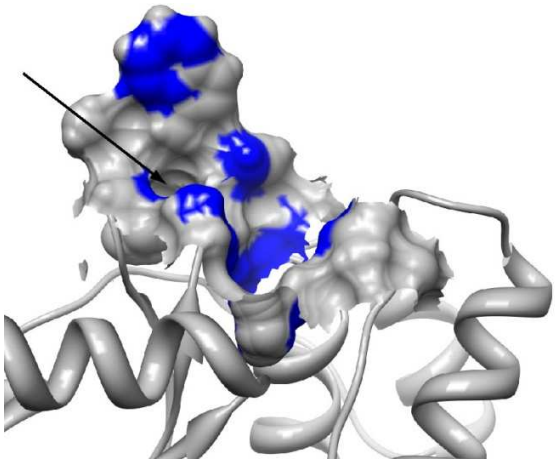

Figure 3.5. PtpA binding pocket with only inhibitor **3.88**-enzyme contact points shown (blue). The arrow indicates the position of an unfilled enzyme pocket adjacent to the docked inhibitor.[14]

Inhibitor Selectivity Profile

Due to the high structural homology of PTP active sites, achieving inhibitor selectivity is a major challenge.[15] Compound **3.88**, however, was found to be highly selective (>70-fold) when tested against a panel of tyrosine and dual-specificity phosphatases, including TC-Ptp, an essential human phosphatase[16] (Table 3.4). This compound was also 11-fold selective for *Mtb*

PtpA versus human low molecular weight phosphatase, HCPtpA, which shows 38% sequence identity to the *Mtb* enzyme (Figure 3.6).[11] Compound **3.88** also did not inhibit *Mtb* PtpB, which was not surprising given the large structural differences between PtpA and PtpB, particularly in the variable loop region (Figure 3.6). This selectivity should enable the use of this inhibitor to further dissect the biochemical role of *Mtb* PtpA.

Table 3.4. Selectivity profile of inhibitor **3.88** versus a panel of human and mycobacterial phosphatases

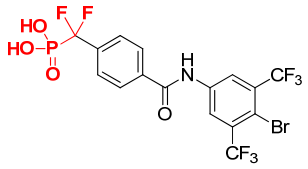

3.88

	Mtb PTPs		Human PTPs					
	PtpA	**PtpB**	**PTP1B**	**TC-Ptp**	**VHR**	**CD45**	**LAR**	**HCPtpA**
K_i (μM)	3.4	>100	>100	>100	>100	>100	>100	14.8
Selectivity	--	>70	>70	>70	>70	>70	>70	11

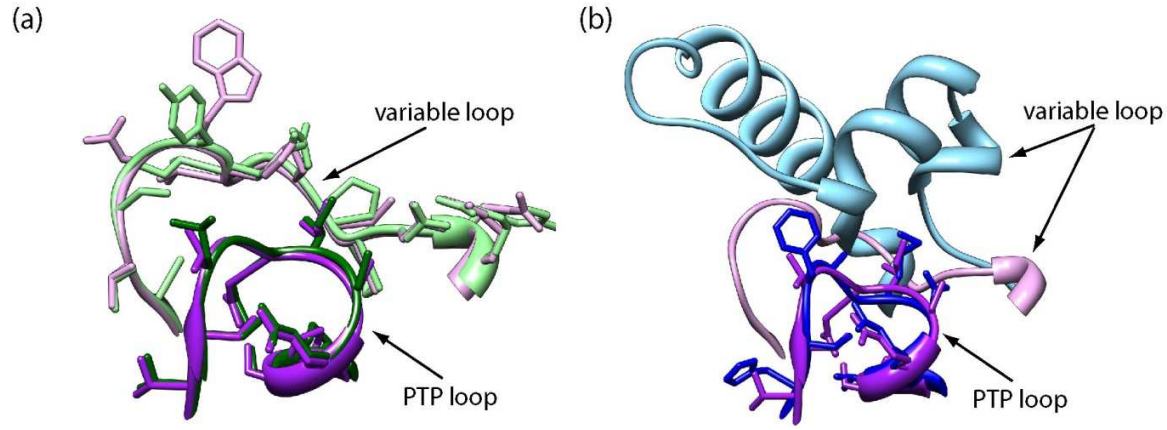

Figure 3.6. Structural overlay of *Mtb* PtpA (purple) with (a) HCPtpA (green) and (b) *Mtb* PtpB (blue), focusing on the PTP and variable loop regions.[14]

Conclusions

In conclusion, we have developed inhibitors with low micromolar affinity for PtpA based on the benzanilide scaffold **3.55**. SAR studies resulted in compound **3.88**, which represents the most potent and selective PtpA inhibitor reported in the literature to date.[3a,b] Molecular modeling highlighted the importance of pi-stacking with Trp48, and hydrogen bonding with active-site residues and His49 for high-affinity binding. Compound **3.88** was additionally found to be over 70-fold selective for PtpA versus a panel of human phosphatases and 11-fold selective over the closely related human homologue HCPtpA. This compound was additionally selective over the other *Mtb* phosphatase PtpB, which, in conjunction with the potent and selective isoxazole inhibitor developed for PtpB (Chapter 1), provides a set of chemical tools for further dissection of the biochemical roles of each of the *Mtb* enzymes, in addition to examination of

potential synergistic effects. Inhibitor **3.88** is currently being evaluated in TB-infected cells, and if found to be cell permeable, will be further evaluated in animal models.

Experimental

General Synthetic Methods

Unless otherwise noted, all reagents were obtained from commercial suppliers and used without further purification. Tetrahydrofuran (THF), dichloromethane (CH_2Cl_2), toluene, and diethyl ether (Et_2O) were dried over alumina under a nitrogen atmosphere. Solvents used for reactions set up in a nitrogen-filled Braun inert atmosphere box, including THF and toluene, were additionally degassed with three consecutive freeze pump thaw cycles and stored over 3Å molecular sieves. Methanol was dried over calcium hydride under a nitrogen atmosphere. All reactions, unless otherwise stated, were performed under inert atmosphere using syringe, cannula, and Schlenk techniques, or set up in a nitrogen-filled Braun inert atmosphere box, with flame or oven-dried glassware. All ^{1}H, ^{13}C, ^{19}F, and ^{31}P NMR spectra were measured with a Bruker DRX-500, AVB-400, AVQ-400 or AV-300 spectrometer. NMR chemical shifts are reported in ppm relative to 1,2-difluorobenzene (-138.9) for ^{19}F NMR and trimethylphosphate (3.0) for ^{31}P NMR. Mass spectrometry (HRMS) was carried out by the University of California, Berkeley Mass Spectrometry Facility.

Synthesis and Analytical Data for DFMP Inhibitors

*Synthesis and Analytical Data for Benzamide Inhibitor **3.88***

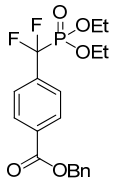

3.11

Compound 3.11. Compound **3.11** was synthesized according to modified literature procedures.[7] A solution of diethyl(bromodifluoromethyl)phosphonate (13.80 g, 44.0 mmol) in DMA (20 mL) in a flame-dried 50 mL flask under an N_2 atmosphere was slowly added to a stirred suspension of activated Zn dust (2.88 g, 44 mmol) in DMA (20 mL) in a flame-dried 250 mL flask under an N_2 atmosphere at 60 °C via cannula addition. After addition was complete, the resulting mixture was sonicated at room temperature for 3 h, followed by addition of CuBr (6.31 g, 44 mmol) in one portion. A solution of benzyl 4-iodobenzoate **3.10**[7] (5.41 g, 16 mmol) in DMA (5 mL) was added dropwise, and the resulting mixture was stirred for 38 h at room temperature. The mixture was diluted with water (50 mL) and ether (50 mL), and was then passed through Celite. The organic layer was separated, washed with brine (1 x 100 mL), dried over anhydrous $MgSO_4$ (s), and filtered. The solvent was removed under reduced pressure to afford crude product, which was then purified via column chromatography to yield **3.11** as a colorless oil (4.68 g, 73% yield). **Analytical data.** ^{1}H NMR (400 MHz, $CDCl_3$): δ 8.16 (d, J = 8.0 Hz, 2H), 7.70 (d, J = 8.0 Hz, 2H), 7.46-7.36 (m, 5H), 5.39 (s, 2H), 4.26-4.11 (m, 4H), 1.30 (t, J = 7.2 Hz, 6H); ^{19}F NMR (376 MHz, $CDCl_3$): δ -108.59 (d, J_{PF} = 109 Hz); ^{31}P NMR (162 MHz,

$CDCl_3$): δ 5.76 (t, J_{PF} = 109 Hz). HRMS-FAB (*m/z*): $[M + H]^+$ calcd for $C_{19}H_{22}F_2O_5P$, 399.1172; found, 399.1177.

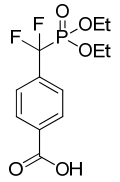

3.12

Compound 3.12. Comopund **3.12** was synthesized by modified literature procedures.[7] A solution of **3.11** (2.50 g, 6.28 mmol) in MeOH (5mL) was added to 10% Pd/C (835 mg, ca. 50% wet) in MeOH (30mL). The reaction mixture was stirred for 16 h under H_2 atmosphere. The catalyst was then removed by filtration through Celite, and the solvent was removed under reduced pressure to give crude **3.12**. The crude product was purified by recrystallization from EtOAc/hexanes to yield **3.12** as a white powder (3.67 g, 86% yield). **Analytical data.** ^{1}H NMR (400 MHz, CD_3OD): δ 8.15 (d, *J* = 8.0 Hz, 2H), 7.70 (d, *J* = 8.0 Hz, 2H), 4.26-4.13 (m, 4H), 1.31 (t, *J* = 7.2 Hz, 6H); ^{19}F NMR (376 MHz, CD_3OD): δ -111.51 (d, J_{PF} = 109 Hz); ^{31}P NMR (162 MHz, CD_3OD): δ 5.73 (t, J_{PF} = 109 Hz). HRMS-FAB (*m/z*): $[M + Na]^+$ calcd for $C_{12}H_{15}F_2O_5PNa$, 331.0523; found, 331.0531.

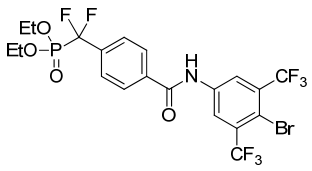

3.103

Compound 3.103. To a solution of **3.12** (98 mg, 0.32 mmol) in dry CH_2Cl_2 (3 mL) in a flame-dried 10 mL flask under an N_2 atmosphere was added oxalyl chloride (55 µL, 0.64 mmol) and a catalytic amount of DMF. The reaction mixture was stirred for 1 h at room temperature, followed by removal of the solvent under reduced pressure, and drying under high vacuum. The resulting acid chloride was dissolved in dry CH_2Cl_2 (2 mL) under an N_2 atmosphere and slowly added to a solution of 4-bromo-3,5-bis(trifluoromethyl)aniline (114 mg, 0.37 mmol) and triethylamine (67 µL, 0.48 mmol) in dry CH_2Cl_2 (3 mL) in a flame-dried 25 mL flask under an N_2 atmosphere. The reaction mixture was stirred at room temperature for 18 h. The solvent was evaporated under reduced pressure to afford crude **3.103**. The crude product was purified via column chromatography to give **3.103** as a white solid (96 mg, 50% yield). **Analytical data**. ^{1}H NMR (400 MHz, CD_3OD): δ 9.07 (br s, 1H), 8.40 (s, 2H), 7.92 (d, *J* = 8.2 Hz, 2H), 7.65 (d, *J* = 7.8 Hz, 2H), 4.29-4.16 (m, 4H), 1.33 (t, *J* = 7.1 Hz, 6H); ^{19}F NMR (376 MHz, CD_3OD): δ -63.47 (s), -108.27 (d, J_{PF} = 114 Hz); ^{31}P NMR (162 MHz, CD_3OD): δ 4.86 (t, J_{PF} = 114 Hz). MS-ESI (*m/z*): $[M + H]^+$ calcd for $C_{20}H_{18}BrF_8NO_4P$, 596.9951; found, 598.0 and 599.0.

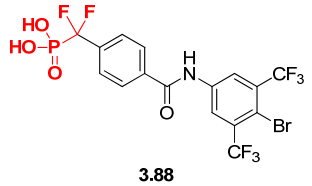

3.88

Compound 3.88. To a stirred solution of **3.103** (35 mg, 0.06 mmol) in $CHCl_3$ (3 mL) was added TMSI (33 µL, 0.22 mmol). The mixture was stirred for 3 h at room temperature. Volatiles were removed under reduced pressure and the residue was dissolved in MeOH (3 mL) and stirred at room temperature for 18 h. The solvent was removed under reduced pressure to give crude **3.88**. The crude product was purified by recrystallization from EtOAc/hexanes to yield **3.88** as a white powder (13 mg, 41% yield). **Analytical data.** ^{1}H NMR (400 MHz, CD_3OD): δ 8.54 (s, 2H), 8.06 (d, J = 8.0 Hz, 2H), 7.77 (d, J = 8.0 Hz, 2H); ^{19}F NMR (376 MHz, CD_3OD): δ -64.40, -112.46 (d, J_{PF} = 109 Hz); ^{31}P NMR (162 MHz, CD_3OD): δ 2.55 (t, J_{PF} = 109 Hz). HRMS-FAB (*m/z*): $[M + H]^+$ calcd for $C_{16}H_{10}{}^{79}BrF_8NO_4P$, 541.9403; found, 541.9406.

General Synthesis of Other Benzamide Inhibitors

Benzamide inhibitors **3.46-3.87** were synthesized by following the general procedures described for the synthesis of **3.88**, using commercially available anilines or amines. Compound **3.45** was synthesized by subjecting intermediate **3.12** to the procedure described for deprotection of **3.103**.

Analytical Data for Selected Benzamide Inhibitors

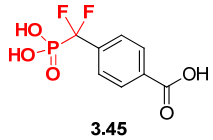

3.45

Compound 3.45. ^{1}H NMR (CD_3OD): δ 7.93 (d, 2H, J = 7.4 Hz), 7.72 (d, 2H, J = 7.4 Hz); ^{19}F NMR (CD_3OD): δ -110.78 (d, J_{FP} = 111 Hz); ^{31}PNMR (CD_3OD): δ 3.38 (br m). HRMS-ESI (*m/z*): $[M - H]^-$ calcd for $C_8H_6O_5F_2P$, 250.9926; found, 250.9916.

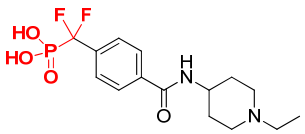

3.46

Compound 3.46. ^{1}H NMR (400 MHz, CD_3OD): δ 7.85 (d, 2H, J = 8.3 Hz), 7.70 (d, 2H, J = 8.3 Hz), 4.13 (m, 1H), 4.03 (quintet, 2H, J = 7.1 Hz), 3.43 (br m, 2H), 3.12 (br m, 2H), 2.17 (br m, 2H), 3.79 (br m, 2H), 1.24 (t, 3H, J = 7.1 Hz); ^{19}F NMR (376 MHz, CD_3OD): δ -108.82 (d, J_{FP} = 99 Hz); ^{31}P NMR (162 MHz, CD_3OD): δ 3.20 (br t, J_{PF} = 99 Hz). HRMS-ESI (*m/z*): $[M + H]^+$ calcd for $C_{15}H_{22}O_4N_2F_2P$, 363.1280; found, 363.1273.

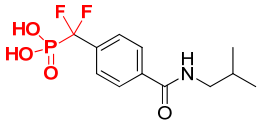

3.47

Compound 3.47. ^{1}H NMR (400 MHz, CD_3OD): δ 7.89 (d, 2H, J = 8.3 Hz), 7.69 (d, 2H, J = 8.3 Hz), 3.20 (d, 2H, J = 6.9 Hz), 1.93 (nonet, 1H, J = 6.9 Hz), 0.96 (d, 6H, J = 6.9 Hz); ^{19}F NMR (376 MHz, CD_3OD): δ -110.60 (d, J_{FP} = 110 Hz); ^{31}P NMR (162 MHz, CD_3OD): δ 4.37 (br t, J_{PF} = 112 Hz). HRMS-ESI (*m/z*): $[M + H]^+$ calcd for $C_{12}H_{17}O_4NF_2P$, 308.0858; found, 308.0852.

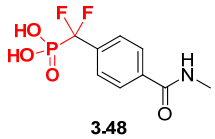

3.48

Compound 3.48. ^{1}H NMR (400 MHz, CD_3OD): δ 7.89 (d, 2H, J = 8.1 Hz), 7.68 (d, 2H, J = 8.1 Hz), 3.09 (s, 3H); ^{19}F NMR (376 MHz, CD_3OD): δ -110.67 (d, J_{FP} = 110 Hz); ^{31}P NMR (162 MHz, CD_3OD): δ 4.34 (br t, J_{PF} = 110 Hz). HRMS-ESI (*m/z*): $[M + H]^+$ calcd for $C_9H_{11}O_4NF_2P$, 266.0388; found, 266.0385.

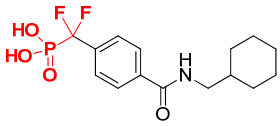

3.49

Compound 3.49. ^{1}H NMR (400 MHz, CD_3OD): δ 7.89 (d, 2H, J = 7.1 Hz), 7.69 (d, 2H, J = 7.1 Hz), 3.22 (d, 2H, J = 6.9 Hz), 3.77 (br m, 4H), 3.71-3.62 (br m, 2H), 1.34-1.18 (br m, 3H), 1.02 (br m, 2H); ^{19}F NMR (376 MHz, CD_3OD): δ -110.65 (d, J_{FP} = 109 Hz); ^{31}P NMR (162 MHz, CD_3OD): δ 4.63 (br m). HRMS-ESI (*m/z*): $[M + H]^+$ calcd for $C_{15}H_{21}O_4NF_2P$, 348.1171; found, 348.1166.

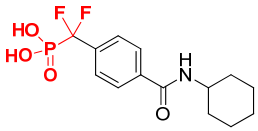

3.50

Compound 3.50. ^{1}H NMR (400 MHz, CD_3OD): δ 7.87 (d, 2H, J = 8.0 Hz), 7.67 (d, 2H, J = 8.0 Hz), 3.88-3.84 (m, 1H), 1.95 (br m, 2H), 3.81 (br m, 2H), 3.68 (br m, 1H), 3.45-1.29 (br m, 4H), 1.27-1.19 (br m, 1H); ^{19}F NMR (376 MHz, CD_3OD): δ -110.63 (d, J_{FP} = 110 Hz); ^{31}P NMR (162 MHz, CD_3OD): δ 4.72 (br m). HRMS-ESI (*m/z*): $[M + H]^+$ calcd for $C_{14}H_{19}O_4NF_2P$, 334.1014; found, 334.1020.

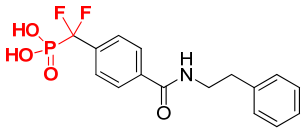

3.51

Compound 3.51. ^{1}H NMR (400 MHz, CD_3OD): δ 7.94 (d, 2H, J = 8.2 Hz), 7.84 (d, 2H, J = 8.2 Hz), 7.34-7.17 (m, 5H), 3.60 (t, 2H, J = 7.4 Hz), 2.91 (t, 2H, 7.4 Hz); ^{19}F NMR (376 MHz, CD_3OD): δ -110.73 (d, J_{FP} = 112 Hz); ^{31}P NMR (162 MHz, CD_3OD): δ 4.49 (br m). HRMS-ESI (*m/z*): $[M + H]^+$ calcd for $C_{16}H_{17}O_4NF_2P$, 356.0858; found, 356.0865.

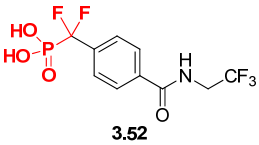

3.52

Compound 3.52. ^{1}H NMR (400 MHz, CD_3OD): δ 7.93 (d, 2H, J = 7.6 Hz), 7.72 (d, 2H, J = 8.0 Hz), 4.10 (q, 2H, J_{HF} = 9.2 Hz); ^{19}F NMR (376 MHz, CD_3OD): δ -72.92 (t, J_{FH} = 9.4 Hz),

-110.78 (d, J_{FP} = 109 Hz); ^{31}P NMR (162 MHz, CD_3OD): δ 4.48 (br m). HRMS-ESI (*m/z*): [M - H]$^-$ calcd for $C_{10}H_8O_4NF_5P$, 332.0117; found, 332.0105.

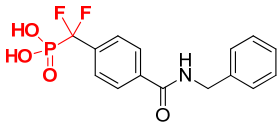

3.53

Compound 3.53. ^{1}H NMR (400 MHz, CD_3OD): δ 7.93 (d, 2H, *J* = 8.1 Hz), 7.70 (d, 2H, *J* = 8.1 Hz), 7.36-7.22 (m, 5H), 4.58 (s, 2H); ^{19}F NMR (376 MHz, CD_3OD): δ -110.57 (d, J_{FP} = 109 Hz); ^{31}P NMR (162 MHz, CD_3OD): δ 4.09 (br t, J_{PF} = 109 Hz). HRMS-ESI (*m/z*): [M + H]$^+$ calcd for $C_{15}H_{15}O_4NF_2P$, 342.0701; found, 342.0712.

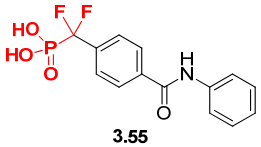

3.55

Compound 3.55. ^{1}H NMR (400 MHz, CD_3OD): δ 8.02 (d, *J* = 8.0 Hz, 2H), 7.74 (d, *J* = 8.0 Hz, 2H), 7.69 (d, *J* = 8.0 Hz, 2H), 7.36 (t, *J* = 7.6 Hz, 2H), 7.15 (t, *J* = 7.6 Hz, 1H); ^{19}F NMR (376 MHz, CD_3OD): δ -112.39 (d, J_{PF} = 109 Hz); ^{31}P NMR (162 MHz, CD_3OD): δ 2.65 (t, J_{PF} = 109 Hz). HRMS-FAB (*m/z*): [M + Na]$^+$ calcd for $C_{14}H_{12}F_2NO_4PNa$, 350.0370; found, 350.0366.

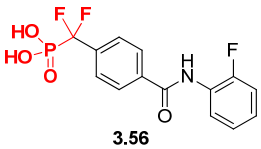

3.56

Compound 3.56. ^{1}H NMR (400 MHz, CD_3OD): δ 8.03 (d, *J* = 7.1 Hz, 2H), 7.80-7.71 (m, 3H), 7.29-7.14 (m, 3H); ^{19}F NMR (376 MHz, CD_3OD): δ -110.70 (d, J_{PF} = 111 Hz), -124.20; ^{31}P NMR (162 MHz, CD_3OD): δ 4.27 (t, J_{PF} = 102 Hz). MS-ESI (*m/z*): [2M + H]$^+$ calcd for $C_{28}H_{23}F_6N2O_8P_2$, 691.0760; found, 691.0.

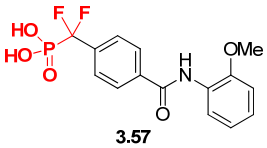

3.57

Compound 3.57. ^{1}H NMR (400 MHz, CD_3OD): 8.02 (d, *J* = 8.0 Hz, 2H), 7.97 (d, *J* = 8.0 Hz, 1H), 7.75 (d, *J* = 8.0 Hz, 2H), 7.19 (t, *J* = 8.0 Hz, 1H), 7.07 (d, *J* = 8.0 Hz, 1H), 6.98 (t, *J* = 8.0 Hz, 1H), 3.91 (s, 3H); ^{19}F NMR (376 MHz, CD_3OD): -112.43 (d, J_{PF} = 109 Hz); ^{31}P NMR (162 MHz, CD_3OD): 2.67 (t, J_{PF} = 109 Hz); HRMS-ESI (*m/z*): [M + 2Na - H]$^+$ calcd for $C_{15}H_{13}F_2NO_5PNa_2$, 402.0295; found, 402.0302.

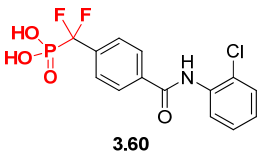

3.60

Compound 3.60. ^{1}H NMR (400 MHz, CD_3OD): δ 8.02 (d, J = 8.0 Hz, 2H), 7.89 (t, J = 2.0 Hz, 1H), 7.75 (d, J = 8.0 Hz, 2H), 7.60 (dd, J = 8.0, 2.0 Hz, 1H), 7.34 (d, J = 8.0 Hz, 1H), 7.15 (dd, J = 8.0, 2.0 Hz, 1H); ^{19}F NMR (376 MHz, CD_3OD): δ -112.44 (d, J_{PF} = 109 Hz). ^{31}P NMR (162 MHz, CD_3OD): δ 2.64 (t, J_{PF} = 109 Hz). HRMS-EI (m/z): $[M + H]^+$ calcd for $C_{14}H_{12}{}^{35}ClF_2NO_4P$, 362.0160; found, 362.0169.

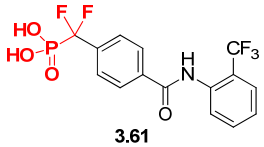

3.61

Compound 3.61. ^{1}H NMR (400 MHz, CD_3OD): δ 8.03 (d, J = 8.0 Hz, 2H), 7.78-7.71 (m, 4H), 7.62-7.60 (m, 1H), 7.54-7.52 (m, 1H); ^{19}F NMR (376 MHz, CD_3OD): δ -61.52, -110.88 (d, J_{PF} = 109 Hz); ^{31}P NMR (162 MHz, CD_3OD): δ 2.60 (t, J_{PF} = 109 Hz). HRMS-FAB (*m/z*): $[M + H]^+$ calcd for $C_{15}H_{12}F_5NO_4P$, 396.0424; found, 396.0424.

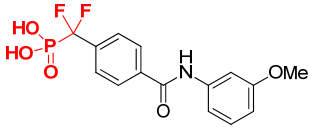

3.62

Compound 3.62. ^{1}H NMR (400 MHz, CD_3OD): 8.01 (d, J = 8.0 Hz, 2H), 7.74 (d, J = 8.0 Hz, 1H), 7.41 (s, 1H), 7.26-7.24 (m, 2H), 6.74-6.72 (m, 1H), 3.81 (s, 3H); ^{19}F NMR (376 MHz, CD_3OD): -112.28 (d, J_{PF} = 109 Hz); ^{31}P NMR (162 MHz, CD_3OD): 2.49 (t, J_{PF} = 109 Hz); HRMS-ESI (*m/z*): $[M + H]^+$ calcd for $C_{15}H_{15}F_2NO_5P$, 358.0655; found, 358.0663.

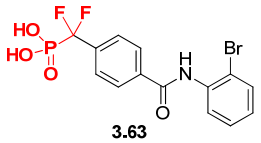

3.63

Compound 3.63. ^{1}H NMR (400 MHz, CD_3OD): δ 8.07 (d, J = 8.0 Hz, 2H), 7.77 (d, J = 8.0 Hz, 2H), 7.72-7.69 (m, 2H), 7.43 (t, J = 7.6 Hz, 1H), 7.21 (d, J = 7.6 Hz, 1H); ^{19}F NMR (376 MHz, CD_3OD): δ -112.45 (d, J_{PF} = 109 Hz); ^{31}P NMR (162 MHz, CD_3OD): δ 2.64 (t, J_{PF} = 109 Hz). HRMS-FAB (*m/z*): $[M + H]^+$ calcd for $C_{14}H_{12}{}^{79}BrF_2NO_4P$, 405.9655; found, 405.9666.

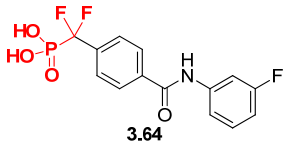

3.64

Compound 3.64. ^{1}H NMR (400 MHz, CD_3OD): δ 8.02 (d, J = 8.0 Hz, 2H), 7.75 (d, J = 8.0 Hz, 2H), 7.69-7.66 (m, 1H), 7.45 (d, J = 8.0 Hz, 1H), 7.38-7.32 (m, 1H), 6.88 (t, J = 8.0 Hz, 1H); ^{19}F NMR (376 MHz, CD_3OD): δ -112.41 (d, J_{PF} = 109 Hz), -115.00; ^{31}P NMR (162 MHz, CD_3OD): δ 2.80 (t, J_{PF} = 109 Hz). HRMS-FAB (*m/z*): $[M + H]^+$ calcd for $C_{14}H_{10}F_3NO_4P$, 344.0300; found, 344.0292.

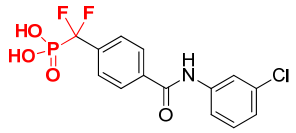

3.67

Compound 3.67. ^{1}H NMR (400 MHz, CD_3OD): δ 8.02 (d, J = 8.0 Hz, 2H), 7.89 (t, J = 2.0 Hz, 1H), 7.75 (d, J = 8.0 Hz, 2H), 7.60 (dd, J = 8.0, 2.0 Hz, 1H), 7.34 (d, J = 8.0 Hz, 1H), 7.15 (dd, J = 8.0, 2.0 Hz, 1H); ^{19}F NMR (376 MHz, CD_3OD): δ -112.44 (d, J_{PF} = 109 Hz); ^{31}P NMR (162 MHz, CD_3OD): δ 2.64 (t, J_{PF} = 109 Hz). HRMS-EI (*m/z*): $[M + H]^+$ calcd for $C_{14}H_{12}{}^{35}ClF_2NO_4P$, 362.0160; found, 362.0169.

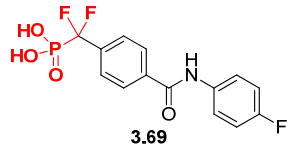

3.69

Compound 3.69. ^{1}H NMR (400 MHz, CD_3OD): δ 8.01 (d, J = 8.0 Hz, 2H), 7.74 (d, J = 8.0 Hz, 2H), 7.70 (dd, J = 8.8, 4.8 Hz, 2H), 7.10 (t, J = 8.8 Hz, 2H); ^{19}F NMR (376 MHz, CD_3OD): δ -112.38 (d, J_{PF} = 109 Hz), -120.72; ^{31}P NMR (162 MHz, CD_3OD): δ 2.71 (t, J_{PF} = 109 Hz). HRMS-FAB (*m/z*): $[M + Na]^+$ calcd for $C_{14}H_{10}F_3NO_4PNa$, 390.0095; found, 390.0102.

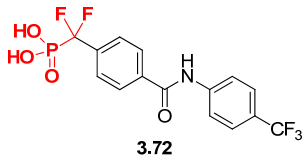

3.72

Compound 3.72. ^{1}H NMR (400 MHz, CD_3OD): δ 8.03 (d, J = 8.0 Hz, 2H), 7.94 (d, J = 8.0 Hz, 2H), 7.76 (d, J = 8.0 Hz, 2H), 7.66 (d, J = 8.0 Hz, 2H); ^{19}F NMR (376 MHz, CD_3OD): δ -64.41, -112.37 (d, J_{PF} = 109 Hz); ^{31}P NMR (162 MHz, CD_3OD): δ 2.59 (t, J_{PF} = 109 Hz). HRMS-FAB (*m/z*): $[M + H]^+$ calcd for $C_{15}H_{12}F_5NO_4P$, 396.0424; found, 396.0423.

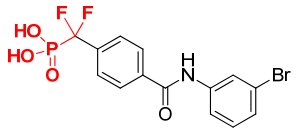

3.74

Compound 3.74. ^{1}H NMR (400 MHz, CD_3OD): δ 8.03-8.00 (m, 4H), 7.75 (d, J = 8.0 Hz, 1H), 7.67-7.65 (m, 1H), 7.29-7.26 (m, 2H); ^{19}F NMR (376 MHz, CD_3OD): δ -112.27 (d, J_{PF} = 109 Hz); ^{31}P NMR (162 MHz, CD_3OD): δ 2.64 (t, J_{PF} = 109 Hz). HRMS-FAB (*m/z*): $[M + H]^+$ calcd for $C_{14}H_{12}{}^{79}BrF_2NO_4P$, 405.9655; found, 405.9650.

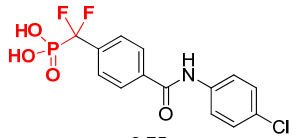

3.75

Compound 3.75. ^{1}H NMR (400 MHz, CD_3OD): δ 8.01 (d, J = 8.0 Hz, 2H), 7.74 (d, J = 8.0 Hz, 2H), 7.72 (d, J = 8.0 Hz, 2H), 7.36 (d, J = 8.0 Hz, 2H); ^{19}F NMR (376 MHz, CD_3OD): δ -112.42 (d, J_{PF} = 109 Hz); ^{31}P NMR (162 MHz, CD_3OD): δ 2.60 (t, J_{PF} = 109 Hz). HRMS-ESI (*m/z*): $[M + 2Na - H]^+$ calcd for $C_{14}H_{10}{}^{35}ClF_2NO_4PNa_2$, 405.9799; found, 405.9815.

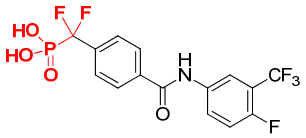

3.77

Compound 3.77. ^{1}H NMR (400 MHz, CD_3OD): δ 8.14 (m, 1H), 8.05-7.92 (m, 3H), 7.82 (s, 1H), 7.75 (m, 1H), 7.31 (m, 1H); ^{19}F NMR (376 MHz, CD_3OD): δ -62.06 (d, J_{FP} = 13 Hz), -121.21. MS-ESI (*m/z*): $[M - H]^-$ calcd for $C_{15}H_9F_6NO_4P$, 413.0252; found 413.0.

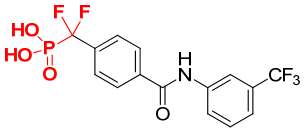

3.78

Compound 3.78. ^{1}H NMR (400 MHz, CD_3OD): δ 8.17 (s, 1H), 8.04 (d, J = 8.0 Hz, 2H), 7.95 (d, J = 8.0 Hz, 1H), 7.76 (d, J = 8.0 Hz, 2H), 7.56 (t, J = 8.0 Hz, 1H), 7.44 (d, J = 8.0 Hz, 1H); ^{19}F NMR (376 MHz, CD_3OD): δ -65.08, -112.39 (d, J_{PF} = 109 Hz); ^{31}P NMR (162 MHz, CD_3OD): δ 2.64 (t, J_{PF} = 109 Hz). HRMS-FAB (*m/z*): $[M + Na]^+$ calcd for $C_{15}H_{11}F_5NO_4PNa$, 418.0244; found, 418.0243.

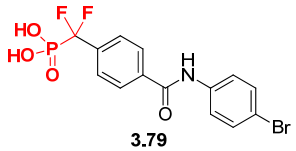

3.79

Compound 3.79. ^{1}H NMR (400 MHz, CD_3OD): δ 8.01 (d, J = 8.0 Hz, 2H), 7.74 (d, J = 8.0 Hz, 2H), 7.67 (d, J = 8.8 Hz, 2H), 7.50 (d, J = 8.8 Hz, 2H); ^{19}F NMR (376 MHz, CD_3OD): δ -112.39 (d, J_{PF} = 109 Hz); ^{31}P NMR (162 MHz, CD_3OD): δ 2.74 (t, J_{PF} = 109 Hz). HRMS-FAB (*m/z*): $[M + H]^+$ calcd for $C_{14}H_{12}{}^{79}BrF_2NO_4P$, 405.9655; found, 405.9650.

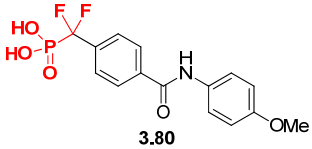

3.80

Compound 3.80. ^{1}H NMR (400 MHz, CD_3OD): 8.01 (d, J = 8.0 Hz, 2H), 7.73 (d, J = 8.0 Hz, 2H), 7.58 (d, J = 8.8 Hz, 2H), 6.93 (d, J = 8.8 Hz, 2H), 3.80 (s, 3H); ^{19}F NMR (376 MHz, CD_3OD): -111.51 (d, J_{PF} = 109 Hz); ^{31}P NMR (162 MHz, CD_3OD): 2.61 (t, J_{PF} = 109 Hz); HRMS-ESI (*m/z*): $[M + 2Na - H]^+$ calcd for $C_{15}H_{13}F_2NO_5PNa_2$, 402.0295; found, 402.0298.

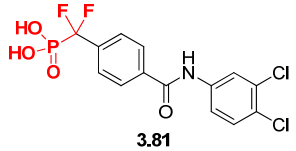

3.81

Compound 3.81. ^{1}H NMR (400 MHz, CD_3OD): 8.06 (d, J = 2.4 Hz, 1H), 8.01 (d, J = 8.0 Hz, 2H), 7.75 (d, J = 8.0 Hz, 2H), 7.64 (dd, J = 8.8, 2.4 Hz, 1H), 7.50 (d, J = 8.8 Hz, 1H); ^{19}F NMR (376 MHz, CD_3OD): -110.86 (d, J_{PF} = 109 Hz); ^{31}P NMR (162 MHz, CD_3OD): 2.56 (t, J_{PF}

= 109 Hz); HRMS-FAB (*m/z*): $[M + H]^+$ calcd for $C_{14}H_{10}{}^{35}Cl_2F_2NO_4P$, 394.9692; found, 394.9685.

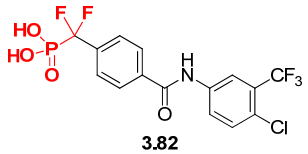

3.82

Compound 3.82. ^{1}H NMR (400 MHz, CD_3OD): δ 8.27 (s, 1H), 8.04 (d, J = 8.0 Hz, 2H), 7.99 (d, J = 8.8 Hz, 1H), 7.75 (d, J = 8.0 Hz, 2H), 7.59 (d, J = 8.8 Hz, 1H); ^{19}F NMR (376 MHz, CD_3OD): δ -64.96, -112.45 (d, J_{PF} = 109 Hz); ^{31}P NMR (162 MHz, CD_3OD): δ 2.62 (t, J_{PF} = 109 Hz). HRMS-FAB (*m/z*): $[M + H]^+$ calcd for $C_{15}H_{11}{}^{35}ClF_5NO_4P$, 430.0034; found, 430.0029.

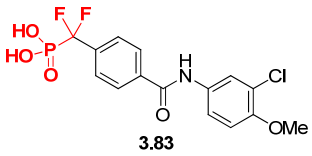

3.83

Compound 3.83. ^{1}H NMR (400 MHz, CD_3OD): 8.00 (d, J = 8.0 Hz, 2H), 7.81 (d, J = 2.4 Hz, 1H), 7.74 (d, J = 8.0 Hz, 2H), 7.57 (dd, J = 8.8, 2.4 Hz, 1H), 7.07 (d, J = 8.8 Hz, 1H), 3.88 (s, 3H); ^{19}F NMR (376 MHz, CD_3OD): -112.35 (d, J_{PF} = 109 Hz); ^{31}P NMR (162 MHz, CD_3OD): 2.67 (t, J_{PF} = 109 Hz); HRMS-FAB (*m/z*): $[M + Na]^+$ calcd for $C_{15}H_{13}{}^{35}ClF_2NO_5PNa$, 414.0086; found, 414.0089.

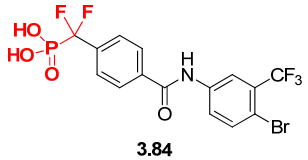

3.84

Compound 3.84. ^{1}H NMR (400 MHz, CD_3OD): δ 8.27 (s, 1H), 8.04 (d, J = 8.0 Hz, 2H), 7.92 (d, J = 7.2 Hz, 1H), 7.79-7.74 (m, 3H); ^{19}F NMR (376 MHz, CD_3OD): δ -64.96, -112.46 (d, J_{PF} = 109 Hz); ^{31}P NMR (162 MHz, CD_3OD): δ 2.62 (t, J_{PF} = 109 Hz). HRMS-FAB (*m/z*): $[M + H]^+$ calcd for $C_{15}H_{11}{}^{79}BrF_5NO_4P$, 473.9529; found, 473.9542.

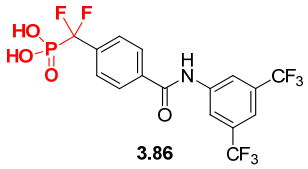

3.86

Compound 3.86. ^{1}H NMR (400 MHz, CD_3OD): δ 8.42 (s, 2H), 8.07 (d, J = 8.0 Hz, 2H), 7.77 (d, J = 8.0 Hz, 2H), 7.71 (s, 1H); ^{19}F NMR (376 MHz, CD_3OD): δ -65.38, -112.46 (d, J_{PF} = 109 Hz); ^{31}P NMR (162 MHz, CD_3OD): δ 2.54 (t, J_{PF} = 109 Hz). HRMS-FAB (*m/z*): $[M + H]^+$ calcd for $C_{16}H_{11}F_8NO_4P$, 464.0297; found, 464.0301.

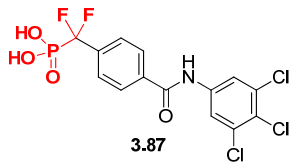

3.87

Compound 3.87. ^{1}H NMR (400 MHz, CD_3OD): 8.02 (d, J = 8.0 Hz, 2H), 7.99 (s, 2H), 7.75 (d, J = 8.0 Hz, 2H); ^{19}F NMR (376 MHz, CD_3OD): -112.45 (d, J_{PF} = 109 Hz); ^{31}P NMR (162 MHz, CD_3OD): 2.56 (t, J_{PF} = 109 Hz). HRMS-ESI (*m/z*): $[M + 2Na - H]^+$ calcd for $C_{14}H_8{}^{35}Cl_3F_2NO_4PNa_2$, 473.9020; found, 473.9033.

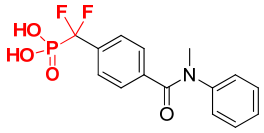

3.96

Compound 3.96. ^{1}H NMR (400 MHz, CD_3OD): 7.43 (d, J = 8.0 Hz, 2H), 7.39 (d, J = 8.0 Hz, 1H), 7.28 (t, J = 7.6 Hz, 2H), 7.22- 7.15 (m, 3H), 3.47 (s, 3H); ^{19}F NMR (376 MHz, CD_3OD): -112.01 (d, J_{PF} = 109 Hz); ^{31}P NMR (162 MHz, CD_3OD): 2.62 (t, J_{PF} = 109 Hz). HRMS-FAB (*m/z*): $[M + 2Na - H]^+$ calcd for $C_{15}H_{13}F_2NO_4PNa_2$, 386.0346; found, 386.0354.

General Synthetic Methods for Other DFMP Inhibitors

Compounds **3.17**, **3.19**, **3.22**, **3.26**, **3.27**, **3.31**, **3.35**, **3.43**, **3.44**, **3.91**, **3.94**, **3.100**, and **3.102** were synthesized as described in the text (vide supra). All compounds were purified by automated reversed-phase C18 column chromatography (linear gradient of 5 to 95% acetonitrile in H_2O with 0.1% trifluoroacetic acid), or by recrystallization.

Analytical Data for Other DFMP Inhibitors

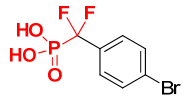

3.17

Compound 3.17. ^{1}H NMR (400 MHz, CD_3OD): δ 7.52 (2H, d, J = 8.0 Hz), 7.65 (2H, d, J = 8.4 Hz); ^{19}F NMR (376 MHz, CD_3OD): δ -110.49 (d, J = 110.9 Hz); ^{31}P NMR (162 MHz, CD_3OD): δ 4.15 (t, J = 109.9 Hz). MS-ESI (*m/z*): $[M + H]^+$ calcd for $C_7H_7BrF_2O_3P$, 286.9206; found 287.0.

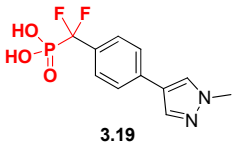

3.19

Compound 3.19. ^{1}H NMR (400 MHz, DMSO-d_6) δ 3.87 (s, 3H), 7.48 (d, J = 8.0 Hz, 2H), 7.66 (d, J = 8.4 Hz, 2H), 7.92 (s, 1H), 8.21 (s, 1H); ^{19}F NMR (376 MHz, DMSO-d_6): δ -107.00 (d, J_{PF} = 108 Hz); ^{31}P NMR (162 MHz, DMSO-d_6): δ 3.04 (t, J_{PF} = 109 Hz). HRMS-ESI (*m/z*): $[M + H]^+$ calcd for $C_{11}H_{12}F_2N_2O_3P$, 289.0548; found, 289.0549.

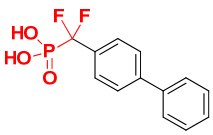

3.22

Compound 3.22. ^{1}H NMR (400 MHz, CD_3OD): δ 7.75-7.63 (m, 6H), 7.45 (t, J = 7.6 Hz, 2H), 7.34 (t, J = 7.4 Hz, 1H); ^{19}F NMR (376 MHz, CD_3OD): δ -113.8 (d, J_{PF} = 113 Hz); ^{31}P NMR (162 MHz, CD_3OD): δ 3.18 (t, J_{PF} = 115 Hz). MS-ESI (*m/z*): $[M - H]^-$ calcd for $C_{13}H_{10}F_2O_3P$, 283.0414; found, 283.0.

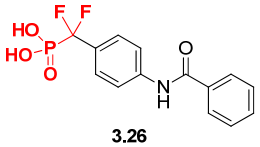

3.26

Compound 3.26. ^{1}H NMR (400 MHz, CD_3OD): δ 7.93 (d, J = 7.6 Hz, 2H), 7.83 (d, J = 8.0 Hz, 2H), 7.61-7.49 (m, 5H); ^{19}F NMR (376 MHz, CD_3OD): δ -111.17 (d, J_{PF} = 113 Hz); ^{31}P NMR (162 MHz, CD_3OD): δ 3.31 (t, J_{PF} = 113 Hz). HRMS-FAB (*m/z*): $[M + H]^+$ calcd for $C_{14}H_{13}F_2NO_4P$, 328.0550; found, 328.0545.

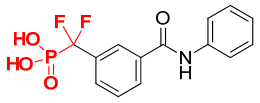

3.31

Compound 3.31. ^{1}H NMR (400 MHz, CD_3OD): δ 7.16 (t, J = 7.4 Hz, 1H), 7.37 (t, J = 7.8 Hz, 2H), 7.64 (t, J = 7.8 Hz, 1H), 7.70 (d, J = 7.6 Hz, 2H), 7.82 (d, J = 7.6 Hz, 1H), 8.06 (d, J = 7.6 Hz, 1H), 8.15 (s, 1H); ^{19}F NMR (376 MHz, CD_3OD): δ -110.56 (d, J_{PF} = 110.2 Hz); ^{31}P NMR (162 MHz, CD_3OD): δ 4.30 (t, J_{PF} = 110.4 Hz). HRMS-ESI (*m/z*): $[M + H]^+$ calcd for $C_{14}H_{13}F_2NO_4P$, 328.0545; found, 328.0551.

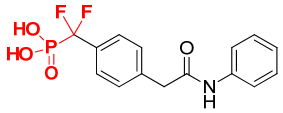

3.35

Compound 3.35. ^{1}H NMR (400 MHz, CD_3OD): δ 3.74 (2H, s), 7.09 (1H, t, J = 7.4 Hz), 7.30 (2H, t, J = 8.0 Hz), 7.47 (2H, d, J = 8.0 Hz), 7.52-7.56 (2H, m), 7.59 (2H, d, J = 8.0 Hz); ^{19}F NMR (376 MHz, CD_3OD): δ -110.03 (d, J = 112.8 Hz); ^{31}P NMR (162 MHz, CD_3OD): δ 4.75 (t, J = 112.6 Hz). HRMS-ESI (*m/z*): $[M + H]^+$ calcd for $C_{15}H_{15}F_2NO_4P$, 342.0701; found, 342.0715.

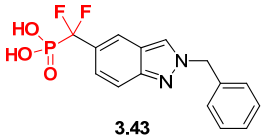

3.43

Compound 3.43. ^{1}H NMR (400 MHz, CD_3OD): δ 5.67 (s, 2H), 7.28-7.39 (m, 5H), 7.52 (d, J = 9.2 Hz, 1H), 7.67 (d, J = 8.8 Hz, 1H), 8.02 (s, 1H), 8.44 (s, 1H); ^{19}F NMR (376 MHz, CD_3OD): δ -108.72 (d, J_{PF} = 114.7 Hz); ^{31}P NMR (162 MHz, CD_3OD) δ 5.05 (t, J_{PF} = 116.0 Hz). HRMS-ESI (*m/z*): $[M + H]^+$ calcd for $C_{15}H_{14}F_2N_2O_3P$, 339.0705; found, 339.0711.

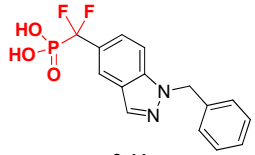

3.44

Compound 3.44. ^{1}H NMR (400 MHz, CD_3OD): δ 5.68 (s, 2H), 7.16-7.32 (m, 5H), 7.62 (s, 2H), 8.06 (s, 1H), 8.17 (s, 1H); ^{19}F NMR (376 MHz, CD_3OD): δ -108.15 (d, J_{PF} = 114.7 Hz); ^{31}P NMR (162 MHz, CD_3OD): δ 5.22 (m). HRMS-ESI (*m/z*): $[M + H]^+$ calcd for $C_{15}H_{14}F_2N_2O_3P$, 339.0705; found, 339.0714.

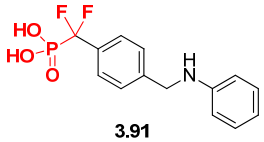

3.91

Compound 3.91. ^{1}H NMR (400 MHz, CD_3OD): δ 7.48 (*AB*q, *J* = 8.4 Hz, 4H), 7.10 (t, *J* = 7.8 Hz, 2H), 6.68 (d, *J* = 8.0 Hz, 2H), 6.64 (t, *J* = 7.4 Hz, 1H), 4.34 (s, 2H); ^{19}F NMR (376 MHz, CD_3OD): δ -106.70 (d, J_{PF} = 109 Hz); ^{31}P NMR (162 MHz, CD_3OD): δ 2.78 (t, J_{PF} = 108 Hz). HRMS-ESI (*m/z*): $[M + H]^+$ calcd for $C_{14}H_{15}F_2NO_3P$, 314.0758; found, 314.0766.

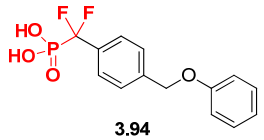

3.94

Compound 3.94. ^{1}H NMR (400 MHz, CD_3OD): δ 7.60 (d, *J* = 8.1 Hz, 2H), 7.47 (d, *J* = 8.0 Hz, 2H), 7.24 (t, *J* = 7.9 Hz, 2H), 6.93-6.90 (m, 3H), 5.08 (s, 2H); ^{19}F NMR (376 MHz, CD_3OD): δ -107.45 (d, J_{PF} = 109 Hz); ^{31}P NMR (162 MHz, CD_3OD): δ 7.01 (br m). HRMS-ESI (*m/z*): $[M + Na]^+$ calcd for $C_{14}H_{13}F_2O_4PNa$, 337.0412; found, 337.0415.

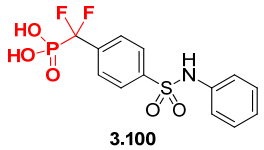

3.100

Compound 3.100. ^{1}H NMR (400 MHz, CD_3OD): δ 7.04-7.13 (m, 3H), 7.19-7.25 (m, 2H), 7.70 (d, *J* = 8.4 Hz, 2H), 7.85 (d, J = 8.4 Hz, 2H); ^{19}F NMR (376 MHz, CD_3OD): δ -110.80 (d, J_{PF} = 106.0 Hz). MS-ESI (*m/z*): $[M + H]^+$ calcd for $C_{13}H_{13}F_2NO_5PS$, 364.0142; found, 364.0.

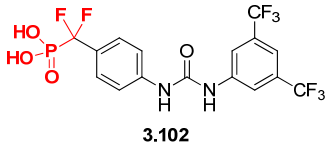

3.102

Compound 3.102. ^{1}H NMR (500 MHz, DMSO-d_6): δ 10.7 (br s, 1H), 10.1 (br s, 1H), 8.22 (m, 2H), 8.10 (m, 2H), 7.61 (m, 1H), 7.32 (m 2H). MS-ESI (*m/z*): $[M + H]^+$ calcd for $C_{16}H_{12}F_8N_2O_4P$, 479.0239; found, 479.0.

Expression and Purification of PtpA

The gene for PtpA was amplified from *Mtb* genomic DNA and cloned into the pET28b vector (Novagen). Protein was expressed in BL21(DH3) cells (Invitrogen). Transformed bacteria were grown to an OD600 of 0.8 in terrific broth and protein expression was induced by the addition of 100 uM isopropyl β-D-1-thiogalactopyranoside. After 18 hours of expression at 20 °C, cells were harvested and resuspended in buffer A (20 mM Tris pH 7.5, 50 mM NaCl), and

protease inhibitor AEBSF. Cell suspensions were sonicated, the lysates centrifuged for 1 hour at 15,000 g, and the cleared lysate loaded onto a metal affinity column. After elution with an imidazole gradient, the His6 tag was cleaved by treatment with 1:1,000 (w/w) trypsin for 10 minutes at rt. The protein was further purified by gel filtration on a S75 Superdex column in buffer A and concentrated to 2.3 mg/mL for phosphatase assays.

Assay Procedures

Determination of Substrate K_M

96-well plates were used with reaction volumes of 100 μL per well. 30 μL of water was added to each well, followed by 5 μL of buffer (stock solution: 1.0 M Tris-HCl, 20 mM $MgCl_2$, pH 7.5), 40 μL of 2-amino-6-mercapto-7-methylpurine riboside (MESG) solution (1 mM), and 10 μL of purine nucleotide phosphorylase (PNP) solution (0.01 U/mL). 5 μL of the appropriate substrate dilution, serially diluted 2.5-fold for a total of 8 different concentrations in DMSO, was then added to the wells, and the plate was covered and incubated at 37 ^oC in a UV-Vis plate reader. The coupled assay was started by addition of 10 μL of 1 μM PtpA, and the reaction progress was monitored at 360 nm at 37 ^oC. The initial rate data collected was used for Michaelis-Menton kinetic analysis, where the K_M and relative k_{cat}/K_M could be obtained. K_M and V_{max} were determined using nonlinear regression analysis on the substrate-velocity data with the equation $v = V_{max}*[S]/(K_M+[S])$.

Determination of Inhibitor K_i

96-well plates were used to run K_i assays, with reaction volumes of 100 μL per well. 45 μL of water was added to each well, followed by 20 μL of sodium citrate buffer (stock solution: 100 mM sodium citrate, pH 6.2, 0.02% Triton X-100), 5 μL of 20 mM EDTA stock solution, 5 μL of 20 mM DTT stock solution, and 10 μL of 1 μM PtpA stock solution. Then 5 μL of the appropriate inhibitor stock solutions, serially diluted 2-fold for a total of 10 different concentrations in DMSO, was added to the wells, and the plate was covered and incubated at 37 ^oC in a UV-Vis plate reader. The reaction was started after 5 minutes of incubation by addition of 10 μL of 2 mM pNPP substrate stock, and reaction progress was monitored at 405 nm with continued incubation at 37 ^oC. The initial rate data collected was used for the determination of K_i values. The kinetic values were obtained from nonlinear regression of substrate-velocity curves in the presence of various concentrations of inhibitor using the equation $v=V_{max}*[S]/(K_M(1+[I]/K_i)+[S])$.

Inhibitor-PtpA Modeling

Receptor Relaxation

The X-ray crystal structure of PtpA (PDB ID 1U2P) was used for all modeling studies.[11] To allow the protein to relax, a short molecular dynamics simulation was run in AMBER 9.0 using the ff03 force field.[9,17] The structure was prepared by removing crystallographic waters and adding an 8.0 Å octagon of TIP3P water and sodium ions using the LEaP accessory.[17] The

system was minimized, slowly melted to 300K, and allowed to equilibrate for 25 ps. The simulation was continued for an additional 150 ps and selected as the final snapshot for docking.

Active Site Identification

To identify where inhibitors might bind, waters were removed from the structure produced by the molecular dynamics simulation, and protein surface invaginations were identified using spheres generated by the DOCK accessory SPHGEN.[18] The putative binding site was characterized by selecting all spheres within a 12 Å radius of the chlorine atom bound to the active-site cysteine nucleophile in the X-ray structure.

Receptor Preparation for Docking

An octagon of TIP3P waters was built around the receptor using the Chimera AmberTools module, followed by removal of any waters >5 Å from any receptor atom, resulting in approximately two shells of water molecules.[19] All waters $\leq$3 Å from the active site spheres described above were then removed. The Chimera (version 1.3) Dock Prep module was used to complete the receptor preparation.[20] To account for the receptor contribution to the score during DOCKing, grids were precomputed to store the van der Waals and electrostatic values for the receptor using the DOCK accessory GRID.[20a]

Compound Preparation for Docking

To validate observed structure-activity relationships, structures **3.55**, **3.88**, and **3.102** were docked onto PtpA. Each compound was drawn and converted to SMILE strings using the JME molecular editor.[21] The SMILE strings were used to create rotamer ensembles of three-dimensional structures in OMEGA.[10] All generated conformations were kept for docking, resulting in any average of 11 conformations per compound. Each conformation was protonated and assigned AM1-BCC charges using the Chimera (version 1.3) AddH and AddCharge modules.[22]

Docking Procedure

The compound conformations were docked using Grid Score in DOCK 6.4 using default parameters.[10] Each conformation was then rescored and ranked using the PB/SA score. The top scoring conformation for each compound was used for comparisons. For compounds **3.55**, **3.88**, and **3.102**, molecular dynamics simulations were also performed on the top-scoring conformation to explore the validity of the docked poses. The same protocol described in the "Receptor Relaxation" section was used. All three simulations were equilibrated after 100 ps, and the simulations were run for a further 50 ps. The snapshot with the ligand heavy atom RMSD closest to the docked pose from the final 50 ps of each simulation was selected for analysis.

PtpA Structure Overlays

The crystal structure of PtpA[11] was overlayed with the structures of HCPtpA (PDB ID 5PNT) and PtpB (PDB ID 1YWF), using Chimera,[14,20a] for comparison of the PTP active-site P-loop and the variable loop of each enzyme. PtpA and HCPtpA have high homology in both loops, but differ in the residue located at position 48 (Trp for PtpA, Tyr for HCPtpA), which was predicted to be important for pi-stacking interactions with our inhibitors. PtpA and PtpB have differences in the P-loop and differ significantly in the sequence and position of the variable loop. These distinctions likely account for the high selectivity of inhibitor **3.55** for PtpA over PtpB.

References

1. Grundner, C.*, et al. Structure* **2007**, *15*, 499-509.
2. Cowley, S. C.*, et al. Res. Microbiol.* **2002**, *153*, 233-241.
3. (a) Chiaradia, L. D.*, et al. Bioorg. Med. Chem. Lett.* **2008**, *18*, 6227-6230; (b) Manger, M.*, et al. ChemBioChem* **2005**, *6*, 1749-1753; (c) Rawls, K. A.*, et al. Bioorg. Med. Chem. Lett.* **2009**, *19*, 6851-6854.
4. (a) Sun, J.-P.*, et al. J. Biol. Chem.* **2003**, *278*, 12406-12414; (b) Shen, K.*, et al. J. Biol. Chem.* **2001**, *276*, 47311-47319; (c) Yao, Z.-J.*, et al. Bioorg. Med. Chem. Lett.* **1998**, *6*, 1799-1810; (d) Puius, Y. A.*, et al. Proc. Natl. Acad. Sci. U. S. A.* **1997**, *94*, 13420-13425.
5. Han, Y.*, et al. Bioorg. Med. Chem. Lett.* **2008**, *18*, 3200-3205.
6. (a) Matsui, T.*, et al. Bioorg. Med. Chem. Lett.* **2002**, *10*, 3807-3815; (b) Yokomatsu, T.*, et al. Tetrahedron* **1997**, *53*, 815-822.
7. Li, Z.*, et al. Bioorg. Med. Chem. Lett.* **1998**, *8*, 2443-2446.
8. (a) Coan, K.*, et al. J. Med. Chem* **2009**, *52*, 2067-2075; (b) Shoichet, B. *J. Med. Chem* **2006**, *49*, 7274-7277; (c) Shoichet, B. *Drug Disc.Today* **2006**, *11*, 607-615; (d) Feng, B. Y.; Shoichet, B. K. *Nat. Protoc.* **2006**, *1*, 550-553; (e) Seidler, J.*, et al. J. Med. Chem* **2003**, *46*, 4477-4486; (f) McGovern, S.*, et al. J. Med. Chem* **2003**, *46*, 4265-4272; (g) McGovern, S.*, et al. J. Med. Chem* **2002**, *45*, 1712-1722.
9. Case, D. A.*, et al.*, *AMBER 9*, University of California, San Francisco, **2006**.
10. Lang, P. T.*, et al. RNA-Publ. RNA Soc.* **2009**, *15*, 1219-1230.
11. Madhurantakam, C.*, et al. J. Bacteriol.* **2005**, *187*, 2175-2181.
12. Case, D. A.*, et al.*, *AMBER 9*, University of California, San Francisco, **2006**.
13. (a) Zsila, F.; Iwao, Y. *BBA-General Subjects* **2007**, *1770*, 797-809; (b) Zsila, F.*, et al. BBA-General Subjects* **2006**, *1760*, 1248-1273; (c) Schuttelkopf, A.*, et al. J. Biol. Chem.* **2006**, *281*, 27278; (d) Rao, F.*, et al. Chem. Biol.* **2005**, *12*, 973-980; (e) Kryger, G.*, et al. Structure* **1999**, *7*, 297-307.
14. Molecular graphics images were produced using the UCSF Chimera package from the Resource for Biocomputing, Visualization, and Informatics at the University of California, San Francisco (supported by NIH P41 RR-01081).
15. (a) Zhang, S.; Zhang, Z.-Y. *Drug Disc.Today* **2007**, *12*, 373-381; (b) Lee, H.*, et al. Biochemistry* **2006**, *45*, 234-240; (c) Moller, N. P. H.*, et al. Handb. Exp. Pharmacol.* **2005**, *167*, 215-262; (d) Vintonyak, V.*, et al. Curr. Opin. Chem. Biol.* **2009**.
16. Tiganis, T.*, et al. J. Biol. Chem.* **1999**, *274*, 27768.
17. Duan, Y.*, et al. J. Comput. Chem.* **2003**, *24*, 1999-2012.
18. Lee, M. C.; Duan, Y. *Proteins* **2004**, *55*, 620-634.
19. Jorgensen, W. L.*, et al. J. Chem. Phys.* **1983**, *79*, 926-935.
20. (a) Pettersen, E. F.*, et al. J. Comput. Chem.* **2004**, *25*, 1605-1612; (b) Kuntz, I. D.*, et al. J. Mol. Biol.* **1982**, *161*, 269-88.
21. Moustakas, D. T.*, et al. J. Comput.-Aided Mol. Des.* **2006**, *20*, 601-619.
22. Shoichet, B.*, et al. J. Comp. Chem.* **1992**, *13*, 380-397.

Chapter 4. Design and Synthesis of Inhibitors for *Staphylococcus aureus*

Abstract: *In this chapter, the design and synthesis of inhibitors for Staphylococcus aureus (S. aureus) is described. Initial lead compounds were identified by screening the full panel of inhibitors described in Chapters 1-3, with isoxazole carboxylic acid inhibitors showing the most promising activity. Our lead compound had activity in both methicillin-sensitive (MSSA) and methicillin-resistant (MRSA) strains of S. aureus (MIC = 8.8 μM or 3.8 μg/mL), suggesting a novel mechanism of action for these inhibitors. Further structure-activity relationships (SAR) were explored by devising a new synthetic route to isoxazole carboxylic acid analogs that allowed for late stage variation of functionality distal to the isoxazole warhead. Analogs were evaluated directly in S. aureus bacteria to determine SAR, leading to the identification of an analog with further improved activity (MIC = 5.0 μM or 2.1 μg/mL versus MRSA strains). The target of our inhibitors is postulated to be phosphatases SaPtpA and SaPtpB, newly discovered enzymes that have not been previously targeted for treatment of Staph infection. Further investigation of inhibitor mechanism of action is in progress, and the synthesis of new inhibitor analogs will be pursued based on the results.*

Authorship

This work was conducted in collaboration with Dr. Christoph Grundner, Tyler Baguley, Dr. Ferric Fang, and Joyce Karlinsev. The inhibitor library was synthesized previously by Dr. Matthew Soellner, Dr. Jun Takeuchi, Dr. Shinichi Imamura, Tyler Baguley, and myself. New inhibitor analogs reported in this chapter were synthesized by Tyler Baguley and myself. Christoph provided enzyme for inhibitor assays and conducted all cell-based assays. Dr. Ferric Fang and Joyce Karlinsev at the University of Washington conducted all experiments with *S. aureus* strains and gram-positive pathogens.

Introduction

Staphylococcus aureus (*S. aureus*) is the causative agent of Staph infections, which range from skin infections such as pimples or boils to more serious or even fatal conditions including pneumonia and sepsis. *S. aureus* is a gram-positive bacteria commonly associated with hospital- and community-acquired infections, and in recent years, has increasingly developed resistance to multiple antibiotics.[1] Methicillin-resistant strains (MRSA) were first reported in the 1960's, and since that time strains resistant to both methicillin and vancomycin (VRSA) have developed, leading to a significant increase in the number of deaths associated with hospital-acquired infections.[2] The wide-spread resistance of *S. aureus* strains to multiple beta-lactam antibiotics underscores the need for the development of new treatments with novel mechanisms of action.

Recently it was reported that *S. aureus* expresses two protein tyrosine phosphatases (PTPs) belonging to the low molecular-weight (LMW-PTP) family, SaPtpA and SaPtpB.[3] The genes encoding these phosphatases were found to be conserved across multiple strains of *S. aureus*, but their function has yet to be determined. By analogy to other pathogenic bacteria, however (*e.g. Mycobacterium tuberculosis* phosphatases PtpA and PtpB described in Chapters 1-3), these phosphatases may play a role in bacterial pathogenesis or survival and they are of interest as potential therapeutic targets. Although *S. aureus* encodes for protein tyrosine kinases,[4] the genes encoding the two phosphatases are not localized on the same operon as the genes encoding the kinases, implying that they may act on targets different than those targeted by the *S. aureus* kinases, including targets in the infection host.

Evaluation of the Inhibitor Library versus *S. aureus*

The entire library of inhibitors previously synthesized for *Mycobacterium tuberculosis* (*Mtb*) phosphatases PtpA and PtpB (Chapters 1-3) was evaluated versus *S. aureus* bacteria to determine if cross-reactivity between pathogenic targets could be achieved with these compounds. Due to the high homology among pathogenic PTPs, cross-reactivity was not unexpected, and indeed, it was found that isoxazole carboxylic acid inhibitors **4.1** and **4.2** previously developed for *Mtb* PtpB had activity versus *S. aureus* (Figure 4.1). Interestingly, all compounds incorporating the isothiazolidinone (IZD) or difluoromethylphosphonic acid (DFMP) warhead showed no activity against the bacteria (data not shown). This could be due to a number of factors, including differences in *S. aureus* cell permeability, undesired reactivity with off-target enzymes, or differing interactions with the target *in vivo*.

In the initial screen, *tert*-octyl compound **4.1** was found to slow bacterial growth after 26 hours of treatment with 50 μM inhibitor, while inhibitor **4.2** completely arrested cell growth

(Figure 4.1). Each of these compounds was assayed in tandem with control cells treated with DMSO, which showed normal growth. Compound **4.2** was further evaluated to confirm bactericidal activity by monitoring the behavior of *S. aureus* cells after treatment with inhibitor over a period of 90 minutes (Figure 4.2). After 90 minutes, bacterial cell numbers were found to remain constant, indicating that cells were not lysed, which would indicate nonspecific cell death, while the number of colony forming units was completely reduced, indicating that the inhibitor is bactericidal.

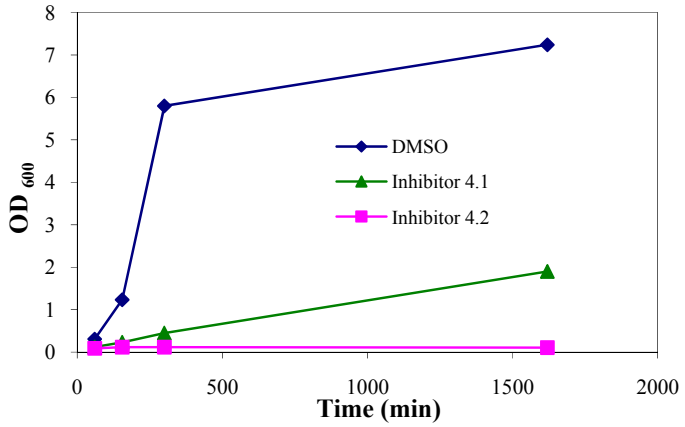

Figure 4.1. Initial lead compounds from inhibitor library screen versus *S. aureus*. The growth of bacterial cells after 26 hours of treatment with DMSO control or 50 μM **4.1** or **4.2** is shown.

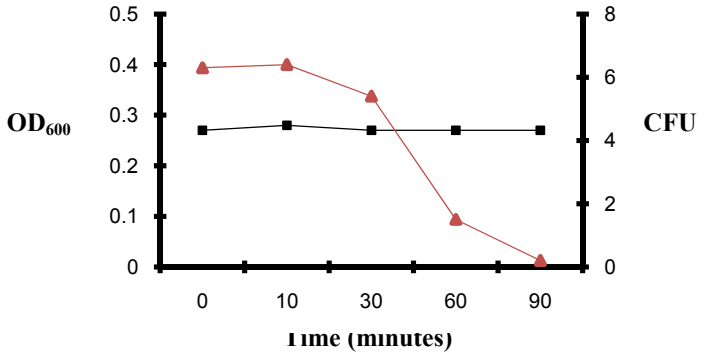

Figure 4.2. Evaluation of **4.2** versus *S. aureus*. Bacteria cell numbers (OD_{600}, shown in black, left axis) remained stagnant, while the number of colonies able to grow back after inhibitor treatment was reduced completely (colony forming units, shown in red, right axis).

Synthesis and Evaluation of Isoxazole Inhibitor Analogs

Deletion Library Synthesis and Evaluation

To determine the features of **4.2** important for bactericidal activity versus *S. aureus*, a small library of deletion analogs was synthesized for exploration of focused structure-activity relationships (SAR, Table 4.1). Cyclohexyl and isopropyl substituted analogs **4.2-4.9** were synthesized via the route describe in Chapter 1 for isoxazole carboxylic acid inhibitors (Scheme

4.1), beginning with Suzuki coupling between the appropriate 4-bromophenol[5] (**4.14**) and the appropriate aryl boronic acid (**4.15**) to arrive at biphenyl phenols **4.16**. Triflation was then followed by Sonogashira coupling with trimethylsilyl acetylene,[6] and removal of the silyl group to afford **4.18**. Copper-mediated formal 1,3-dipolar cycloaddition with ethyl-2-chloro-2-(hydroximino)acetate was then followed by saponification to give the desired isoxazole inhibitors (**4.20**).

Table 4.1. Deletion analogs synthesized for evaluation versus *S. aureus*

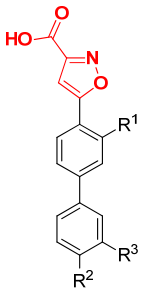

#	R^1	R^2	R^3	#	R^1	R^2	R^3	#	R^1	R^2	R^3
4.2		F	CF_3	**4.6**		F	CF_3	**4.10**	H	F	CF_3
4.3		F	H	**4.7**		F	H	**4.11**	H	F	H
4.4		H	CF_3	**4.8**		H	CF_3	**4.12**	H	H	CF_3
4.5		H	H	**4.9**		H	H	**4.13**	H	H	H

Scheme 4.1. Synthesis of deletion analogs **4.2-4.9**

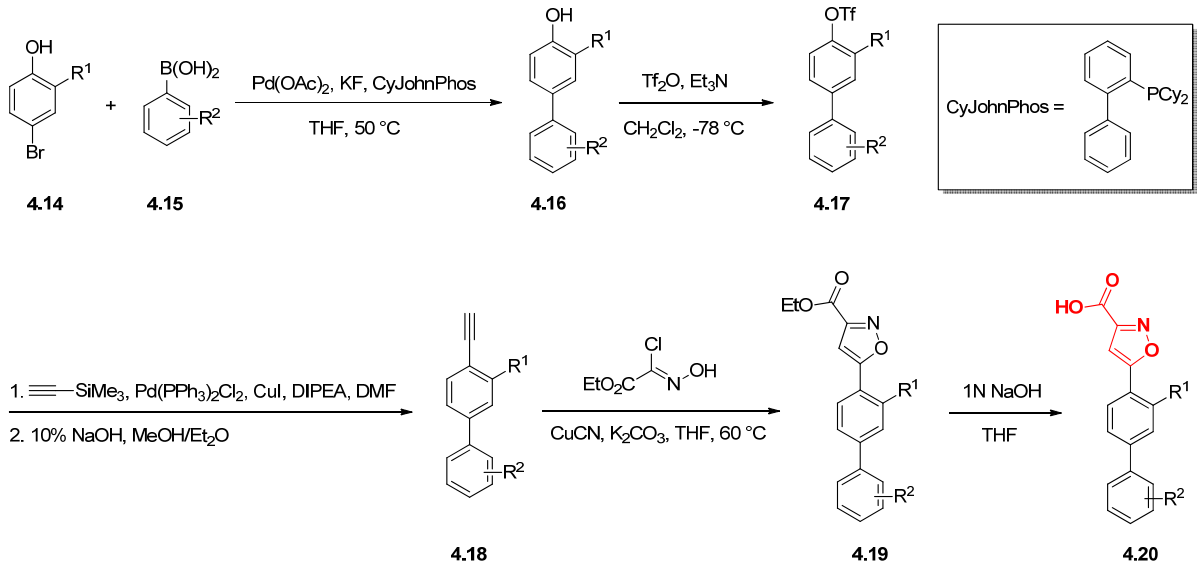

Unsubstituted isoxazole analogs **4.10-4.13** were synthesized via modified literature procedures,[7] beginning with Claisen condensation between 4-bromoacetophenone (**4.21**) and diethyl oxalate to form enol **4.22** (Scheme 4.2). This product was then treated with hydroxylamine hydrochloride to affect hydroxylimine formation followed by cyclization and concomitant dehydration to afford isoxazole **4.23**. Compound **4.23** was then coupled with the appropriate aryl boronic acid **4.24**, followed by saponification to arrive at isoxazole carboxylic acids **4.26**.

Scheme 4.2. Synthesis of unsubstituted deletion analogs **4.10-4.13**

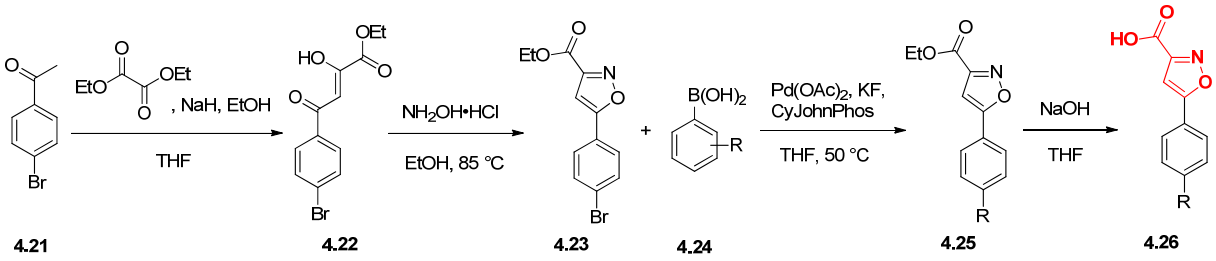

Upon evaluation of the deletion library versus *S. aureus* bacteria (strain ISP479), it was found that only compounds incorporating cyclohexyl groups *ortho* to the isoxazole warhead (**4.2-4.5**) had activity, suggesting the importance of this bulky alkyl group (Figure 4.3). Approximate MIC values were obtained in the initial screen (*i.e.* using two-fold dilutions of inhibitor for a total of six data points – actual MIC values are between 12 and 24 µM for compounds **4.2-4.5**). For the cyclohexyl analogs, modest changes in activity depending upon the substituents on the bottom aryl ring were also observed.

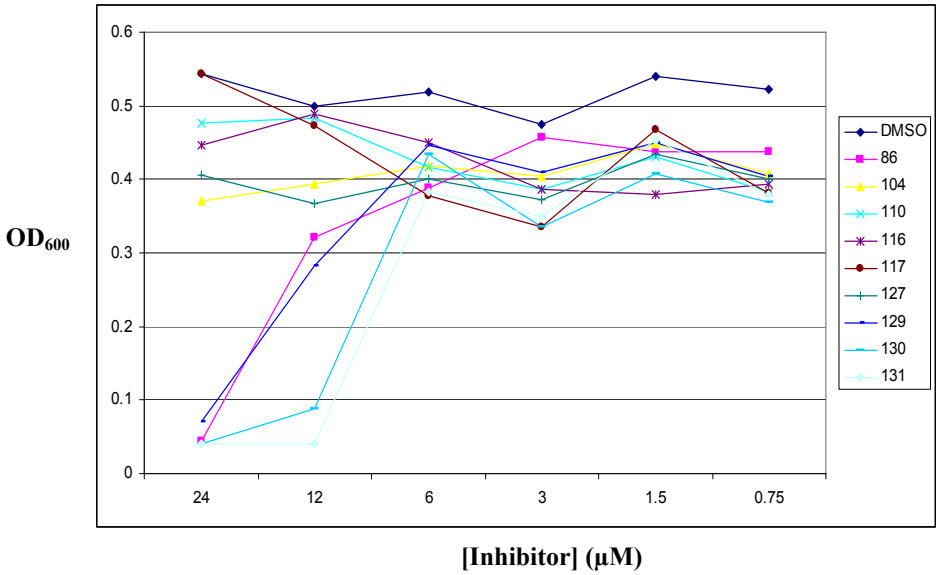

Figure 4.3. Evaluation of compounds **4.2-4.5**, **4.7**, **4.9-4.11**, and **4.13** in *S. aureus* bacterial cells at 24, 12, 6, 3, 1.5, and 0.75 µM inhibitor concentrations. Only analogs with an *ortho* cyclohexyl group had activity as compared to DMSO control.

Cyclohexyl Analog Synthesis and Evaluation

With the importance of the *ortho* cyclohexyl group established, we desired a route to further probe SAR at the site of the distal aromatic ring. The synthetic route used initially to access isoxazole inhibitors (Scheme 4.1) limits efficiency for exploration of SAR at this position since this piece is incorporated early in the sequence. We therefore developed an alternative route to access these compounds that enables efficient late-stage incorporation of the distal aromatic ring by coupling triflate intermediate **4.34** with various aryl boronic acids in the second to last step, followed by deprotection to afford the final inhibitors (Scheme 4.3).

To synthesize these analogs, commercially available **4.27** was first subjected to lithium-halogen exchange with *n*-butyllithium, followed by addition to cyclohexanone to afford alcohol **4.28**. Hydrogenolysis in the presence of sulfuric acid removed both the alcohol and benzyl protecting group to afford **4.29**. Iodination with iodine monochloride was followed by selective deiodination with *N*-methylmorpholine to afford **4.31**.[8] This reaction was monitored carefully by GC to prevent overdeiodination, which would regenerate **4.29**. The identity of **4.31** was additionally independently confirmed by NOE spectroscopy using authentic samples of each constitutional isomer. Compound **4.31** was then coupled with stannane **4.32**[9] to arrive at isoxazole **4.33**. Triflation then afforded key intermediate **4.34**, which was coupled with a variety of aryl boronic acids and saponified to rapidly arrive at a large number of analogs (**4.36**).

Scheme 4.3. Synthesis of analogs of **4.2** for further SAR exploration

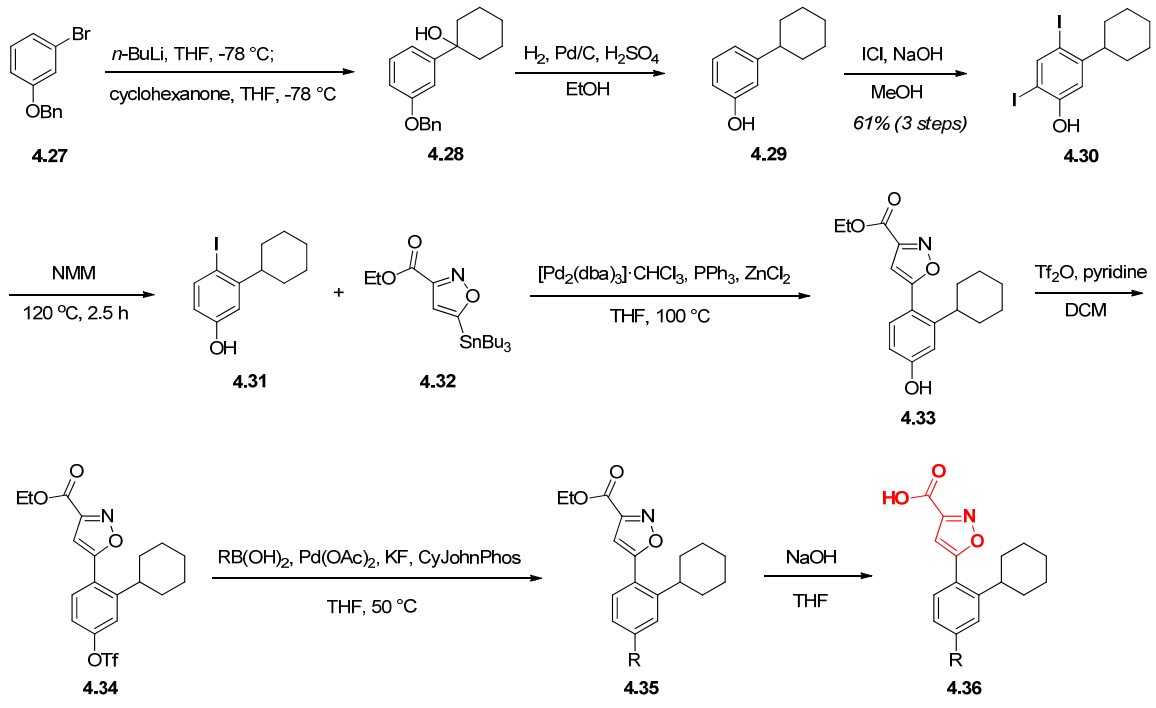

Table 4.2 shows the MIC values obtained thus far for compounds **4.2-4.5** and **4.37-4.59**, which were all made via the route described in Scheme 4.3 using commercially available aryl boronic acids. Electron donating and withdrawing substituents at the *ortho*, *meta*, and *para* positions were examined (**4.37-4.51**), in addition to combinations of these substituents (**4.52-**

4.54). Compared to the benchmark compound **4.2** (MIC = 8.8 µM), only compound **4.37** showed improved activity (MIC = 5.0 µM). Several compounds with electron withdrawing substituents had comparable activity to **4.2** (**4.4**, **4.48**, **4.49**, **4.52** and **4.53**), with MIC values between 5 and 10 µM. Acidic carboxylic acid groups (**4.42** and **4.47**) proved ineffective, potentially due to cell permeability that might be expected from the second negatively charged site at physiologically relevant pH. Fused heterocycle **4.55** also showed weak activity in comparison to the lead scaffold. Pyridyl compounds **4.57-4.59** were synthesized because these functionalities maintain the electron deficient characteristics present in the most potent compound (**4.37**) while providing the potential for lowering the LogP of the inhibitors. These analogs are currently undergoing evaluation in *S. aureus* bacterial cells, and the synthesis of other analogs incorporating commercially available boronic acids is in progress. Once sufficient initial SAR is established, other aryl groups will be explored, including modifications of commercially available boronic acids to extend functionality off of the distal aryl ring.

Table 4.2. Evaluation of isoxazole analogs in *S. aureus* cells

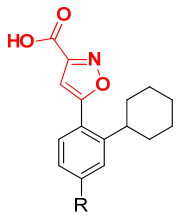

#	R	MIC (µM)	#	R	MIC (µM)	#	R	MIC (µM)
4.2	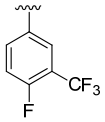	8.8	**4.43**		20	**4.51**	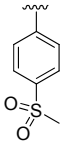	>40
4.5		>40	**4.44**		20	**4.52**	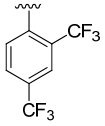	10
4.37	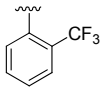	5.0	**4.45**		40	**4.53**	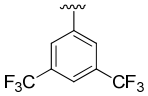	10
4.38		20	**4.46**	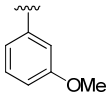	>40	**4.54**	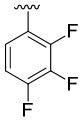	20
4.39		20	**4.47**	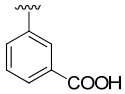	>40	**4.55**	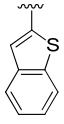	>40
4.40	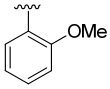	40	**4.48**	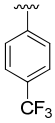	10	**4.56**		nd[a]

4.41		40	**4.49**	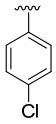	10	**4.57**		nd[a]
4.42	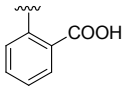	>40	**4.3**	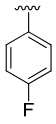	18	**4.58**		nd[a]
4.4	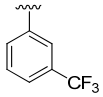	12	**4.50**	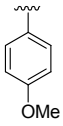	>40	**4.59**		nd[a]

[a]nd = not yet determined; assays are in progress for these compounds.

To evaluate the mechanism of action of these inhibitors, compound **4.2** was tested versus five laboratory strains and six clinical isolates, including methicillin-sensitive (MSSA) and methicillin-resistant (MRSA) strains (Table 4.3). Since clinical and laboratory isolates vary greatly in terms of expression of virulence factors and efflux pumps, and because significant resistance has developed towards the commonly used antibiotic methicillin, this experiment was crucial in evaluating whether the activity of **4.2** was due to a novel mechanism of action. Gratifyingly, the MIC value for compound **4.2** remained constant in all strains tested, including MSSA and MRSA strains, indicating that the compound is acting via a novel mechanism distinct from that causing methicillin resistance. Compound **4.2** is also currently undergoing evaluation versus human HeLa cells to test whether the observed activity is specific for bacterial cells over human cell lines, and to evaluate toxicity.

Table 4.3. MIC values of inhibitor **4.2** against a panel of methicillin-sensitive (MSSA) and methicillin-resistant (MRSA) *S. aureus* strains

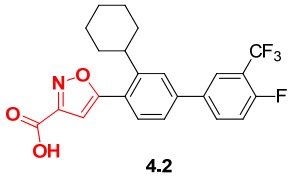

4.2

Strain	Resistance	MIC (μM)
Clinical isolate 1	MSSA	8.8
Clinical isolate 2	MSSA	8.8
Clinical isolate 3	MSSA	8.8
Newman	MSSA	8.8
ISP479	MSSA	8.8
Col	MRSA	8.8
USA300	MRSA	8.8
MW2	MRSA	8.8
Clinical isolate 4	MRSA	8.8
Clinical isolate 5	MRSA	8.8
Clinical isolate 6	MRSA	8.8

Inhibitors **4.2** and **4.37** are also currently being used to generate resistance mutants that are expected to have reduced MIC values when treated with these compounds. If the development of resistance mutants takes more than a single step, then the compounds may have utility as antibiotics. Additionally, since the suspected targets of these compounds are the phosphatases SaPtpA and SaPtpB, these enzymes will be isolated and the K_i values of our inhibitors measured against each to determine if a correlation exists with *in vivo* MIC values. Resistant *S. aureus* strains could also be examined for mutations in the gene that encodes these phosphatases to determine whether this is responsible for the observed resistance. Finally, phosphatase overexpressor *S. aureus* strains are being developed to determine if these mutants confer an increase in MIC values upon treatment with our compounds. Together, these data would provide good evidence that the targets of our inhibitors are the two phosphatases expressed by *S. aureus*, and would additionally guide future inhibitor development.

Conclusions

Upon screening the library of inhibitors previously developed for *Mtb* phosphatases PtpA and PtpB (Chapters 1-3), isoxazole inhibitor **4.2** was found to have potent *in vivo* activity versus *S. aureus* bacteria (MIC = 8.8 μM or 3.8 μg/mL). SAR exploration led to the identification of compound **4.37** with further improved potency (MIC = 5.0 μM or 2.1 μg/mL), which is comparable to the commonly used antibiotics methicillin and vancomycin (MIC = <3 and 0.5 μg/mL, respectively, for sensitive strains). Significantly, compound **4.2** was active versus methicillin-sensitive and resistant strains alike, suggesting a novel mechanism of action and providing a promising starting point for the development of new antibiotics for the treatment of Staph infection. The synthesis of other isoxazole compounds based on lead compound **4.2** is currently underway to further explore SAR and improve potency. Compounds **4.2** and **4.37** are also being used to generate resistance mutants that will be evaluated to determine whether the two phosphatases expressed by *S. aureus*, SaPtpA and SaPtpB, are the targets *in vivo*. X-ray crystallographic analysis of these compounds with SaPtpA is also underway, and may provide an avenue for further compound development.

Experimental

General Synthetic Methods

Unless otherwise noted, all reagents were obtained from commercial suppliers and used without further purification. Tetrahydrofuran (THF), dichloromethane (CH_2Cl_2), toluene, and diethyl ether (Et_2O) were dried over alumina under a nitrogen atmosphere. Solvents used for reactions set up in a nitrogen-filled Braun inert atmosphere box, including THF and toluene, were additionally degassed with three consecutive freeze pump thaw cycles and stored over 3Å molecular sieves. Methanol was dried over calcium hydride under a nitrogen atmosphere. All reactions, unless otherwise stated, were performed under inert atmosphere using syringe, cannula, and Schlenk techniques, or set up in a nitrogen-filled Braun inert atmosphere box, with flame or oven-dried glassware. All ^{1}H, ^{13}C, ^{19}F, and ^{31}P NMR spectra were measured with a Bruker DRX-500, AVB-400, AVQ-400 or AV-300 spectrometer. NMR chemical shifts are reported in ppm relative to 1,2-difluorobenzene (-138.9) for ^{19}F NMR and trimethylphosphate

(3.0) for ^{31}P NMR. Mass spectrometry (HRMS) was carried out by the University of California, Berkeley Mass Spectrometry Facility.

Selected Isoxazole Inhibitor Synthesis and Analytical Data

Unsubstituted Analogs

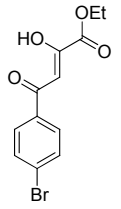

4.22

Compound 4.22. Compound **4.22** was synthesized via modified literature procedures.[7] 4-Bromoacetophenone (1.0 g, 5.0 mmol) was added to a flame-dried 3-necked round bottomed flask under N_2 and dissolved in THF (12 mL). Catalytic ethanol was added (1 drop), followed by sodium hydride. A solution of diethyl oxalate (1.0 mL, 7.5 mmol) in THF (3 mL) was then added dropwise via addition funnel. The resulting mixture was stirred at room temperature for 3 h and then diluted with ether (15 mL). The reaction was then quenched with 2N HCl (15 mL). The organic layer was washed with 2N HCl (2 x 15 mL), then brine (1 x 15 mL), dried over anhydrous Na_2SO_4 (s) and filtered. The solvent was removed under reduced pressure to provide crude product which was purified via automated silica gel chromatography (linear gradient of 2 to 20% EtOAc in hexanes) to yield compound **4.22** as an orange solid (0.97 g, 65% yield). **Analytical data.** Analytical data was found to match that reported in the literature[7]: ^1H NMR (400 MHz, $CDCl_3$) δ 15.19 (s, 1H), 7.90 – 7.83 (m, 2H), 7.71 – 7.62 (m, 2H), 7.03 (s, 1H), 4.41 (q, J = 7.1 Hz, 2H), 1.42 (t, J = 7.1 Hz, 3H).

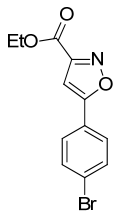

4.23

Compound 4.23. Compound **4.23** was synthesized via modified literature procedures.[7] Compound **4.22** (300 mg, 1.0 mmol) was dissolved in ethanol (2.5 mL) in a 10 mL flask under N_2, followed be addition of hydroxylamine hydrochloride (208 mg, 3.0 mmol). The resulting mixture was heated to reflux (85 ºC) in an oil bath for 1 h. The reaction mixture was then cooled in an ice bath until a white solid formed. The reaction mixture was filtered to collect the solid, which was washed with ice-cold ethanol, and then recrystallized from ethanol to give **4.23** as a white solid (215 mg, 73% yield). **Analytical data.** Analytical data was found to match that reported in the literature[7]: ^1H NMR (400 MHz, $CDCl_3$) δ 7.68 (d, J = 8.5 Hz, 2H), 7.64 (d, J = 8.7 Hz, 2H), 6.93 (s, 1H), 4.48 (q, J = 7.1 Hz, 2H), 1.44 (t, J = 7.1 Hz, 3H).

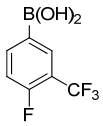

4.60

Compound 4.60. Compound **4.60** was synthesized as described in Chapter 1 (compound **1.175**).

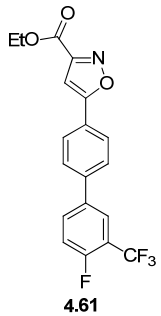

4.61

Compound 4.61. Compound **4.23** (100 mg, 0.34 mmol) was added to a 10 mL Schlenk flask in an inert atmosphere box, followed by 3-(trifluoromethyl)-4-fluoro-phenylboronic acid **4.60** (105 mg, 0.51 mmol), potassium fluoride (59 mg, 1.0 mmol), palladium acetate (7.6 mg, 0.10 mmol), 2-(dicyclohexylphosphino)biphenyl (18 mg, 0.15 mmol), and THF (0.34 mL). The flask was then sealed under a N_2 atmosphere, and the reaction mixture was heated to 50 °C with stirring for 18 h. The reaction mixture was then diluted with EtOAc (5 mL) and filtered through a pad of celite. The solvent was removed under reduced pressure to provide the crude product as a yellow oil, which was purified via automated silica gel chromatography (linear gradient of 2 to 25% EtOAc in hexanes) to yield compound **4.61** as an off-white solid (104 mg, 81% yield). **Analytical data.** ^{1}H NMR (400 MHz, $CDCl_3$): δ 7.94 – 7.88 (m, 1H), 7.87-7.75 (m, 2H), 7.71 – 7.65 (m, 1H), 7.36 – 7.28 (m, 2H), 7.02 – 6.96 (m, 1H), 4.49 (q, J = 7.1 Hz, 2H), 1.46 (t, J = 7.1 Hz, 3H); ^{19}F NMR (376 MHz, $CDCl_3$): δ -61.37 (d, J = 12.5 Hz), -115.67 (s).

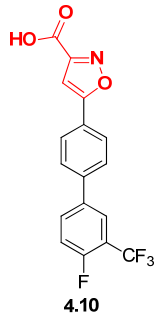

4.10

Compound 4.10. Compound **4.61** (20 mg, 0.040 mmol) was added to a 20 mL flask and dissolved in THF (1 mL). NaOH (1N solution, 1 mL) was then added, and the reaction mixture was stirred at ambient temperature for 2 h. The solvent was removed under reduced pressure, and EtOAc (10 mL) and HCl (2N, 10 mL) were added to the resulting residue. The organic layer was separated and washed with 2N HCl (4 × 10 mL) and brine (1 × 10 mL). The organic layer was then dried over anhydrous $NaSO_4$ (s) and filtered, and the solvent was removed under reduced pressure to give crude product, which was dissolved in minimal dimethylsulfoxide (1 mL) and purified via automated reversed-phase C18 column chromatography (linear gradient of 15 to 95% acetonitrile in H_2O with 0.1% trifluoroacetic acid) to give compound **4.10** as a white

powder (17 mg, 18% yield). **Analytical data.** ^{1}H NMR (400 MHz, 1:1 CD_3OD:$CDCl_3$) δ 7.77 (d, *J* = 7.4 Hz, 2H), 7.73-7.64 (m, 2H), 7.54 (d, *J* = 7.7 Hz, 2H), 7.19 (t, *J* = 9.4 Hz, 1H), 6.87 (s, 1H); ^{19}F NMR (376 MHz, $CDCl_3$) δ -58.55 (d, *J* = 12.5 Hz), -113.27 (s); HRMS-ESI (*m/z*): [M - H]$^-$ calcd for $C_{17}H_8F_4NO_3$, 350.0446; found, 350.0434.

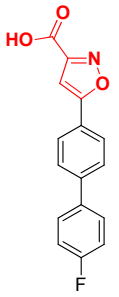

4.11

Compound 4.11. Compound **4.11** was synthesized via procedures analogous to those described for compound **4.10**. **Analytical data.** ^{1}H NMR (400 MHz, 1:1 CD_3OD:$CDCl_3$): δ 7.71-7.62 (m, 2H), 7.50-7.44 (m, 2H), 7.43-7.34 (m, 2H), 6.98-6.89 (m, 2H), 6.78 (s, 1H); ^{19}F NMR (376 MHz, $CDCl_3$) δ -111.33 (s); MS-ESI (*m/z*): [M + H]+ calcd for $C_{16}H_{11}FNO_3$, 284.2539; found, 284.0.

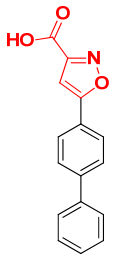

4.13

Compound 4.13. Compound **4.13** was synthesized via procedures analogous to those described for compound **4.10**. **Analytical data.** ^{1}H NMR (400 MHz, CD_3OD): δ 7.96 (d, *J* = 8.2 Hz, 2H), 7.79 (d, *J* = 8.2 Hz, 2H), 7.68 (d, *J* = 7.6 Hz, 2H), 7.47 (t, *J* = 7.6 Hz, 2H), 7.38 (t, *J* = 7.6 Hz, 2H), 7.16 (s, 1H); MS-ESI (*m/z*): [M + H]+ calcd for $C_{16}H_{12}NO_3$, 266.0739; found, 266.0.

Ortho-Substituted Analogs

Compounds **4.2-4.9** were synthesized as described in Chapter 1 (see compounds **1.170-1.173**). All other analogs were made via the procedures described below.

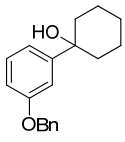

4.28

Compound 4.28. 1-Benzyloxy-3-bromobenzene (15.0 g, 0.60 mol) was added to an oven-dried flask under N_2, followed by THF (102 mL). The resulting solution was cooled to -78 ºC, and *n*-butyllithium (27 mL of a 2.5 M solution in hexanes, 0.70 mol) was added dropwise via

addition funnel, keeping the internal temperature at -78 ºC. The resulting mixture was stirred for 15 minutes at -78 ºC. In a separate flask, cyclohexanone (7.1 mL, 0.70 mol) was dissolved in THF (57 mL), cooled to -78 ºC and added via cannula to the first solution over 30 minutes. The resulting solution was stirred for 1 h at -78 ºC, followed by quenching the reaction with water while the reaction vessel was open to the atmosphere. The aqueous layer was extracted with EtOAc (3 x 150 mL). The combined organic layer was then washed with brine, dried over anhydrous $NaSO_4$ (s), and filtered. The solvent was removed under reduced pressure to provide crude product (16.1 g, 72% pure by NMR), which was taken on without further purification. **Analytical data.** ^{1}H NMR (400 MHz, $CDCl_3$) δ 7.47-7.42 (m, 2H), 7.42 – 7.36 (m, 2H), 7.36 – 7.28 (m, 1H), 7.28-7.24 (m, 1H), 7.20 – 7.16 (m, 1H), 7.12-7.07 (m, 1H), 6.86 (dd, *J* = 8.1, 2.5 Hz, 1H), 5.07 (s, 2H), 1.91 – 1.59 (m, 10H).

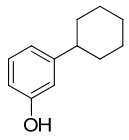

4.29

Compound 4.29. Compound **4.28** (16.1 g, 0.600 mol) was dissolved in ethanol (570 mL) in a 1 L flask. 10 wt% palladium on carbon (2.9 g, 50 mg per mmol of **4.28**) was then added, followed by sulfuric acid (3.5 mL, 0.70 mol). The reaction apparatus was evacuated and backfilled 5 times using a hydrogen balloon, and the mixture stirred under a hydrogen atmosphere for 24 h. 10N NaOH was added dropwise until neutral pH was reached, and then the entire mixture was filtered through celite, eluting with EtOAc. The resulting solution was concentrated under reduced pressure to remove volatiles, and then the remaining aqueous solution was extracted with EtOAc (3 x 25 mL). The combined organic layer was washed with brine (1 x 50 mL), dried over anhydrous $NaSO_4$ (s), and filtered. The solvent was removed under reduced pressure to provide crude **4.29**, which was taken on without further purification (9.7 g, 91% pure by NMR). **Analytical data.** Analytical data was found to match that of previous literature reports[10]: ^{1}H NMR (400 MHz, $CDCl_3$) δ 7.15 (t, *J* = 7.8 Hz, 1H), 6.79 (d, *J* = 7.6 Hz, 1H), 6.71 – 6.67 (m, 1H), 6.64 (m, 1H), 4.72 (s, 1H), 2.50-2.39 (m, 1H), 1.92 – 1.70 (m, 5H), 1.46 – 1.30 (m, 5H).

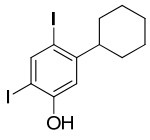

4.30

Compound 4.30. Compound **4.30** was synthesized via modified literature procedures.[8] Compound **4.29** (3.8 g, 0.20 mol) was dissolved in MeOH (62 mL) in a 250 mL flask under N_2, followed by addition of NaOH (2.8 g, 0.70 mol). ICl (7.8 g, 0.50 mol) was added to a glass addition funnel and dissolved in MeOH (48 mL), and the resulting solution was added dropwise to the solution of compound **4.29** under N_2. The resulting solution was stirred at room temperature for 30 minutes, and the reaction was then quenched with 10% w/v Na_2SO_3 (40 mL). Volatile solvents were removed under reduced pressure to provide an aqueous solution that was diluted with 2N HCl (40 mL) and extracted with EtOAc (3 x 50 mL). The combined organic layer was washed with brine (1 x 50 mL), dried over anhydrous $NaSO_4$ (s), and filtered. The solvent was removed under reduced pressure to provide crude **4.30**, which was purified via

automated silica gel chromatography (linear gradient of 2 to 25% EtOAc in hexanes) to yield compound **4.30** as a light yellow solid (5.5 g, 61% yield over 3 steps). **Analytical data.** ^{1}H NMR (400 MHz, $CDCl_3$) δ 8.03 (s, 1H), 6.88 (s, 1H), 5.18 (s, 1H), 2.66 (t, *J* = 11.9 Hz, 1H), 1.91-1.72 (m, 5H), 1.50-1.36 (m, 2H), 1.36-1.16 (m, 3H).

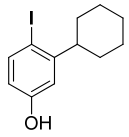

4.31

Compound 4.31. Compound **4.31** was synthesized via modified literature procedures.[8] Compound **4.30** (1.6 g, 3.6 mmol) was dissolved in *N*-methylmorpholine (15 mL) in a 50 mL flask under N_2 and heated to 120 ºC in an oil bath for 2.5 h. The reaction was monitored carefully by GC to minimize formation of completely deiodinated byproduct **4.29**. After cooling to room temperature, the reaction solution was diluted with EtOAc (15 mL) and 2N HCl (15 mL). The organic layer was washed with 2N HCl (2 x 15 mL), and the aqueous layer was back extracted with EtOAc (1 x 30 mL). The combined organic layer was washed with 10% w/v Na_2SO_3 (50 mL), dried over anhydrous $NaSO_4$ (s), and filtered. The solvent was removed under reduced pressure to provide crude **4.31** as a brown oil, which was taken on without further purification (1.1 g, 83% pure by NMR). **Analytical data.** ^{1}H NMR (400 MHz, $CDCl_3$) δ 7.63 (d, *J* = 8.5 Hz, 1H), 6.72 (d, *J* = 3.0 Hz, 1H), 6.43 (dd, *J* = 8.5, 3.0 Hz, 1H), 4.68 (s, 1H), 2.76 – 2.64 (m, 1H), 1.93 – 1.68 (m, 5H), 1.51 – 1.20 (m, 5H).

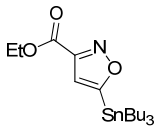

4.32

Compound 4.32. Compound **4.32** was synthesized according to literature procedures.[9,11] Ethyl 2-chloro-2-(hydroxyimino)acetate (4.8 g, 0.30 mol) was dissolved in CH_2Cl_2 (96 mL) in a 250 mL flask under N_2. Tributylstannylacetylene (10.0 g, 0.300 mol) was added, followed by K_2CO_3 (4.8 g, 0.40 mol). The resulting mixture was stirred at room temperature for 5 h. The reaction mixture was then diluted with water (100 mL), and the organic layer was separated. The aqueous layer was extracted with CH_2Cl_2 (3 x 50 mL), and then the combined organic layer was washed with brine (1 x 150 mL), dried over anhydrous $NaSO_4$ (s), and filtered. The solvent was removed under reduced pressure to provide crude **4.32** as a yellow oil, which was purified via automated silica gel chromatography (linear gradient of 0 to 10% EtOAc in hexanes) to yield compound **4.32** as a colorless oil (7.6 g, 56% yield). **Analytical data.** Analytical data was found to match that reported in the literature[9,11]: ^{1}H NMR (400 MHz, $CDCl_3$) δ 6.80 (s, 1H), 4.44 (q, *J* = 7.1 Hz, 2H), 1.62 – 1.51 (m, 6H), 1.42 (t, *J* = 7.1 Hz, 3H), 1.38 – 1.26 (m, 6H), 1.22 – 1.15 (m, 6H), 0.89 (t, *J* = 7.3 Hz, 9H).

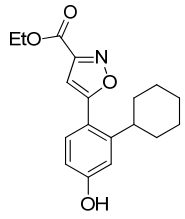

4.33

Compound 4.33. Compound **4.31** (1.1 g, 3.5 mmol) was added to a 50 mL Schlenk flask in an inert atmosphere box, followed by **4.32** (1.5 g, 3.5 mmol), zinc chloride (474 mg, 3.50 mmol), tris(dibenzylideneacetone)dipalladium-chloroform adduct (216 mg, 0.210 mmol), triphenylphosphine (183 mg, 0.700 mmol), and THF (17 mL). The flask was then sealed under a N_2 atmosphere, and the reaction mixture was heated to 90 °C with stirring for 5 h. The reaction mixture was then diluted with EtOAc (10 mL) and filtered through a pad of celite. The solvent was removed under reduced pressure to provide the crude product, which was purified via automated silica gel chromatography (linear gradient of 5 to 25% EtOAc in hexanes) to yield compound **4.33** as a light yellow oil (462 mg), which was taken on without further purification. **Analytical data.** MS-ESI (*m/z*): $[M + H]^+$ calcd for $C_{18}H_{22}NO_4$, 316.1471; found, 316.1.

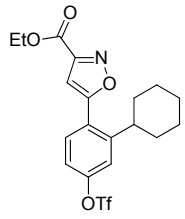

4.34

Compound 4.34. Compound **4.33** (462 mg, 1.50 mmol) was added to a 25 mL flask and dissolved in CH_2Cl_2 (7 mL) under N_2. The resulting solution was then cooled to 0 °C, and Et_3N (0.60 mL, 4.4 mmol) was added, followed by dropwise addition of a solution of triflic anhydride (0.50 mL, 3.0 mmol) in CH_2Cl_2 (29 mL). Once addition of triflic anhydride was complete, the reaction mixture was stirred for 1 h at 0 °C. The reaction was then quenched carefully with H_2O (10 mL) with the reaction vessel open to air. The aqueous layer was then extracted with CH_2Cl_2 (3 x 10 mL). The combined organic layer was then washed with aqueous saturated $NaHCO_3$ (1 × 30 mL) and brine (1 x 30 mL). The organic layer was dried over anhydrous Na_2SO_4 (s) and filtered. The solvent was removed under reduced pressure to provide crude product, which was purified via automated silica gel chromatography (linear gradient of 3 to 25% EtOAc in hexanes) to yield compound **4.34** as an oily orange solid (227 mg, 90% pure by NMR), which was taken on without further purification. **Analytical data.** ^{1}H NMR (400 MHz, $CDCl_3$) δ 7.61 (d, J = 8.6 Hz, 1H), 7.31 (d, J = 2.5 Hz, 1H), 7.21 (dd, J = 8.6, 2.5 Hz, 1H), 6.79 (s, 1H), 4.48 (q, J = 7.1 Hz, 2H), 2.90 – 2.76 (m, 1H), 1.92-1.70 (m, 5H), 1.45 (t, J = 7.1 Hz, 3H), 1.42 – 1.27 (m, 5H); ^{19}F NMR (376 MHz, $CDCl_3$) δ -71.89 (s).

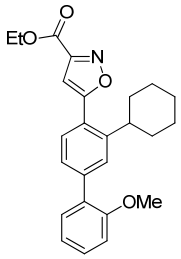

4.62

Compound 4.62. Compound **4.34** (75 mg, 0.17 mmol) was added to a 10 mL Schlenk flask in an inert atmosphere box, followed by 2-methoxyphenylboronic acid (38 mg, 0.25 mmol), K_2CO_3 (46 mg, 0.34 mmol), palladium acetate (1.5 mg, 0.007 mmol), triphenylphosphine (8.8 mg, 0.030 mmol), and dioxane (0.74 mL). The flask was then sealed under a N_2 atmosphere, and the reaction mixture was heated to 95 °C with stirring for 23 h. The reaction mixture was then diluted with EtOAc (5 mL) and filtered through a pad of celite. The solvent was removed under reduced pressure to provide the crude product as an orange oil, which was purified via automated silica gel chromatography (linear gradient of 2 to 35% EtOAc in hexanes) to yield compound **4.62** as an off-white solid (63 mg, 93% yield). **Analytical data.** ^{1}H NMR (400 MHz, $CDCl_3$) δ 7.59 (dd, *J* = 9.8, 4.7 Hz, 2H), 7.49 (dd, *J* = 8.0, 1.7 Hz, 1H), 7.36 (d, *J* = 7.5 Hz, 2H), 7.12 – 6.97 (m, 2H), 6.78 (s, 1H), 4.50 (q, *J* = 7.1 Hz, 2H), 3.85 (s, 3H), 2.96-2.84 (m, 1H), 1.99 – 1.71 (m, 5H), 1.60 – 1.18 (m, 8H).

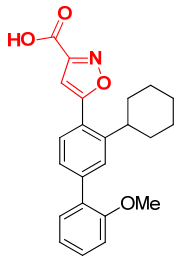

4.40

Compound 4.40. Compound **4.62** (63 mg, 0.16 mmol) was added to a 20 mL flask and dissolved in THF (4 mL). 1N NaOH (4 mL) was then added and the reaction mixture was stirred at ambient temperature for 2 h. The solvent was removed under reduced pressure, and EtOAc (4 mL) and 2N HCl (5 mL) were added. The organic layer was separated and washed with 2N HCl (4 × 10 mL) and brine (1 × 10 mL). The organic layer was then dried over anhydrous $NaSO_4$ (s) and filtered, and the solvent was removed under reduced pressure to give crude product, which was dissolved in minimal dimethylsulfoxide (1 mL) and purified via automated reversed-phase C18 column chromatography (linear gradient of 15 to 95% acetonitrile in H_2O with 0.1% trifluoroacetic acid) to give compound **4.40** as a white powder (15 mg, 33% yield). **Analytical data.** ^{1}H NMR (500 MHz, MeOD) δ 7.56 (m, 1H), 7.52 (d, *J* = 8.0 Hz, 1H), 7.41 (dd, *J* = 8.0, 1.3 Hz, 1H), 7.33 (t, *J* = 7.8 Hz, 1H), 7.29 (dd, *J* = 7.5, 1.3 Hz, 1H), 7.07 (d, *J* = 8.3 Hz, 1H), 7.01 (t, *J* = 7.5 Hz, 1H), 6.85 (s, 1H), 3.79 (s, 3H), 2.86 (t, *J* = 11.8 Hz, 1H), 1.90-1.78 (m, 4H), 1.77-1.68 (m, 1H), 1.57 – 1.24 (m, 5H); HRMS-FAB (*m/z*): $[M + H]^+$ calcd for $C_{23}H_{24}NO_4$, 378.1700; found, 378.1698.

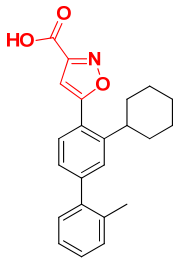

4.41

Compound 4.41. Compound **4.41** was synthesized via procedures analogous to those described for compound **4.40**. **Analytical data.** ^{1}H NMR (500 MHz, MeOD): δ 7.58 (d, J = 7.9 Hz, 1H), 7.36 (s, 1H), 7.32 – 7.16 (m, 5H), 6.71 (s, 1H), 2.95 (m, 1H), 2.26 (s, 3H), 1.85 (m, 4H), 1.74 (m, 1H), 1.56 – 1.24 (m, 5H); HRMS-FAB (*m/z*): $[M + H]^+$ calcd for $C_{23}H_{24}NO_3$, 362.1751; found, 362.1750.

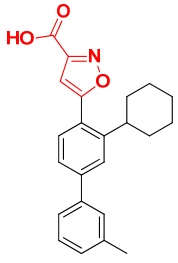

4.44

Compound 4.44. Compound **4.44** was synthesized via procedures analogous to those described for compound **4.40**. **Analytical data.** ^{1}H NMR (500 MHz, MeOD): δ 7.66 (d, J = 1.5 Hz, 1H), 7.61 (d, J = 8.0 Hz, 1H), 7.54 (dd, J = 8.1, 1.8 Hz, 1H), 7.49 – 7.40 (m, 2H), 7.34 (t, J = 7.6 Hz, 1H), 7.20 (d, J = 7.5 Hz, 1H), 6.87 (s, 1H), 2.90 (t, J = 11.8 Hz, 1H), 2.42 (s, 3H), 1.93-1.71 (m, 5H), 1.67 – 1.32 (m, 5H); HRMS-FAB (*m/z*): $[M + H]^+$ calcd for $C_{23}H_{24}NO_3$, 362.1751; found, 362.1750.

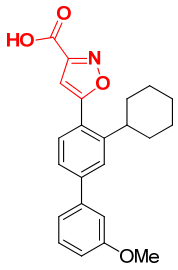

4.46

Compound 4.46. Compound **4.46** was synthesized via procedures analogous to those described for compound **4.40**. **Analytical data.** ^{1}H NMR (500 MHz, MeOD): δ 7.70-7.58 (m, 2H), 7.53 (dd, J = 8.1, 1.8 Hz, 1H), 7.37 (t, J = 8.0 Hz, 1H), 7.22 (d, J = 7.8 Hz, 1H), 7.20-7.14 (m, 1H), 6.95 (dd, J = 8.0, 2.2 Hz, 1H), 6.70 (s, 1H), 3.86 (s, 3H), 2.96 (m, 1H), 1.87 (m, 4H), 1.77 (m, 1H), 1.65-1.50 (m, 2H), 1.51 – 1.29 (m, 3H); HRMS-FAB (*m/z*): $[M + H]^+$ calcd for $C_{23}H_{24}NO_4$, 378.1700; found, 378.1694.

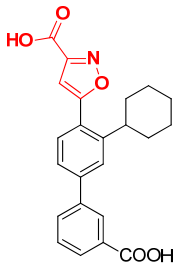

4.47

Compound 4.47. Compound **4.47** was synthesized via procedures analogous to those described for compound **4.40**. **Analytical data.** ^{1}H NMR (500 MHz, MeOD) δ 8.40 (s, 1H), 8.31 (s, 1H), 8.06 (m, 1H), 7.92 (m, 1H), 7.76 (m, 1H), 7.67 – 7.56 (m, 2H), 6.92 (s, 1H), 2.94 (m, 1H), 2.65 (s, 1H), 1.98-1.73 (m, 4H), 1.72-1.53 (m, 2H), 1.50 – 1.25 (m, 4H); MS-ESI (*m/z*): $[M + H]^+$ calcd for $C_{23}H_{22}NO_5$, 392.1420; found, 392.0; MS-ESI (*m/z*): [M + H]+ calcd for $C_{23}H_{22}NO_5$, 392.1420; found, 392.0.

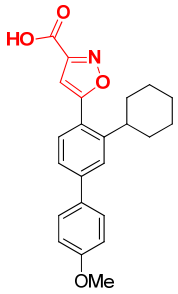

4.50

Compound 4.50. Compound **4.50** was synthesized via procedures analogous to those described for compound **4.40**. **Analytical data.** ^{1}H NMR (500 MHz, MeOD): δ 7.64-7.56 (m, 4H), 7.50 (dd, J = 8.2, 1.9 Hz, 1H), 7.02 (d, J = 8.9 Hz, 2H), 6.69 (s, 1H), 3.84 (s, 3H), 3.00-2.91 (m, 1H), 1.91-1.82 (m, 4H), 1.82-1.72 (m, 1H), 1.65-1.53 (m, 2H), 1.49-1.32 (m, 3H); HRMS-FAB (*m/z*): $[M + H]^+$ calcd for $C_{23}H_{24}NO_4$, 378.1700; found, 378.1689.

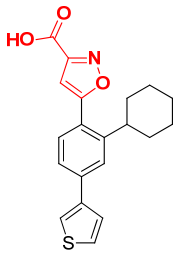

4.56

Compound 4.56. Compound **4.56** was synthesized via procedures analogous to those described for compound **4.40**. **Analytical data.** ^{1}H NMR (500 MHz, MeOD): δ 7.81-7.69 (m, 2H), 7.66 – 7.54 (m, 2H), 7.51 (d, J = 2.2 Hz, 2H), 6.68 (s, 1H), 2.95 (t, J = 11.9 Hz, 1H), 1.85 (m, 4H), 1.77 (d, J = 11.1 Hz, 1H), 1.60 (m, 2H), 1.41 (dt, J = 27.7, 12.5 Hz, 3H); HRMS-FAB (*m/z*): $[M + H]^+$ calcd for $C_{20}H_{20}NO_3S$, 354.1158; found, 354.1157.

Assay Protocols

Minimum Inhibitory Concentration Assay

S. aureus strains were grown from freezer stocks in Tryptic Soy Broth (5 mL, TSB) at 37 ºC for 19-20h. ON cultures ($1x10^{10}$ CFU/mL) were diluted in Muller Hinton Broth (MHB) with 2% NaCl to $1x10^{6}$ CFU/mL. 50 µL of this stock was used in the assay ($5x10^{6}$ CFU/mL). The CFU were determined by diluting with PBS and plating on TSB plates. Inhibitor stocks were diluted with MHB with 2% NaCl for a starting concentration of 8.75 µM. Assays were performed at 37 ºC in microtiter plates and the plate was read after 20h incubation.

References

1. Wang, G.*, et al. J. Clin. Microbiol.* **2006**, *44*, 3883-3886.
2. (a) Centers for Disease Control and Prevention, **2010**, "Healthcare-Associated Methicillin Resistant *Staphylococcus aureus* (HA-MRSA)"; (b) Centers for Disease Control and Prevention, **2010**, "VISA / VRSA: Vancomycin-Intermediate/Resistant *Staphylococcus aureus*"
3. Soulat, D.*, et al. J. Bacteriol.* **2002**, *184*, 5194-5199.
4. Cozzone, A.*, et al. Arch. Microbiol.* **2004**, *181*, 171-181.
5. Klarmann, E.*, et al. J. Am. Chem. Soc.* **1933**, *55*, 4657-4662.
6. (a) Hosokawa, S.*, et al. Tetrahedron Lett.* **2007**, *48*, 7305-7308; (b) Takemura, I.*, et al. Tetrahedron Lett.* **2006**, *47*, 6673-6676; (c) Zbinden, K.*, et al. Bioorg. Med. Chem. Lett.* **2005**, *15*, 5344-5352.
7. (a) Riahi, A.*, et al. Org. Biomol. Chem.* **2009**, *7*, 4248-4251; (b) Roy, A. K.; Batra, S. *Synthesis* **2003**, 2325-2330; (c) Liu, G.*, et al. J. Med. Chem* **2003**, *46*, 4232-4235.
8. Hermann, G.*, et al. Synth. J. Synth. Org. Chem.* **2008**, 221-224.
9. (a) Lee, J. S.*, et al. Bioorg. Med. Chem. Lett.* **2003**, *13*, 4117-4120; (b) Kondo, Y.*, et al. Tetrahedron Lett.* **1989**, *30*, 4249-4250.
10. Costa, B. R. d.; Mattson, M. V. *J. Labelled Compd. Radiopharm.* **1991**, *29*, 63-74.
11. Sakamoto, T.*, et al. Tetrahedron* **1991**, *47*, 5111-5118.